The Molecular and Systemic Underpinnings of Cardiomyocyte Metabolism and Cardiac Inflammation in Heart Failure: Roles for Oxidized Lipids and Pannexin 1 Channels

Caitlin Marie Pavelec
Fort Wayne, Indiana

Bachelor of Science, Chemistry, Spanish, University of Wisconsin-Madison, 2019

A Dissertation presented to the Graduate Faculty
of the University of Virginia in Candidacy for the Degree of
Doctor of Philosophy

Department of Pharmacology

University of Virginia
May, 2024

Table of Contents

Chapter 1 – Introduction

Chapter 2 – Methods

Chapter 3 – Pannexin 1 Channels Control Cardiomyocyte Metabolism and Neutrophil Recruitment During Non-ischemic Heart Failure

List of Figures

Acknowledgements

I hope from this body of work that is quite obvious the completion of a PhD does not happen without collaboration and support. I am so proud of this work and so happy to have done this with so many people, while this process was not without lows and hardships, I believe I am better scientist and human being for it.

I would first like to thank my family: Mom, Dad, and Nick. Thank you for always picking up my phone calls and answering my text no matter what hour it was (mostly too early). I appreciate you all understanding the holidays cut short or where I wasn't totally mentally present, and I hope those become fewer in the future. Moreover, thank you for trekking around cities to watch me run and cheer me on even when you probably had better things to do or talking to me about running for endless hours. You guys have demonstrated what true love and support is and I am eternally grateful for that!

To Jack, the yin to my yang and my other half. I know it was a wild ride when we decided to start this whole process long distance, but we made it through. I'm so glad to have you around me every day and to continue growing this life we've built together. You are always there to just sit while I work, and that presence and support means more than anything. You also know when to help me take a break and step back, which I so desperately need, and I can't wait to see what the future holds for us. I can't promise I won't be stressed over work again, because that would be a lie, but I know I can rely on you to be there when it happens. I couldn't have done this and more without you by my side.

Next, I would like to thank the Leitinger Lab. When I joined the lab quite literally as the world shut down, I didn't really know what I was in for, but now I realize how

amazing you all were to take me under your wings. To Scott and Clint, you both shaped my being as both a scientist and as a person. Thank you for the endless coffee and chatting. Thank you for helping me understand the basics and listening while I explained my next hypothesis and experimental design. Moreover, thank you for being not just my co-workers but friends. I am happy you both welcomed me in and taught me everything you knew and more. To Anna, you have grown so much in this last year, and I can't wait to see what you become. I'm so glad to have you join the lab not only for your help but for making me explain my science in a better way. To Hannah and Emily, my undergraduates throughout this process, thank you for being my right hands. You both made my time in lab not only more fulfilling scientifically, but also personally. I know you both will have amazing careers and I hope you look back on our time with fond memories, mostly. To the newest members of the lab: Kyla, Daniel, and Priyanka, while we haven't known each other long I am so excited to see what you all do and watch the lab grow.

To my thesis committee, thank you for your support and constructive criticism. You all pushed me to be a better scientist and know how to answer the tough questions. I have no doubts that without your guidance this dissertation would look very different. You also provided the collaborative support I needed to complete this work and for that I will be always grateful.

To my PI, Norbert Leitinger. You took a chance on me when we both were in a moment of need, and I'd like to think that worked out pretty well for the both of us. You have taught me so much more than just how to be a scientist. You have taught me that

we don't "believe" anything in science because realistically the data speaks for the findings. You have taught me how to find the holes in a piece of work and how to know when you've filled them with your own data. You've taught me how to present my science and the importance of a title, something I will take with me and use for the rest of my career. Finally though, you taught me that we are more than our work. Hobbies and other interests are what make us people and you should lean into that in times of joy but also those low moments. I know you pushed me in subtle ways to achieve more than I knew I was capable of and for that all I can say is thank you. I look forward to more collaboration in the future.

I would like to thank all of the friends I've made in Charlottesville! The running group from Greenberry's coffee every morning has been central to my happiness, and I am so glad I started showing up one Sunday. You have been there for every stage of this PhD and will be there after, thanks for keeping me on my toes and helping keep me sane. To Melissa, you have become my person through this whole process, and I couldn't imagine a better friend. We've hit some highs and many lows, but it seems fitting that we're finishing this process together.

Finally, to my grandfathers who won't be here to see this. I know you would both be proud to see the woman I've become. You both always supported my love of science and told me about the value of education. Thank you for listening from heaven and I'll see you again someday.

I'll end on a quote that kept me going through this: "When life gets you down, you what you gotta do? Just keep swimming." – Dory, Finding Nemo

Abstract

Proper contractile function of the heart is central to life. At the cellular level availability of ATP to allow for proper contraction within the cardiomyocyte is required to ensure that synchronous beating occurs. Generating this ATP and maintaining a sufficient pool is necessary to keep this required physiological process running.

In the first part of this dissertation, we explore a novel role for pannexin 1 (PANX1) in regulating cardiomyocyte glycolytic metabolism and how the deletion of the channel in cardiomyocytes impacts disease onset during non-ischemic heart failure. We find that deletion of PANX1 in cardiomyocyte shifts cells to a hyper-glycolytic state at baseline and further simulation with a beta-adrenergic agonist does not raise glycolytic bioenergetics as observed in control cells. Additionally, we determined that cardiomyocyte specific deletion of PANX1 protects mice against isoproterenol induced hypertrophy and significantly decreases neutrophil infiltration into the myocardium.

In the second part of this dissertation, we seek to understand how oxidized lipids regulate the heart in a murine model of HFpEF induced by high fat high sucrose (HFHS) feeding. We determine that using a liver-inducible AAV8 to drive scFv-E06 expression we lower plasma oxidized phospholipids after HFHS feeding. Additionally, we find that scFv-E06 protects mice from cardiac and metabolic dysfunction induced by HFHS feeding. Finally, we explore potential mechanisms by which this may be occurring and that scFv-E06 expression may protect by different mechanisms in a sex-dependent manner.

In conclusion, this work identifies novel regulators of cardiomyocyte metabolism and injury response in multiple murine models of heart failure. These findings reveal novel therapeutic targets which may fill gaping holes in clinical heart failure treatment.

Chapter 1 - Introduction:

1.1 Cardiomyocytes and other functional cells of the heart: Cardiomyocytes are the function cell of the heart serving as the contractile force used to produce the heartbeat and pump blood throughout the circulatory system. Cardiomyocytes are a specialized type of muscle cell which relies on the influx and efflux of calcium to cause the contraction of actin/myosin filaments in a concerted effort[1,2]. Individual myocytes are linked in multiple manners including through the nervous system and as well as through gap-junctions which together allow the synchronous beating of the myocardium[3]. The nervous system innervation of the sino-atrial and atrial-ventricular nodes acts as conduction points to synchronize the pumping action between the chambers of the myocardium, while the gap junctions allow for communication between individual myocytes which propagates the contractile signals[2,3]. The sequence of different chambers being activated to pump creates the characteristic lub-dub of the heart-beat, but the individual cellular communication creates the concerted effort which provides enough force to move blood through the system.

Inside the cardiomyocyte there is a unique sarcomere structure that contains the actin thin filaments and myosin thick filaments. The thick filament contains: myosin II which is the predominate isoform in healthy cardiac muscle; titan which acts as template for the sarcomere; and myosin binding protein- C which is proposed to modulate the interaction between myosin and actin[2,4]. The thin filament contains the actin filament which is interspersed with troponin T and troponin I in cardiomyocytes, additionally tropomyosin present in this filament protects the myosin binding sites on the actin

filament. Influx of calcium activates troponin and causes a conformational change in tropomyosin exposing the binding site for the myosin head on the thick filament[5]. When the myosin head is exposed, it hydrolyzes ATP to ADP + P_i which bind to myosin in the formation of the actin-myosin cross bridge structure. Binding of actin and myosin liberates the ADP + P_i allowing for the reorientation of the myosin head to the center of the sarcomere which causes the power generation of contraction. At this point myosin is released from the actin filament and rebinds to unhydrolyzed ATP[2].

In disease contraction can go awry in multiple ways including a deficit of ATP and the composition of the thick filament proteins. As this process relies so heavily on ATP, without sufficient energy sources proper contractile forces cannot be generated and the heart fails to beat with appropriate regularity or force[6]. Furthermore, each of the proteins included in this contractile mechanism has multiple isoforms which have different affinities for their ligands and binding partners. For examples β-myosin, which is the predominant form in the healthy adult heart also has an α-myosin isoform which is more predominate in most diseases characterized by cardiac dysfunction[7].

While cardiomyocytes make up 90% of the cell volume of the myocardium, by cell number they only account for 30-40% of cells present[8]. Endothelial cells, fibroblasts, and resident immune cell populations account for the majority of the remaining cells[8,9]. Endothelial cells line the capillary network which innervates the densely-packed cardiomyocytes. This network is responsible for oxygen delivery locally, as well as passage of fuel sources and transport of damage signals released into the extracellular environment by cardiomyocytes[10]. Moreover, the endocardial surface (the inside surface

of the ventricle) is lined with a layer of endothelial cells which contacts the inner-most layer of cardiomyocytes as well as the blood which is pumped through the ventricle[11]. Endothelial cells in the capillary are central to maintaining proper contractile function in the adult myocardium. Previous work demonstrated that without endothelial cells in the myocardium, cardiomyocytes had reduced responsiveness to intracellular Ca^{2+} concentrations and behaved as though they had decreased resting muscle length[10].

Fibroblasts are present between the cardiomyocytes and provide structure as well as secreted factors to the myocardium[8,12,13]. Fibroblasts secrete a careful balance of extracellular matrix proteins such as collagens and fibronectin to provide structure and space between cardiomyocytes, as well as matrix metalloproteinases, to degrade extracellular matrix and prevent build-up of fibrotic tissue. While fibroblasts have a basal level of activity, they can also be further activated into the myofibroblast like state. Fibroblasts shift to this activated state in response to stimuli including cytokines, excess mechanical stress, and damage signals such as ATP and other purinergic signals. In this state, collagen production and excretion are increased often to serve as a replacement to myocytes which have undergone apoptosis or necrosis. While this replacement fibrosis is necessary to prevent cardiac rupture, it becomes pathological when the fibrosis between myocytes prevents proper myocyte-myocyte communication causing desynchrony of the contractile forces[14]. Additionally, the type of collagen, collagen 1 instead of collagen 3, which is excreted changes the mechanical properties of the myocardium causing the heart to work harder and decreasing contractile efficiency[15]. Cardiac fibrosis is a major hallmark for a variety of diseases, including heart failure, but attempts to modulate the fibrotic

content of the heart with therapies has not improved patient outcomes. In a clinical trial using pirfenidone, an antifibrotic compound which reduces growth factor and procollagen production, patients with HFpEF showed improvement in ECM-volume but not left-ventricle cardiac function parameters after 52 weeks of treatment compared with placebo controls[16]. While this demonstrates that antifibrotic therapy has potential for patients with HF, these trials further indicate the need for improved antifibrotic compounds.

Finally, the myocardium has a resident immune cell population which consists mainly of monocytes, though some low level of B and T-cells are also present[8,9]. Resident immune cells in the heart are characterized by their CCR2- marking compared with CCR2+ infiltrating populations[8]. These cells are responsible for patrolling and contending with low levels of inflammatory stimuli, such as small amounts of cell death or progression of stress signals from myocytes for short periods of time. In addition, it has been shown that these cells are necessary for proper electrical coupling and general maintenance of the myocardium[17]. CCR2- monocytes are capable of proliferation in response to larger damage signals as well as release of pro-inflammatory cytokines to recruit circulatory monocytes to the site of injury[18,19].

1.2 Cardiomyocyte Metabolism in Disease: Proper contractile function of the heart requires, at the level of the cardiomyocyte, sufficient cellular energy in the form of accessible ATP. Adult cardiomyocytes rely on fatty acids as their main fuel source to generate ATP, but they are metabolically flexible and can use glucose, branched-chain amino acids, or ketones as needed[6]. The metabolic flexibility of cardiomyocytes is key to their ability to adapt to increased energy demands during physiological: exercise or

pregnancy, and pathological: hypertension or heart failure, stress. During heart failure, cardiomyocytes demonstrate an increased demand for ATP due to more frequent but less effective contraction[20]. In order to meet this increased energy demand, cardiomyocytes shift their metabolism from utilizing fatty acids to utilizing glucose, which is accompanied by increased glycolysis[21]. This switch resembles the reliance on glucose and glycolysis in fetal cardiomyocytes[6,22]. Initially this increase in glycolysis provides the needed increase in ATP, but the role for this switch in chronic pathologies is hotly-debated. While some recent work has demonstrated that decreased reliance on fatty acid oxidation confers greater resistance to ischemia reperfusion injury and promotes cardiomyocyte proliferation in mice deficient in the mitochondrial fatty acid transporter *Cpt1b*, the paradigm in the field is that this switch will become pathological if allowed to progress unchecked for prolonged disease[23]. The most recent findings suggest that a metabolic shift to glucose utilization by cardiomyocytes protects against cardiac injury, but more work to understand cardiomyocyte metabolism is needed.

1.3 Heart Failure - disease and pathology: Heart failure affects more than 5 million Americans each year with a five-year survival rate of less than 50%[24]. The number of patients diagnosed is continuing to increase as the understanding of heart failure pathology changes and the average age of the human population increases with it. Heart failure can be broken down into two categories: heart failure with preserved ejection fraction (HFpEF) and heart failure with reduced ejection fraction (HFrEF). This classification is dependent on whether the ejection fraction of the heart is above 40%, HFpEF, or less than 40%, HFrEF those these classification even have changed as more is

discovered about the disease of heart failure as a whole[24,25]. Historically, congestive heart failure which is the more classical diagnosis only encompassed patients that fell within the diagnosis of HFrEF, but a fuller understanding of the mechanisms underlying the disease have further stratified patients. HFpEF accounts for about 70% of the diagnoses in the last five-years with that number expected to continue to increase[24].

Mechanistically, both forms of heart failure are characterized by an increase in the fibrotic content of the myocardium as well as a chronic infiltration of immune cells into the myocardium[13,25]. These processes are temporally associated with cardiomyocyte hypertrophy, which while initially thought to be compensatory, becomes pathological under the non-resolving conditions of heart failure[26]. These processes together cause cardiac pump dysfunction, resulting in the cardiac muscle having decreased efficiency and increased energy demand. When left unchecked, this ultimately leads to a decrease in function which ends in HFrEF.

HFrEF can occur as a progressive disease which initially starts with unchecked HFpEF, where no treatment results in the slow progression of the disease to a HFrEF state, or can be caused by an acute cardiac event like myocardial infarction. The progression of heart failure from HFpEF to a HFrEF is associated with cardiometabolic co-morbidities such as obesity, hypertension, and type-2 diabetes, as well as factors such as age and renal disease[27]. In addition to the co-morbidities, HFpEF has proven difficult to treat as traditional therapies used with HFrEF including beta-blockers, angiotensin converting enzyme inhibitors, angiotensin receptor blockers, and diuretics have had limited success in HFpEF patients[28]. To date, only SGLT2 inhibitors have proven successful in improving

cardiac function for HFpEF patients[28,29]. While, HFrEF has more therapeutic options than HFpEF, most of these therapies treat the symptoms of HFrEF targeting the renin/angiotensin and aldosterone signaling axis, rather than treating the disease-causing mechanism[25]. Furthermore, while beta-blockers target the hypertrophic signaling in the cardiomyocyte to manage the disease progression patients become desensitized to this class of compounds over time making their use effective but temporally limited[30]. This reveals a much-needed space for therapeutic development which is both effective at preventing disease progression and treating disease mechanism instead of symptoms.

1.4 Chronic Inflammation in Heart Failure: Though the myocardium has a resident immune cell population which is monocyte driven, under pathological conditions the resident immune cells are far outnumbered by infiltrating immune populations[9,17,31]. Neutrophils (CD11b$^+$, Ly6g$^+$) initiate the immune cascade acting as first responders[32]. Neutrophils are central players by releasing oxidants as well as proteases to contend with tissue damage, further propagating the pro-inflammatory signaling which recruits other populations and more neutrophils to the damaged area. Recently neutrophils have been classified as N1 or N2, similar to the classification given to macrophages historically[33]. N1 neutrophils are the classical first responders and considered to be pro-inflammatory releasing cytokines such as IL1β, IL12, and TNFα[34,35]. In ischemic injury models, these N1 neutrophils are most prevalent the first five days after injury, at which point N2 neutrophils significantly increase[36]. N2 neutrophils are marked by expression of CD206 and IL10, which have both also historically been used as M2 markers[37,38]. In most pathologies, N1 neutrophils comprise the majority of the neutrophil population through-

out the course of disease, though the N2 population increases in late stages of disease as pro-resolving cytokines dominate[32,33].

The next responder called by the release of pro-inflammatory cytokines by neutrophils and other damage signals from the resident cardiac cells is macrophages[17,19]. Resident cardiac macrophages are proliferative and add to the leukocyte population in the myocardium during injury with a CCR2$^-$ surface marker[39]. Infiltrating macrophages are identified by their CCR2$^+$ surface marker. Infiltrating macrophages efferocytose dying cardiomyocyte in response to damage signals released from these cells including ATP and pro-apoptotic markers such as cytochrome c[18,40,41]. Initial polarization of these macrophages skews towards a pro-inflammatory phenotype which increase macrophage numbers and promotes the release of cytokines such as IL-1β, IL-6, and TNFα[39,42,43]. In ischemic injury, the temporal regulation of macrophage infiltration and polarization from a pro-inflammatory to a pro-resolving state has been well studied, but in chronic cardiac damage this is less well understood as pro-resolving macrophages never dominate the population[39,43]. This is concurrent with the chronic inflammation phenotype described in these diseases including coronary artery disease, atherosclerosis, chronic hypertension, and obesity[44–46].

Chapter 2 – Methods:

Animals: Cardiomyocyte-specific Panx1-deficient mice were generated by crossing *Panx1$^{loxP/loxP}$* (Panx1$^{fl/fl}$) mice[47] with B6.FVB-Tg(Myh6-cre)2182Mds/J (MyHC6-Cre)[48] (strain #011038) obtained from the Jackson Laboratory. For breeding purposes, mice hemizygous for the MyHC6 Cre were cross with Panx1$^{fl/fl}$ mice to give littermate mice of Panx1$^{loxP/loxP}$ MyHC6$^{wt/wt}$ (Panx1$^{fl/fl}$) and Panx1$^{loxP/loxP}$ MyHC6 $^{Cre/wt}$ (Panx1^{MyHC6}). All animals were maintained at the University of Virginia Center for Comparative Medicine in a pathogen-free vivarium facility. Mice were maintained on a 12-hour light/dark cycle and provided ad libitum access to standard rodent chow (Teklad 7912) and water. All experiments performed were approved by the University of Virginia Animal Care and Use Committee (protocol #3444). All experiments were performed using age-matched littermate controls. Genotyping was performed via PCR from tail clip biopsies after proteinase K digestion in DirectPCR tail lysis buffer (Viagen Biotech 102-T). PCR of genomic DNA was performed using Apex Taq Master Mix and allele-specific primers as previously described[49].

B6.Cg-Speer6-ps1$^{Tg(Alb-Cre)21Mgn}$/J (The Jackson Laborartory 003574) (Alb Cre) mice were purchased at 8 weeks of age and maintained at the University of Virginia Center for Comparative Medicine in a pathogen-free vivarium facility. Mice were maintained on a 12-hour light/dark cycle and unless otherwise described provided ad libitum access to standard rodent chow (Teklad 7912) and water. At 12 weeks of age, mice were injected with either AAV8-GFP (Penn Vector Core) or AAV8-scFv-E06 (10^{11} genome copies/ 100 µL in sterile PBS). At 14 weeks of age, mice were randomized by body weight across viral

vector, and fed either chow control diet or high fat high sucrose diet (40% fat, 12% sucrose) (ResearchDiets D12327Mi) for 12 or 16-weeks respectively.

Isoproterenol induction of heart failure: 8–10-week-old male mice were treated daily with isoproterenol or saline vehicle for 14 days to induce heart failure as previously described. Isoproterenol (medchem: HYB0468) was freshly prepared daily in sterile saline prior to injection (15 mg/kg/day) and administered by intraperitoneal injection. Mice were weighed daily to monitor for excessive weight loss and appropriate dose administration.

Isoproterenol progression of heart failure: For longer-term administration of isoproterenol, osmotic pumps (Alzet 2004) were filled with isoproterenol in sterile saline plus 0.02% acetic acid and mice were weighed prior to implantation to administer 15mg/kg/day according to pump rate specifications. Pumps were equilibrated overnight in sterile saline prior to implantation. 8–10-week-old male mice were anesthetized using isoflurane and implantation sites were exposed after hair removal with Nair hair removal lotion with aloe and lanolin. Mice were administered bupivicane analgesic and sites were sterilized with three washes of betadine and ethanol wipes. Pumps were implanted in a subcutaneous pocket on the back of the mouse and surgical clips were placed for wound closure. Mice were placed on a heating-pad and isoflurane anesthesia was maintained for the length of the procedure. Surgical clips were removed 10-14 days after placement.

Immunofluorescence staining: Hearts were harvested and fixed for 4 hours in 10% zinc-buffered formalin prior to fixation in 50% ethanol. Tissues were paraffin embedded and cryosectioned to 7μm thickness and mounted. Slides were deparaffinized. Briefly, sections

were submerged in Histo-Clear (Electron Microscopy Sciences 64110-01) (3x10 minutes), 100% ethanol (2x3 minutes), 95% ethanol (2x3 minutes), 70% ethanol (1x3 minutes), and PBS (1x5 minutes). Antigen retrieval was performed using citrate-based solution (Vector Laboratories H-330) where slides were submerged in antigen retrieval solution and heated to boiling for 20 minutes, slides were then cooled for 10 minutes at room temperature and 10 minutes at $4^{\circ C}$. Tissue sections were then blocked for 1 hour in antibody blocking buffer (0.2% TritonX, 1mL donkey serum) at room temperature. Antibody blocking buffer was removed and replaced with antibody blocking buffer containing primary antibody (1:100) overnight at $4^{\circ C}$. Sections were then washed (3xPBS for 5 minutes) and incubated in antibody blocking buffer containing secondary antibody (1:500) for 1 hour at room temperature protected from light. Sections were washed (3xPBS) and counterstained with DAPI (Thermo Fisher Scientific D3571) before mounting. Sections were imaged on an Olympus Fluoview 1000 and are representative images of composite z-stacks. Analysis (thresholding, manual counting, and fluorescence intensity quantification) were performed in ImageJ.

Quantification of Cardiomyocyte cross-sectional area: Hearts were prepared as indicated in immunofluorescence staining. Sections were stained with cTnnt (1:100 - Abcam ab8295) during primary incubation and DAPI (1:500 - Thermo Fisher D3571) and Wheat-Germ-Agglutinin-Alexa Fluor 647 (5 µg/m – Thermo Fisher W32466) during secondary incubation. Sections were imaged on an Olympus Fluoview 1000 confocal microscope with five images per mouse taken in the left ventricle across two sections. 50 round nucleated cardiomyocytes per mouse were outlined across the images and were analyzed in ImageJ.

Flow cytometry of infiltrating cardiac leukocytes: Primary infiltrating leukocytes were isolated from cardiac tissue by non-Langendorff perfusion previously described[50]. Briefly, hearts were sequentially perfused with EDTA buffer, perfusion buffer, and digestion buffer containing collagenase until hearts appeared soft. Hearts were then mechanically dissociated with scissors and pipetted up and down. Cells were washed through a 100μm cell strainer to create a single cell suspension. Myocytes were isolated by centrifugation at 120 x g for 5 minutes. Supernatants (containing non-myocyte cells) were transferred to clean tubes and pelleted by centrifugation at 300 x g for 5 minutes. Pellets were treated with ACK lysis buffer for 1 minutes and then resuspended in 1mL of FACS buffer (PBS, 2mM EDTA, and 1%BSA). Splenocytes were isolated by grinding through a 100μm cell strainer and washing with PBS containing 2mM EDTA. Samples were then incubated with ACK lysis buffer for 2 minutes and spun at 400 x g for 5 minutes. All samples were then counted and resuspended at 100μL per 100,000 cells in PBS. Cells were stained with LIVE/DEAD Yellow (1:1000) (Thermo Scientific L34967) for 30 minutes on ice. Fc-receptors were then blocked for 15 minutes using FcBlock (BioRad – BUF041A). Cells were pelleted by centrifugation (300 x g,5 minutes) and resuspended in FACS buffer (100μL per 100,000 cells) and stained with fluorophore-conjugated antibodies (1:100) for 1 hour on ice. See tables for antibodies included below. Cells were washed in PBS (x3) after staining. Flow cytometry collection and deconvolution was performed on an Cytek Northern Lights 3 laser Spectral Flow Cytometer. Automatic deconvolution was performed using single stains generated from splenocytes. Gating and post-hoc analysis was performed with FCS-Express 7.18.

Representative gating is presented for all flow cytometry experiments in supplemental figures.

RNA-Sequencing: Hearts of mice were removed after whole body perfusion with 10mL of PBS, weighed, and snap frozen at -80^C prior to analysis. For some experiments, isolated cardiomyocytes were suspended in 1mL of TRIzol^{TM} (Invitrogen) and stored at -80^{oC} for further analysis[50]. After chloroform incubation and centrifugation per manufacture instructions RNA-containing phase was diluted with 70% ethanol 1:1 and RNA isolation was performed using RNeasy Mini Kit (Qiagen). For tissues, Total RNA was isolated using RNeasy Mini Kit (Qiagen) after lysis in RLT buffer with bead homogenization. Total RNA quantity and quality were then assessed on a NanoDrop 2000 spectrophotometer (Thermo Fisher Scientific). Library preparation including quality metrics, sequencing, and clustering were performed by Novogene (Sacramento, CA). Sample integrity was assessed prior to library preparation using the Bioanalyzer 2110 system with an RNA Nano 6000 Assay Kit (Agilent Technologies). One hundred fifty-base paired-end sequencing was performed using an Illumina NovaSeq platform according to manufacture instructions. Fastq files were processed using in-house perl scripts from Novogene to obtain clean reads. Clean reads were aligned to the mouse reference genome using Hisat2 v2.0.5. FeatureCounts was used to calculate read numbers for each gene and fragments of per kilobase of transcript sequence per millions base pairs sequenced (FPKM) were calculated. Differential expression analysis was performed using DESeq2. Differentially expressed genes (DEG) were assigned by criteria of P-value adjusted < 0.05 (-Log(p-value) > 1.3).

KEGG pathway analysis and Gene Ontology pathway analysis was performed on DEG using clusterProfiler.

Echocardiography: 8–16-week-old male mice were anesthetized using isoflurane. The chest was exposed after hair removal and a four-lead electrocardiogram (ECG) was collected during the procedure. Images were collected using a VevoView 1100 system. Images were collected in the long-axis (B-mode) and short axis (M-mode) on mice serially throughout the experimental period. Serial collection began prior to disease induction and occurred every two-weeks during disease progression. Images were analyzed using Vevo Lab. Left-ventricle (LV) end-diastolic, end-systolic volume, and wall thickness were assessed, and ejection fraction calculated.

Blood Pressure Assessments using Radiotelemetry: Blood pressure was measured using telemetry equipment (Data Sciences International, DSI) as previously described[51]. Mice were surgically implanted with radiotelemetry units (PA-C10 or HD-X10). Briefly, while under isoflurane anesthesia, the catheter of a radiotelemetry unit was placed in the left carotid artery and positioned such that the probe reached the aortic arch. The radio-transmitter was placed in a subcutaneous pouch at the right flank. Buprenorphine was used as an analgesic. Mice were allowed to recover for seven days prior to the initiation of recordings. Baseline blood pressure measurements, including systolic pressure, diastolic pressure, mean arterial pressure (MAP) and heart rate, were recorded every minute for a continuous period of 5 days using Dataquest A.R.T. 20 software (DSI). Diurnal (inactive period) MAP was measured during animal's light cycle (6:00 a.m. to 5:59 p.m.) and nocturnal (active period) MAP was measured during the animal's dark

cycle (6:00 p.m. to 5:59 a.m.).

Antibodies: Antibodies used in these studies were rabbit monoclonal anti-Panx1 (Cell Signaling - #91137), rabbit monoclonal anti-CCR2 (Abcam – ab273050), rat monoclonal anti-Ly6g (R&D Systems – MAB1037), mouse monoclonal anti-cardiac troponin T (Abcam – ab8295), and wheat germ agglutinin (Invitrogen – W32466). Flow cytometry antibody used include CD45 rat anti-mouse APC eFluor 780 (Invitrogen - 47-0451-80), CD11b rat anti-mouse FITC (Invitrogen - 11-0112-82), CD163 rat anti-mouse PE (Invitrogen - 12-1631-80), CD86 rat anti-mouse SuperBright 436 (Invitrogen - 62-0869-41), LIVE/DEAD Yellow Cell Stain for 405 (L34967), Ly6g rat anti-mouse PE-Cyanine5 (Invitrogen - 15-9668-80), F4/80 anti-mouse APC (eBioscience 17-4801-82), CD64 anti mouse PerCP-710 (Invitrogen – 46-0641-80), CD24 anti mouse PE-Cyanine7 (Invitrogen 25-0242-82).

Cell culture: H9c2 rat myoblasts were obtained from ATTC and maintained in high-glucose DMEM supplemented with 10% heat-inactivated FBS, 15 mM sodium bicarbonate (Glibco), 1mM sodium pyruvate (Glibco), and 1% Pen-Strep. Cells were passaged when they reached 70% confluency on tissue culture (TC) treated dishes using 0.25% trypsin (Glibco).

siRNA-Mediated Knock-Down of Panx1: H9c2 cells in 12 or 24 well TC treated plates or 10cm TC treated dishes were washed in sterile PBS and then incubated with OptiMEM (Glibco). Cells were treated with RNAiMax Lipofectamine and siRNA against Panx1 or negative control silencer #1 (Ambion - 197003) per the manufacturer's instructions. Experiments were performed 72 hours after transfection with the siRNA.

RNA isolation and quantitative reverse transcription PCR: RNA was isolated from approximately 75,000 H9c2 rat myoblasts or isolated cardiomyocytes or immune cells from one mouse heart and lysed in RLT lysis buffer. RNA was isolated using the RNeasy Mini Kit (QIAGEN) according to the manufacturer's instructions. RNA was quantified using a NanoDrop spectrophotometer (Thermo Fisher Scientific), and complementary DNA (cDNA) libraries were generated using the iScript cDNA Synthesis Kit (Bio-Rad). Quantitative reverse transcription PCR was performed using TaqManFast Advanced Master Mix (Thermo Fisher Scientific) and TaqMan primers (mouse *Panx1* mm0045091 , mouse *Panx2* mm01308054, mouse *Panx3* mm00552586, mouse *Gja1* mm00439105, mouse *Gja5* mm00433619– Invitrogen) (Rat *Panx1* Rn01447976_m1 – Thermo Fisher Scientific) for genes of interest on a CFX Connect real-time PCR instrument (Bio-Rad). Relative gene expression was determined using *18S* (4333760 – Thermo Fisher Scientific) or *Hprt* (mm01545399 – Invitrogen) as a housekeeping gene. Quantitative reverse transcription PCR was performed using SensiMix SYBR Green reagent and primer pairs for genes of interest on a CFV Connect real-time PCR instrument where TaqMan primers were not used. Relative gene expression was determined using *Hprt* as a housekeeping gene. Primer sequences were verified against genes of interest using NCBI Primer-BLAST.

ATP release measurements: H9c2 cells were plated at 80,000 cells per well in a 48 well dish and put in serum free media overnight prior to experimental treatment. Cells were incubated with Panx1 inhibitors (spironolactone 50 μM in serum free media) or vehicle control for 1 hour prior to stimulation. ARL (Tocris 1283) (300 μM) was added for 30 minutes prior to stimulation. Cells were then stimulated with vehicle (PBS), isoproterenol

(2 or 20 µM in sterile PBS), or phenylephrine positive control (10 µM) for 15 minutes. One-third of the media in the well was carefully collected with care taken to not bump cells in the bottom of the well and placed on ice. ATP concentrations were assessed by CellTiterGlo (Promega G7571) and compared to standard curve prepared by combining serum free H9c2 media with ATP disodium salt (Tocris 3245).

Dye Uptake Assay: H9c2 cells were plated at 1000,000 cells per well in a 12 well dish and incubated with Panx1 inhibitors (spironolactone 50 µM, carbenoxolone 50 µM, or probenecid 1mM) or vehicle control for 1 hour prior to stimulation. Cells were stimulated with vehicle (PBS), isoproterenol (2 or 20 µM in sterile PBS), or phenylephrine positive control (10 µM) for 1 hour at the same time as Yo-Pro-1 dye (Thermo Fisher Scientific Y3603) (1µM) was added to the media. Media was removed and cells were washed prior to detachment with trypsin (0.25%). Cells were spun at 400 x g for 5 minutes and resuspended in PBS with LIVE/DEAD Yellow (1:1000) for 30 minutes. Cells were pelleted and washed in Annexin V binding buffer three times and then resuspended in Annexin V AlexaFluor 568 (Thermo Fisher Scientific A13202) (1:500) (AV) for 10 minutes. Cells were washed and resuspended in FACS buffer as described above. Cells were analyzed by flow cytometry on an Attune NxT. Single stain controls were performed using H9c2 cells for initial intensity. FMO were collected and used for deconvolution prior to gating. Cells were gated for LIVE/DEAD Yellow and AV negative and the percentage of cells positive for Yo-Pro-1 was assessed as compared to vehicle stimulation.

Glycolytic Stress Test, Mitochondrial Stress Test, and ATP Production assay: After treatment with control or Panx1-targeting siRNA as described above, H9c2 rat myoblasts

were plated (40,000 cells per well) in complete medium in XFe96 cell culture microplate and allowed to settle for one hour at room temperature before overnight culture. The following day cells were treated with ISO (20µM) for 1 hour in complete medium. Immediately prior to the assay the media was changed to glycolytic stress test medium (Sigma Aldrich D5030) supplemented with 143 mM NaCl and 2mM L-glutamine (Gibco 25030 – 081), mitochondrial stress test medium (Corning 50-003-PB), or ATP production medium (Agilent 103575-100). Glycolytic activity was assessed by measurement of extracellular acidification rate on a Seahorse XFe96 instrument (Agilent Technologies). The rate of pH change was measured every 13 minutes for a 3-minute interval before sequential challenge with 1) 20mM glucose (Sigma Aldrich D9434), 2) 1 µM oligomycin (Sigma Aldrich 75351), and 3) 80 mM 2-deoxyglucose (Sigma Aldrich D8375). Basal ECAR was measured as post-glucose ECAR minus post 2-DG ECAR, and maximal ECAR was measured as post-oligomycin ECAR minus post-2DG ECAR. Mitochondrial activity was assessed by measurement of O_2 consumption rate on a Seahorse XFe96 instrument (Agilent Technologies). The rate of O_2 change was measured every 13 minutes for a 3-minute interval before sequential challenge with 1) 1 µM oligomycin (Sigma Aldrich 75351), 2) 2 µM BAM15 (Cayman Chemical Company 17811) and 3) 10 µM antimycin A (Sigma-Aldrich, A8674) and 10 µM rotenone (Sigma-Aldrich, R88751G). Maximal OCR was measured as post-BAM15 OCR minus post-antimycin A/rotenone OCR. ATP production was assessed by measurement of proton extrusion rate (PER) on a Seahorse XFe96 instrument (Agilent Technologies). The PER was measured every 13 minutes for a 3-

minute interval before sequential challenge with 1) oligomycin and 2) antimycin A and rotenone according to manufacture instructions.

2-NDB Glucose Uptake: H9c2 rat myoblasts were plated in a black, clear bottom 96 well plate and allowed to adhere overnight in complete media. Cells had been cultured with either control or Panx1 siRNA for 48 hours in OptiMem media prior to plating. The following day cells were treated with ISO (20μM) for 1 hour or vehicle control. After stimulation media was removed and replaced with glucose free DMEM as described above in the presence of 2-NDB glucose for 4 hours. The uptake of fluorescent 2-NBDG was assessed according to manufacturer's instructions (Cayman Chemicals - Glucose Uptake Cell-Based Assay Kit) on a Synergy HTX plate reader (BioTek).

CytoTox Cell Death Assay: H9c2 rat myoblasts were plated in a clear bottom 96 well plate and allowed to adhere overnight in complete phenol red free media. Cells had been cultured with either control or Panx1 siRNA for 48 hours in OptiMem media prior to plating. The following day cells were treated with ISO (2,20μM) or phenylephrine (10 μM) for 15 minutes or vehicle control. After stimulation media was removed and LDH presence in the media was assessed according to manufacturer's instructions (Promega- CytoTox Non-radioactive cytotoxicity assay) on a Synergy HTX plate reader (BioTek).

Serum Creatinine: Whole blood was collected from mice via cardiac puncture and placed into serum separating tubes (BD Microtainer – 365967) for 30 minutes at room temperature. Serum was separated by centrifugation (1500 x g, 5 minutes) and snap frozen on dry ice. Serum creatinine was measured at 520 nm after addition of sodium

picrate according to manufacturer's instructions (Pointe Scientific - Creatinine Reagent Set C75391250) using a known standard (Pointe Scientific C75391250).

Glucose Tolerance Test (GTT): Mice were fasted for 16 hours in chip bedding with ad libitum access to water and weighed prior to the start of the test. Blood glucose was tested and then glucose solution (1 mg/g in sterile water) was injected via intraperitoneal injection. Blood glucose was measured at 15, 30, 60, and 120 minutes via tail vein nick using glucometer (CVS).

Insulin Tolerance Test (ITT): Mice were fasted for 6 hours in chip bedding with ad libitum access to water and weigh prior to the start of the test. ITT tested occurred at minimum 7 days after GTT testing. Insulin (0.75 U/kg) (100 U/mL Hummulin R – Lilly) was administered via intraperitoneal injection and blood glucose was measured 15, 30, 60, and 120 minutes after injection.

Body Composition Analysis: Fat and lean mass body composition analysis was performed using EchoMRI Body Composition Analyzer via magnetic resonance imaging. Analysis was performed every two weeks from the start of diet.

Cardiac MRI Cine Imaging: Mice were anesthetized using isoflurane and imaging was performed using a 9.4 Tesla Bruker BioSpin MRI scanner using ParaVision 360 operating software. Four chamber and serial 2 chamber cine imaging were performed after cardiac localization and planning. Image analysis was performed using Segment for LV mass, diastolic, and systolic functional measurements[52].

Statistics: Statistical analyses were performed in Prism 9 (GraphPad). The presence of statistical outliers was assessed by a ROUT test (2%), and identified outliers were excluded

from analysis. Statistical outliers were identified for data show in Figure 4E, F, which were excluded from analysis. Statistical tests were performed with two-tailed analysis. Comparisons between two groups was conducted by Welch's or Student's t-test, while comparisons between more than two groups were made by one-way analysis of variance or mixed-effects analysis. Sidak's multiple comparisons test was performed as post-hoc analysis where appropriate. Mixed effects analysis was used for paired data with more than two groups. A p-value of less than 0.05 was considered statistically significant. Data are represented as mean ± the standard error of the mean. Image analysis was performed on 3-5 averaged images per mouse across a minimum of two cardiac sections. Data points shown for imaging are representative of the average across a mouse, with each data point representative of individual mice.

Data Availability: Sequencing data reported in this manuscript are deposited in the NCBI Gene expression Omnibus. All data needed to evaluate the conclusions of this manuscript are present in the manuscript, present in the supplementary figures, or available upon request to the corresponding author. Graphics were prepared using BioRender. Panx1^{MyHC6} mice can be provided by N.L. upon completion of a materials transfer agreement with the University of Virginia School of Medicine. Requests may be submitted to N.L. ().

Chapter 3: ***Pannexin 1 Channels Control Cardiomyocyte Metabolism and Neutrophil Recruitment During Non-Ischemic Heart Failure***

Abstract:

Pannexin 1 (PANX1), a ubiquitously expressed ATP release membrane channel, has been shown to play a role in inflammation, blood pressure regulation, and myocardial infarction. However, a possible role of PANX1 in cardiomyocytes in the progression of heart failure has not yet been investigated. We generated a novel mouse line with constitutive deletion of PANX1 in cardiomyocytes (Panx1^{MyHC6}). PANX1 deletion in cardiomyocytes had no effect on unstressed heart function but increased the glycolytic metabolism both *in vivo* and *in vitro*. *In vitro*, treatment of H9c2 cardiomyocytes with isoproterenol led to PANX1-dependent release of ATP and Yo-Pro-1 uptake, as assessed by pharmacological blockade with spironolactone and siRNA-mediated knock-down of PANX1. To investigate non-ischemic heart failure and the preceding cardiac hypertrophy we administered isoproterenol, and we demonstrate that Panx1^{MyHC6} mice were protected from systolic and diastolic left ventricle volume increases and cardiomyocyte hypertrophy. Moreover, we found that Panx1^{MyHC6} mice showed decreased isoproterenol-induced recruitment of immune cells (CD45$^+$), particularly neutrophils (CD11b$^+$, Ly6g$^+$), to the myocardium. Together these data demonstrate that PANX1 deficiency in cardiomyocytes impacts glycolytic metabolism and protects against cardiac hypertrophy in non-ischemic heart failure at least in part by reducing immune cell recruitment. Our study implies PANX1 channel inhibition as a therapeutic approach to ameliorate cardiac dysfunction in heart failure patients.

Introduction

3.1 Pannexin Channels: Pannexin channels are integral members of the cell membrane landscape. A three membered family of membrane channels which are known to be differentially regulated, Pannexin 1 (PANX1) is the most well studied of the three family members and is ubiquitously expressed[51,53,54]. PANX1 has been localized to the plasma membrane in most cell types, as well as recent work which has shown potential localization to the mitochondria in cardiomyocytes[55]. While PANX1 is ubiquitously expressed, PANX2 has been shown to be most robustly expressed in the central nervous system, though expression has been shown in a multitude of cell types including systems such as skin and brown adipose tissue[56]. PANX2 has been shown to be localized to cytoplasmic compartments with minimal identification of the channel at the plasma membrane[57]. Finally, PANX3 which was originally thought to be primarily expressed in bone and skin, has been shown to be expressed in a wide variety of tissues. PANX3 localization has been shown at multiple membranes including not only the plasma membrane as an ATP release channel, but also at the golgi and ER membrane[58]. PANX1 and PANX3 have both been shown to release ATP in response to many types of stimuli in their respective cell types, which serves as a link between one cell and another as part of the purinergic signaling axis[59,60].

PANX1 is a heptameric channel, which has been shown to activated by its C-terminus[61]. Many modes of activation have been identified for PANX1 including cleavage of the C-terminal tail by caspase 3, alpha$_{1D}$-adrenergic receptor activation, β3-adrenergic receptor activation, and β1-adrenergic receptor activation causing phosphorylation of

PANX1 at Ser206 in a cAMP dependent mechanism[51,53,55]. Additionally, there is evidence that the channel may be able to activate by stretch of the cells in a mechanical mechanism[62]. The open probability of PANX1 follows a quantized mechanism whereby increasing the number of C-termini which are cleaved increased the conductance of the channel linearly[62]. Moreover, while multiple modes of channel activation have been described, the channel is known to release a variety of metabolites less than 1 kDa in size[63]. ATP is the most well characterized metabolite released through PANX1, serving as a damage signal to recruit immune cells known as a "find me" signal[59,63]. ATP is also used as the standard to measure *in vitro* channel activation. Meanwhile, **Medina et al.** described that other metabolites of interest including spermidine and UDP-glucose can also be released through the channel during apoptosis[63].

A role for PANX1 has been previously described in multiple models of cardiovascular disease including hypertension, inflammation, abdominal aortic aneurism, and myocardial infarction[64–68]. As previously discussed PANX1 can be activated via alpha$_{1D}$-adrenergic receptor activation, and this has been shown to play an important role in physiological regulation of blood pressure where ATP released through PANX1 serves as a vasoconstrictive signal for smooth-muscle cells[51]. Several pharmacologic compounds including probenecid, carbenoxolone, and the FDA-approved heart failure therapeutic spironolactone have been identified as PANX1 channel blockers[64,69,70]. Furthermore, spironolactone which is a primary therapy for heart failure patients, has been identified as both a mineralocorticoid receptor antagonist as well as PANX1 blocker[64,71–73]. Using a PANX1 global knock-out mouse in a model of myocardial ischemia-reperfusion, PANX1^{-/-}

mice were protected from cardiac dysfunction and infarct size[55]. Endothelial cell specific

PANX1 knock-out mice were also protected in a mouse model of myocardial infarction and

this was linked with decreases in CCR2^{+} infiltrating leukocytes[68]. Finally, release of ATP

from cardiomyocytes through PANX1, which caused fibroblast activation *in vitro,* has

previously been described[74]. While these prior studies have strongly implied PANX1 as a

therapeutic target for cardiovascular diseases, the role for PANX1 in cardiomyocytes

specifically and in the regulation of chronic cardiac pathologies, including heart failure,

remains to be elucidated[75].

3.2 Heart Failure and the Innate Immune Response: Heart failure, which affects five

million Americans each year and has a five-year survival rate of less than 50 percent, can

be divided in to two sub-pathologies: heart failure with reduced ejection fraction (HFrEF)

and heart failure with preserved ejection fraction (HFpEF); HFpEF is the more

predominant form and its prevalence is on the rise[24,28]. While several effective therapies

are available for patients with HFrEF, HFpEF has limited treatment options underscoring

the need to identify new therapeutic strategies[27]. Pathological features of heart failure

include cardiac hypertrophy, chronic inflammation, and interstitial fibrosis of the heart

muscle, which together result in reduced cardiac contractile function[25]. Current

pharmacologic interventions for HFrEF include treatments with beta-blockers, loop

diuretics, angiotensin converting enzyme (ACE) inhibitors, angiotensin receptor blockers,

and sodium glucose transporter 2 (SGLT2) inhibitors[25,76,77]. These therapies target the

renin-angiotensin/ aldosterone systems and the adrenergic signaling axes, providing more

symptom management rather than improving function of the cardiac muscle[76]. Moreover,

previous clinical trials have targeted TNF-α signaling, modulated the immune system using intravenous immunoglobulins[78], or decreased fibroblast activation with pirfenidone[79] (an antifibrotic which down regulates growth factors and procollagens I and II), have not lead to significant improvements in patient outcomes. To prevent cardiac muscle decline, it is necessary to devise novel therapeutic approaches which directly target the mechanisms of heart failure progression.

In response to local hypoxia or chronic beta-adrenergic stimulation, two conditions known to cause cardiac hypertrophy and heart failure, cardiomyocytes release damage signals such as ATP[74] and secrete pro-inflammatory cytokines, which leads to the recruitment of macrophages and neutrophils and efferocytosis of dying cardiomyocytes[39,78]. Initially, recruited leukocytes promote the repair of damaged myocardium by stimulating resident fibroblasts to secrete extracellular matrix, and by inducing angiogenesis to provide needed oxygenation and nutrients to the healing cardiac muscle[17,80]. While this acute inflammatory response is necessary to activate fibroblasts and prevent excessive cardiomyocyte death, chronic activation of both the innate and adaptive immune responses has been shown to exacerbate heart failure progression[9,40,78,81]. The immune cell cascade and timeline for resolution of inflammation after ischemic myocardial infarction has been well characterized, however, it is less well understood how immune cells are recruited to the injured myocardium in chronically developing non-ischemic heart failure[82].

3.3 Purinergic Signaling in neutrophil recruitment*: PANX1 serves as a key signaling axis in the purinergic signaling cascade. Purinergic signaling is comprised of a group of channels known to release purinergic nucleotides including ATP and adenosine and the receptors which bind these ligands. This signaling can act in an autocrine manner signaling to other microdomains within the same cell or as a paracrine function signaling locally to other cells to communicate cellular damage and cause chemotaxis. Though much of the work done with PANX1 heavily implicates the role for PANX1 dependent ATP release, previous studies have demonstrated that a wide variety of metabolites can be released through PANX1[63]. Other metabolites including ADP, UTP, and UDP-glucose have been identified in the supernatant of media collected from PANX1 dependent activation[63].

These ligands as well as others are all known to play roles in paracrine signaling, or "find me signals" from damage cells such as cardiomyocytes .These metabolites serve as ligands for many purinergic receptors present on neutrophils, including P2Y14, P2Y2,P2X1, and P2X7 which have been previously demonstrated to play key roles in chemotaxis and leukocyte migration into tissues during disease[83–86]. Studies in human neutrophils identified UDP-glucose as being the ligand for P2Y14 using a P2Y14 specific inhibitor[84]. Further work in a P2Y14 deficient mouse in a model of COVID infection demonstrated that P2Y14 global deletion reduced neutrophil recruitment to the lung[87]. Finally, in a model of kidney ischemia reperfusion injury pre-treatment with P2Y14 specific antagonist, PPTN, prior to injury reduced neutrophil, Ly6G$^+$, CD11b$^+$, and monocyte, CD11b$^+$, Ly6C$^+$, recruitment in to the kidney[88]. P2Y2 has been shown to bind ATP and UTP, both ligands which have been seen in to be released in a PANX1-dependent manner from

apoptotic cells[63,86]. ATP serves as a chemotaxis signal binding the P2Y2 receptor in neutrophils, which then initiates a positive feedback loop of further ATP release and then hydrolyzed ATP binding to A3 receptors on the neutrophils as a means of communicating directionality to the leading edge of the neutrophil[89]. While P2Y14, which binds UDP-glucose, is more specific to neutrophil populations over other leukocytes, receptors such as P2X1 and P2Y2, which binds ATP are found on many cell types in the myocardium including myocytes themselves, platelets, and multiple immune cell populations include both resident monocytes and invading early responders such as neutrophils[90,91]. In a global deletion P2X1 mouse testing a pancreatitis model, neutrophil recruitment to the pancreas was significantly decreased, while in this same model administration of apyrase, an enzyme which catalyzes the hydrolysis of ATP to AMP, serum MPO was significantly reduced[85]. Taken together these two findings closely link ATP binding to P2X1 receptors as playing a key role in neutrophil recruitment. Finally, P2X7 which is also known to bind ATP has been previously demonstrated to be influential in bacterial killing and the sterile immune response during serve organ damage[92,93]. In a model of severe sterile liver injury, ATP release from hepatocytes was shown to recruit neutrophils to the injury site via chemokine gradient and P2X7 knock-out or pharmacological inhibition significantly reduced this recruitment to the injury site[93].

Taken together, this body of literature demonstrates that purinergic signaling in neutrophils plays a key role neutrophil migration and activation during sterile injury. Additionally, the ligand receptor pairs have been well explored when it comes to those expressed in neutrophils. However to this point, it is not entirely understood how these

signals are released from injured cells, and even less so cardiomyocytes, especially in the context of chronic sterile injury such as non-ischemic heart failure.

3.4 Brief Summary of Chapter: Here we report that PANX1 channels can be activated in cardiomyocytes through beta-adrenergic receptor stimulation. Using mice with a cardiomyocyte-specific PANX1 deletion (Panx1[MyHC6]), we demonstrate a crucial role for PANX1 channels in the development of non-ischemic heart failure. Panx1[MyHC6] mice were protected against isoproterenol-induced [94,95] cardiac hypertrophy, systolic dysfunction, and neutrophil infiltration into the myocardium. Furthermore, we find that PANX1 deletion facilitates glucose utilization and increases glycolytic gene expression as well as glycolytic rate. Finally, we demonstrate that PANX1 deletion decreases immune response genes in cardiomyocytes which is concurrent with a decrease in immune cell, specifically neutrophil, recruitment Taken together our findings implicate PANX1 channels as promising therapeutic targets in non-ischemic heart failure and cardiac hypertrophy.

Results

3.5 Isoproterenol Activates Pannexin 1 channels in Cardiomyocytes:

Previous studies have demonstrated that Pannexin 1 (PANX1) channels are activated in response to β3 and α_{1D}-adrenergic receptor stimuli[51,53]. A recent study demonstrates beta-adrenergic receptor 1-dependent activation of Panx1 channels in cardiomyocytes via cAMP/PKA-mediated phosphorylation on Serine 206[54]. To activate Panx1 channels we used isoproterenol, a pan β-adrenergic receptor agonist, in H9c2 rat myoblasts which endogenously express all β-adrenergic receptor family members and Panx1[96–98]. We tested Panx1 channel opening by measuring both ATP release into the culture media and dye (Yo-Pro-1) uptake into cells. After stimulation with 2 or 20µM isoproterenol, H9c2 cells released significantly more ATP into the extracellular media compared to vehicle stimulation (**Figure 3.1A**). Isoproterenol-induced ATP release was abolished by either siRNA mediated knock-down of Panx1 (successful knock-down is demonstrated by significantly decreased mRNA and protein levels (**Figure 3.7A,B**)), or pharmacological channel inhibition with spironolactone[64] (**Figure 3.1A,C**). Cell viability was not affected at either dose of isoproterenol (**Figure 3.7C**).

Additionally, using a flow-cytometry based approach, we found that stimulation with 20µM isoproterenol caused a significant increase in Yo-Pro-1 positive, Annexin V negative H9c2 cells compared with vehicle stimulation (**Figure 3.1B**, representative gating **Figure 3.7D**). Isoproterenol-induced Yo-Pro-1 uptake was significantly decreased after siRNA-mediated Panx1 knock-down (**Figure 3.1B, Figure 3.7D**), and blunted with PANX1 channel blockade by spironolactone, carbenoxolone, or probenecid (**Figure 3.1D**). Taken

together, these data demonstrate that PANX1 channel opening in cardiac myoblasts as a result of β-adrenergic receptor stimulation leads to the release of ATP.

3.6 Generation and characterization of a mouse with Pannexin 1 deletion specifically in cardiomyocytes

To investigate the role of PANX1 channels in cardiomyocytes *in vivo*, we generated a cardiomyocyte-specific PANX1 null mouse by crossing Panx1 floxed mice[47] with mice expressing Cre recombinase under the control of the alpha myosin heavy chain promoter (MyHC6). Confirmation of successful recombination was demonstrated by the presence of a null band on PCR analysis of genomic DNA isolated from the hearts of Panx1^{MyHC6} mice, which was not present in the hearts of Panx1$^{fl/fl}$ mice or other tested organs (liver, kidney) from either mouse genotype (**Figure 3.8A**). Levels of *Panx1* mRNA (by qPCR) and PANX1 protein (by immunofluorescence) were significantly decreased in isolated cardiomyocytes and cardiac troponin t (cTnnt) positive cells, respectively, from Panx1^{MyHC6} mice (**Figure 2A**, S2B) demonstrating the specificity of the Panx1 deletion in cardiomyocytes. Additionally, we see no concomitant changes in *Panx2*, *Panx3*, *Gja1* (Cx43), or *Gja5* (Cx40) mRNA (by qPCR) in isolated cardiomyocytes from Panx1^{MyHC6} mice compared with Panx1$^{fl/fl}$ mice (**Figure 3.8C**). Panx1^{MyHC6} mice had no obvious gross developmental defects when compared to their Panx1$^{fl/fl}$ littermates as examined by body mass, organ mass, or tibial length at 12 weeks of age (**Figure 3.8D-G**). Furthermore, assessment of cardiac function via 2D-echocardiography showed no significant differences in end-systolic or end-diastolic volume, wall thickness, or ejection fraction at baseline (**Figure 3.2B-E, Figure 3.8L**). Finally, blood pressure measurements by radiotelemetry in

12-week-old male mice demonstrated no differences in mean arterial pressure, systolic or diastolic pressure, or heart rate in Panx1^MyHC6 mice when compared to littermate Panx1^fl/fl mice (**Figure 3.8H-K**).

3.7 Pannexin 1 deletion shifts cardiomyocyte metabolism from oxidative phosphorylation to glycolysis.

To explore effects of PANX1 deficiency on the cardiomyocyte transcriptome *in vivo*, we performed bulk RNA-sequencing on cardiomyocytes isolated from hearts of Panx1^MyHC6 and Panx1^fl/fl mice, which identified 1281 and 727 uniquely expressed genes, respectively (**Figure 3.3A**). There were 1069 significantly differentially expressed genes between the genotypes, with 793 down-regulated and 276 up-regulated (**Figure 3.3B**). Gene ontology (GO) Term and KEGG pathway analysis revealed that Panx1 deletion mainly affected pathways involved in intercellular communication, cell adhesion and gap junction function, namely "cell-cell" and "Wnt signaling", "microtubule-based movement", "ECM-receptor interactions", "leukocyte trans endothelial migration", and "cell adhesion molecules", among others involved in inflammation and cytoskeletal organization (S3A, B). KEGG Pathway analysis was corroborated by significantly lower expression of transcripts of the claudin and cadherin family and their receptors (*Cdh1, Cldn7, Cdhr3, Cdhr4*), as well as increased expression of Transport and Golgi Organization protein 2 Homolog (*Tango2*) , which has been associated with altered mitochondrial energy metabolism in humans[99,100] (**Figure 3.3B**).

Pannexin channels have been demonstrated to control cellular metabolism, specifically the regulation of glucose homeostasis and glycolytic metabolism[101–104]. A

previous study by Adamson et al. demonstrated that Panx1 channel function is required for insulin-induced glucose metabolism in white adipocytes[105]. To assess whether loss of PANX1 impacted these pathways in cardiomyocytes, we analyzed the genes associated with key glycolytic enzymes in PANX1-deficient cardiomyocytes. Our data demonstrate increased expression of glycolytic pathway genes in cardiomyocytes isolated from Panx1[MyHC6] mice compared to their floxed controls. Of note, we found a significantly higher levels of the glucose transporter *Slc2a4* (Glut4), which is the predominant isoform in cardiomyocytes (**Figure 3.3C**). This finding was specific to Glut4 as we do not find any specific changes in Glut1 or Glut3, the other predominant isoforms in cardiomyocytes (S3I).

To determine if the observed transcriptional increase in genes involved in glycolysis impacts cellular metabolism and glucose utilization, we first performed glucose uptake assays to determine if the increase in *Slc2a4* transcripts impacted intracellular glucose content. Intracellular 2NBD-glucose levels were significantly increased after stimulation of H9c2 cells with isoproterenol, which was abrogated after siRNA-mediated knock down of PANX1 (**Figure 3.3F**).

Next, we performed a glycolytic stress test (GST) using a Seahorse extracellular flux analyzer on H9c2 cells that had been treated with either Panx1 siRNA or control siRNA to determine if increased glucose uptake affected cellular bioenergetics. PANX1 knock-down alone resulted in significantly increased basal and maximal extracellular acidification rate (ECAR). The magnitude of increase was even further increased by treatment with isoproterenol (**Figures 3.3D, E,** representative trace **Figure 3.9C**). Conversely, when we

performed a mitochondrial stress test (MST) we found that PANX1 knock-down alone was sufficient to significantly decrease maximal oxygen consumption rate (OCR) (**Figure 3.3H**, representative trace **Figure 3.9D**). Taken together this demonstrates that PANX1 knock-down drives H9c2 cells to a more glycolytic state, which mimics the shift seen after isoproterenol treatment in control cells. Moreover, we performed an ATP production assay to determine the contribution of mitochondrial and glycolytic ATP production to the total ATP production rate. We found that isoproterenol treatment of H9c2 rat myoblasts drives an increase in total ATP production, which is predominantly glycolytic. PANX1-knock-down similarly significant increases the total ATP production rate through a significantly higher glycolytic ATP production rate compared to control siRNA treated cells (**Figure 3.3I, Figure 3.9F-H**). Though cardiomyocyte metabolism and ATP production was significantly changed by PANX1 deletion *in vitro*, intracellular ATP content is not significantly different (**Figure 3.9E**). Taken together these data demonstrate a key role for PANX1 channels in regulating glucose uptake and glycolytic rate in H9c2 cardiomyocytes.

3.8 Panx1 deficiency in cardiomyocytes protects against isoproterenol-induced cardiac hypertrophy and cardiac dysfunction in non-ischemic heart failure

To examine the role of Panx1 channels in regulating cardiomyocyte function of the heart under stress, we induced cardiac hypertrophy preceding non-ischemic heart failure using an established protocol where we repeatedly administered isoproterenol via intraperitoneal injection for 14 days at a dose of 15mg/kg/day[94,106]. We established this timepoint as an early measure of disease progression, where cardiac hypertrophy is the predominant phenotype. We performed 2D-echocardiography prior to the beginning of

the study to collect baseline measurements and then again after 14 days at the model

endpoint (**Figure 3.4A**). As shown previously, before the start of the treatment Panx1$^{fl/fl}$

and Panx1^{MyHC6} mice displayed no overt differences in cardiac function (Figure 3.2B-E) or

weight (**Figure 3.10A**). Repeated isoproterenol administration resulted in significantly

increased heart weight in Panx1$^{fl/fl}$ mice, but not in Panx1^{MyHC6} mice (**Figure 3.4B, Figure

3.10B**). Cardiomyocyte hypertrophy (as measured by cardiomyocyte cross sectional area

by wheat germ agglutinin (WGA) staining) was significantly increased in hearts of in

Panx1$^{fl/fl}$ mice compared with Panx1^{MyHC6} mice after isoproterenol treatment (**Figure 3.4C**).

Furthermore, treatment with isoproterenol caused significant increases in both

end-systolic and end-diastolic volume of the left ventricle in Panx1$^{fl/fl}$ mice as measured

by echocardiography (**Figure 3.4D-F, Figure 3.10H**). Panx1^{MyHC6} mice did not have

significant increases in either metric compared to their baseline and had significant less

change compared to Panx1$^{fl/fl}$ age and sex-matched controls (**Figure 3.4D-F, Figure 3.10H**).

Finally, Panx1$^{fl/fl}$ mice had a trending decrease in ejection fraction after isoproterenol

treatment, while Panx1^{MyHC6} had no change (**Figure 3.10G**). We determined that this

disparity was likely caused by heart-intrinsic functional defects and not systemic vascular

or renal damage, as we observed no differences in blood pressure or serum creatinine

between Panx1$^{fl/fl}$ and Panx1^{MyHC6} mice after treatment with isoproterenol (**Figure 3.10C-

F**).

Additionally, to assess cardiac fibrosis found at later stages of non-ischemic heart

failure and to examine if Panx1 deficiency would also protect against fibrotic changes and

disease progression, we induced non-ischemic heart failure by administration of

isoprotererenol for 28 days (15/mg/kg/day) by subcutaneous implantation of osmotic pump (**Figure 3.11A**). Prolonged isoproterenol treatment caused a significantly greater increase in Collagen 1 (COL1A1) content in the myocardium of Panx1$^{fl/fl}$ mice compared to Panx1^{MyHC6} mice, as determined by immunofluorescence staining (**Figure 3.11B**). Moreover, functional analysis by echocardiography revealed that Panx1^{MyHC6} mice had a trending higher percent fractional shortening and a significantly decreased wall thickness compared with age and sex matched Panx1$^{fl/fl}$ controls (**Figure 3.11C,D**). These findings indicate a protective effect of cardiomyocyte-specific deletion of PANX1 in the later stages of non-ischemic heart failure.

These data demonstrate that cardiomyocyte-specific deletion of PANX1 is cardioprotective against cardiac hypertrophy and interstitial fibrosis during the progression of non-ischemic heart failure.

3.9 Pathways involved in the immune response and fatty-acid metabolism are down regulated in the hearts of Panx1^{MyHC6} mice during non-ischemic heart failure

To elucidate potential mechanisms that are involved in the protection from cardiac hypertrophy and dysfunction observed in Panx1^{MyHC6} mice, we performed bulk RNA-sequencing on whole hearts of Panx1$^{fl/fl}$ and Panx1^{MyHC6} mice after 14-day administration of isoproterenol. These whole heart tissues contained all cell types known to make-up the myocardial tissue including cardiomyocytes, endothelial cells, resident and non-resident immune cells, and fibroblasts predominantly[8]. We identified 1592 genes which were significantly differentially expressed between the two genotypes, with 594 genes

downregulated and 998 upregulated in Panx1^{MyHC6} mice compared to Panx1$^{fl/fl}$ controls (**Figure 3.5A**).

KEGG pathway and GO Term analysis on the differentially expressed genes identified regulatory pathway families including "hematopoietic cell lineage", "cell adhesion molecules", "B-cell receptor signaling pathway", and "Rheumatoid arthritis", all of which suggested significant changes in molecules associated with immune cell recruitment and infiltration. Moreover, we identified "fatty acid degradation", "fatty acid metabolism", and "cardiac muscle contraction", implicating a metabolic shift in the absence of PANX1 channels or at minimum a greater proportion of functional cardiomyocytes to the Panx1^{MyHC6} sample compared with Panx1$^{fl/fl}$. Furthermore, identified GO Terms indicated changes in plasma membrane proteins, specifically transporters and ion channels, as well as "oxidoreductase activity", "scavenger receptor activity", and "hydrolase activity", implicating the possible shift in the oxidative stress state.

Further analysis of genes associated with fatty acid beta-oxidation (as identified through WikiPathways) demonstrated overall decreased expression of this group of genes in hearts from Panx1^{MyHC6} mice with non-ischemic heart failure, while some genes such as *Lipc* (encoding the lipase C hepatic type), were expressed at higher levels (**Figure 3.5B**). Interestingly, a lowered reliance on fatty acid beta-oxidation during ischemic stress has been previously associated with increased cardiomyocyte viability[23].

Examination of genes involved in the inflammatory response identified lower expression of *Cd40*, *Il2ra*, and *Il2* in hearts of Panx1^{MyHC6} mice compared to their Panx1$^{fl/fl}$

counterparts (**Figure 3.5C**), suggesting a lower immune cell load in the hearts as CD40 and IL-2 expression are associated with a wide range of leukocyte populations[107]. Additionally, we observed lower expression of *Lamb1* (encoding Laminin subunit beta 1) and *Lama5* (encoding laminin subunit alpha 5) as well as *Vtn* (encoding Vitronectin) suggestive of decreased cell-cell adhesion and fibrosis (**Figure 3.5C**).

Since PANX1 channel function has been associated with activation of a variety of purinergic receptors[54,66,67,108], we examined the expression of purinergic signaling receptors and other associated molecular regulators in our RNA-Seq dataset (WikiPathway "Purinergic signaling"). We found lower expression of *P2yr1*, *P2rx1*, *P2ry14,* and *Adora2a* in hearts of Panx1[MyHC6] mice (**Figure 3.5D**) compared to Panx1^{fl/fl} controls. This finding is particularly interesting as *P2rx1, P2yr14*, and *Adora2a* have all been previously associated with chemotaxis and activation of immune cells, particularly neutrophils[90,109].

Together these data identify that PANX1 deficiency in cardiomyocytes causes significant transcriptomic changes in genes associated with inflammation, immune cell recruitment, metabolism and oxidative phosphorylation, all of which may contribute to the protection of Panx1[MyHC6] mice from cardiac hypertrophy and progressive heart failure in a model of isoproterenol induced non-ischemic heart failure.

3.10 Neutrophil infiltration is significantly blunted in Panx1[MyHC6] mice during heart failure induced by isoproterenol

To determine the contribution of cardiomyocytes to the findings of the whole heart, most notably to the inflammatory state in isoproterenol-injured hearts, we performed bulk RNA-Seq on the isolated cardiomyocytes from Panx1^{fl/fl} and Panx1[MyHC6]

mice after 14-days of isoproterenol administration. We identified 1439 differentially expressed genes with the majority being downregulated in Panx1-deficient cardiomyocytes (1037 down, 402 up) (**Figure 3.12A**). Further analysis of genes associated with "inflammation response" (WikiPathways) revealed decreased expression of many of the genes identified as being regulatory in inflammation including Zap70, Lack, Fn1, Col1a2, and multiple cytokine receptors (**Figure 3.6A**). This was corroborated by the finding of the GO Terms "immune response" and "immune system process", which were significantly enriched with genes downregulated in the isolated cardiomyocyte fraction of Panx1^{MyHC6} mice compared to Panx1$^{fl/fl}$ mice (**Figure 3.6A**).

To determine whether the observed inflammatory gene regulation patterns was reflective of perturbed leukocyte recruitment to the hearts of Panx1^{MyHC6} mice, we isolated the non-myocyte fractions from the hearts of Panx1$^{fl/fl}$ and Panx1^{MyHC6} mice after 14-day treatment with isoproterenol and examined leukocyte populations by flow cytometry (representative gating **Figure 3.12B**). The number of total leukocytes (CD45$^+$) as well as neutrophils (Ly6g$^+$, CD11b$^+$) were significantly lower in the hearts of Panx1^{MyHC6} mice (**Figure 3.6B, C, Figure 3.12B**). These findings were confirmed by immunofluorescence imaging of the left ventricle of hearts from Panx1$^{fl/fl}$ and Panx1^{MyHC6} mice. In accordance with the flow cytometry data, the number of Ly6g$^+$ puncta per field in the hearts of Panx1^{MyHC6} mice was significantly lower compared to hearts from Panx1$^{fl/fl}$ mice (**Figure 3.6D, Figure 3.12C**).

Of note, there was no significant difference in the total number of macrophages (F4/80$^+$, CD11b$^+$) present in Panx1^{MyHC6} mouse hearts during non-ischemic heart failure

(**Figure 3.6E, Figure 3.12D**). Further analysis of macrophage subsets showed no differences in macrophages with the co-stimulatory macrophage activation marker CD86 (F4/80^{+}, CD11b^{+}, CD86^{+}), which was confirmed with qPCR on isolated immune cells from a separate cohort of mice, or macrophages with the anti-inflammatory marker CD163 (F4/80^{+}, CD11b^{+}, CD163^{+}/CD86^{-}) (**Figure 3.6E, Figure 3.12D, E**). Finally, we observed no differences in dendritic cells (CD11b^{+}, CD24^{+}) (**Figure 3.6E, Figure 3.12D**).

While we did not observe any changes in cell populations, we did find significant decreased in *Il1b and Cxcl2*, M1 macrophage activation markers, expression in isolated immune cells from the myocardium of Panx1^{MyHC6} after 14-day isoproterenol treatment relative to immune cells isolated from Panx1$^{fl/fl}$ mice (**Figure 3.12E**). Furthermore, we did not find detectable levels of *Chil3*, an M2 macrophage activation marker, in in isolated immune cells from the myocardium Panx1$^{fl/fl,}$ which we were able to observe in isolated immune cells from Panx1^{MyHC6} mice (**Figure 3.12E**). Taken together these data, demonstrate that while cell populations of macrophages have not changed the inflammatory and activation state of these populations has significantly shifted.

These data demonstrate a critical role for PANX1 expressed in cardiomyocytes in recruiting immune cells, specifically neutrophils, to the myocardium in response to chronic beta-adrenergic stimulation. This finding is in line with previous work which demonstrates that PANX1-dependent ATP release recruits neutrophils to the endothelium during acute inflammatory disease[65].

Discussion

The role of ATP, adenosine, and other purinergic signaling molecules as both autocrine and paracrine signals in the myocardium has long been understood and exploited clinically, using compounds such as clopidogrel and adenosine[110]. However, the underlying mechanisms for release of purinergic compounds in non-ischemic heart failure still need to be investigated[111,112].

To examine the role of PANX1 in cardiomyocytes, we generated a novel mouse with cardiomyocyte-specific deletion of PANX1 (Panx1^{MyHC6}). We found that Panx1^{MyHC6} mice shift the baseline metabolic state of their cardiomyocytes toward a more glycolytic phenotype, concurrent with increased glucose uptake, GLUT4 transporter expression, and glycolytic ATP production. After isoproterenol-induced non-ischemic heart failure, PANX1^{MyHC6} mice are protected from pathological cardiac hypertrophy and dysfunction. We also find that in Panx1^{MyHC6} mouse hearts during isoproterenol-induced cardiac hypertrophy there is a decrease in gene expression of fatty-acid beta oxidation- associated genes. Finally, PANX1 deficiency in cardiomyocytes blunts neutrophil recruitment to the myocardium during isoproterenol-induced non-ischemic heart failure.

Two previous studies by Adamson *et al.* and Senthivinayagam *et al.* found that deletion of PANX1 in either white or brown adipose tissue exacerbated diet-induced obesity, specifically by increasing susceptibility to insulin resistance, establishing that PANX1 plays a critical role in glucose homeostasis in the adipose tissue[53,105]. Since cardiomyocytes are among the most energy-demanding cell types requiring high levels of

ATP needed for contraction, we examined the role for PANX1 in control of cardiomyocyte metabolism. We demonstrate that PANX1 deletion induces a metabolic shift in the cardiomyocyte by priming the cardiomyocyte toward a glycolytic state at baseline. Consequently, PANX1-deficient cardiomyocytes are less responsive to stress induced by beta-adrenergic receptor activation. We found a significant increase in *Slc2a4* expression in isolated primary murine cardiomyocytes of Panx1[MyHC6] mice, which is matched by increased glucose uptake, glycolytic rate, and glycolytic ATP production in PANX1 knock-down H9c2 myoblasts *in vitro*[22]. This glycolytic phenotype has previously been observed in fetal cardiomyocytes and is associated with increased proliferative capacity[6,22]. Furthermore, increased glucose availability and glycolytic rate in unstressed situations leads to better outcomes and is associated with increased regenerative capacity after ischemic/ reperfusion injury[23,113].

RNA-Sequencing of isolated cardiomyocytes from Panx1[MyHC6] and Panx1[flfl] mice with non-ischemic heart failure revealed significantly decreased expression of genes associated with immune system function. Previous work established that PANX1 deletion in endothelial cells decreases the immune cell recruitment to the myocardium after a myocardial infarction, without further specifying a particular immune cell population[68]. We find that deletion of PANX1 in cardiomyocytes decreases overall immune cell recruitment, which was driven specifically by a significant decrease of neutrophils. Immune cell recruitment to the myocardium has been shown to exacerbate cardiomyocyte damage and impairment of myocardial function[78,114]. Therefore, the decrease in immune cells in the myocardium of mice with PANX1-deficient

cardiomyocytes suggests that PANX1 may serve to propagate or initiate the sterile immune response in the myocardium during times of chronic cardiac stress[9]. The changes in gene expression reveal an overall decreased chronic inflammatory state of the myocardium in Panx1[MyHC6] mice after isoproterenol induced heart failure.

While our observations of neutrophil recruitment by PANX1 are in the context of isoproterenol-induced non-ischemic heart failure, PANX1 activation in cardiomyocytes may also be important in ischemic heart failure or after ischemia-reperfusion injury. Future investigations will elucidate if the effects on neutrophil infiltration attributed to cardiomyocyte-specific deletion of PANX1 vary by injury type, which will provide opportunities to develop therapies that are specific to the type of cardiac injury.

ATP is known to serve as recruitment or "find me" signal for immune cells during inflammation[115,116] and apoptosis[63,117]. While we do not identify the responsible receptors on neutrophils, our RNA sequencing data demonstrate that expression of key purinergic receptors, namely P2X1, P2Y1, and P2Y14, is decreased in the whole heart tissue of Panx1[MyHC6] mice during isoproterenol-induced heart failure. Of these P2Y1 and P2Y14 can be associated with decreased neutrophil recruitment[86]. Moreover, we cannot rule out other purinergic molecules that could be released through PANX1 potentially driving the neutrophil recruitment. P2Y1 binds ADP which could be generated from local exonucleases acting on the ATP released via PANX1 or could be released from PANX1 itself. Furthermore, we see a decreases in ADORA2A which could be attributed to decrease in neutrophil presence as adenosine released from neutrophils serves to orient neutrophil migration[86]. Additionally, P2Y14 on neutrophils binds UDP-glucose[83], which can also be

released through PANX1[63,86]. Therefore, a combination of signaling molecules released by PANX1, including ATP and UDP-glucose, may be necessary for the infiltration of neutrophils into the myocardium during non-ischemic heart failure.

Historically, treatment of heart failure in patients has focused on therapies which treat the symptoms of the disease, such as edema and dyspnea, rather than directly targeting cardiac function or preventing functional decline of the cardiac muscle. These current clinical therapeutic avenues are limited in impacting the immune cell infiltrate or fibrosis, which are key mechanisms leading to disease progression. Previously clinical trials have identified that spironolactone, a mineralocorticoid receptor antagonist (MRA) and PANX1 blocker, can improve patient outcomes in both all-cause mortality and sudden cardiac death in patients with established disease over a placebo[64,71,73]. However, the understanding for why this therapy is more beneficial than others in lowering blood pressure is not yet well understood. Our findings demonstrate that deletion of PANX1 in cardiomyocytes improves cardiac function and decreases cardiac hypertrophy as measured by echocardiography. We find that Panx1$^{fl/fl}$ mice have significant increases in left ventricular end-diastolic and end-systolic volume in isoproterenol induced heart failure. Conversely, Panx1^{MyHC6} do not have any significant increase, and the percent change from baseline in left ventricular volume at both these points is significantly less than their Panx1$^{fl/fl}$ counterparts. With this in mind, we speculate that one secondary mechanism of action for spironolactone in heart failure may be PANX1 channel blockade. PANX1 channel blockade globally may improve patient outcomes by preventing immune cell recruitment, as has been shown in multiple mouse

models[67,117,118]. Furthermore, modulating cardiomyocyte metabolism to increase glucose uptake may prevent an energy imbalance which is thought to be a driving factor in cardiac muscle function decline. Additionally, the decreased immune cell recruitment may explain why patients with lower natriuretic peptide levels see greater benefit from spironolactone therapy compared to their more diseased counterparts[72]. PANX1 blockade is effective in preventing immune cell infiltration, but has not been shown to reverse previously sustained damage which is more severe in patients with a higher disease burden[78].

Taken together our study illustrates how PANX1 deletion in cardiomyocytes protects against the progression of non-ischemic heart failure. We demonstrate that PANX1 channel opening can be induced by beta-adrenergic receptor stimulation in cardiomyocytes. Cardiomyocyte-specific deletion in mice (Panx1^{MyHC6}) impacts their cardiac glycolytic metabolism, which we attribute to a higher expression of *Slc2a4* and increased glucose uptake. Panx1^{MyHC6} mice are protected from isoproterenol-induced non-ischemic heart failure and cardiac hypertrophy, which we demonstrate to be at least in part due to a decrease in neutrophil recruitment. Our findings identify PANX1 in cardiomyocytes as a therapeutic target to prevent severe cardiac tissue damage in non-ischemic heart failure, which may also be relevant for developing therapies targeted at PANX1 for other forms of heart failure such as HFpEF.

Limitations

Our study is limited by the ability to discern the metabolite or metabolites released through PANX1 activation *in vivo* which results in neutrophil infiltration. Further, we

understand that our model is limited in that it does not examine the role for PANX1 in ischemic injury or the context of ischemia reperfusion injury which can both cause heart failure. We utilize a novel mouse which has constitutive deletion PANX1, therefore we are unable to determine the role for PANX1 in initiation versus the progression of disease. Finally, we use a non-contractile cell line for our *in vitro* studies which does not fully recapitulate the *in vivo* physiology of the myocardium.
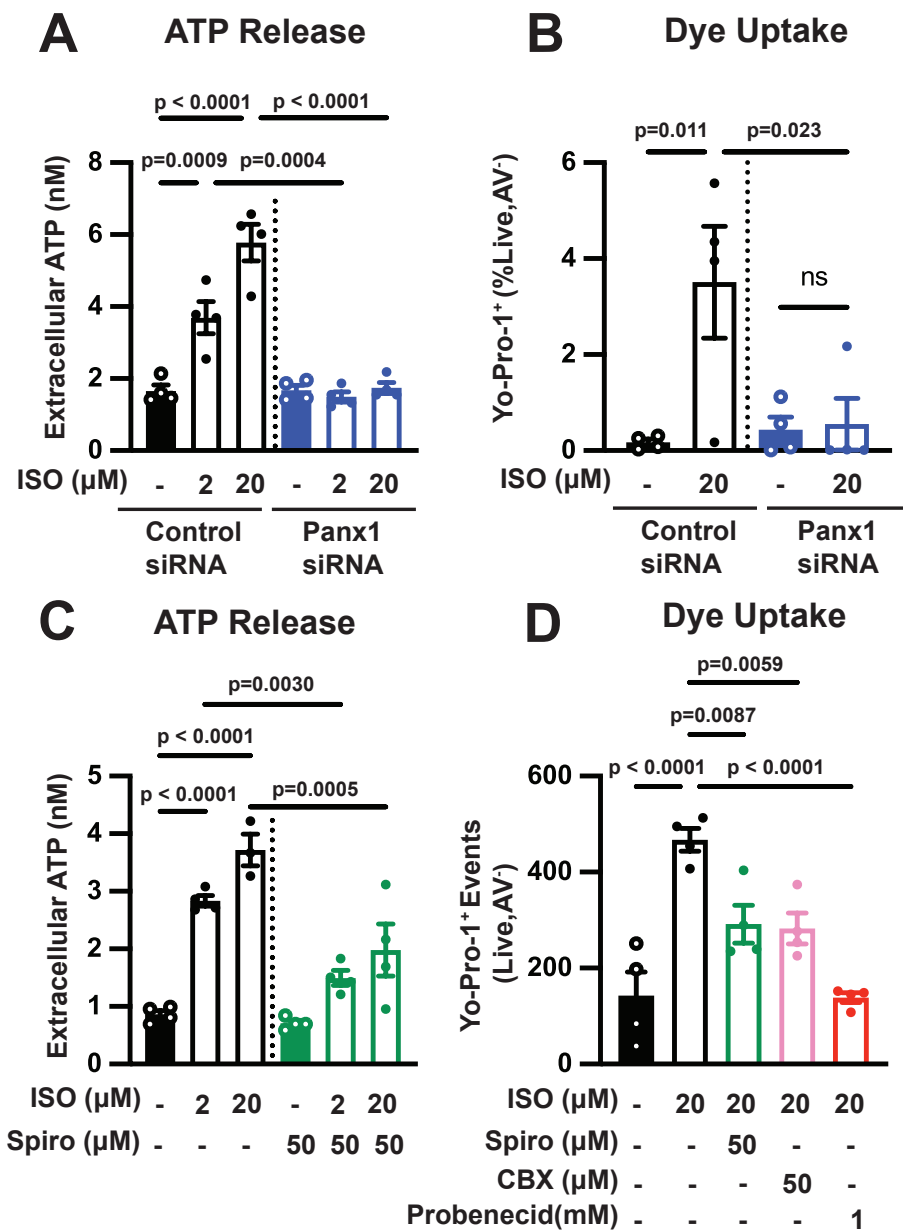
Figure 3.1: Beta-adrenergic receptor stimulation activates Pannexin 1 channels in cardiomyocytes *in vitro*

A) H9c2 were transfected with either control or Panx1-targeting siRNA for 72 hours and extracellular concentration of ATP was measured after 15 minutes of stimulation with isoproterenol (ISO) (2 and 20µM) or vehicle control. (N=4)

B) Flow cytometric analysis of Yo-Pro-1 dye uptake by control of Panx1-targeting siRNA treated H9c2 cells after stimulation with 20µM ISO (gated for live, annexin V⁻ cells). (N=4)

C) H9c2 cells were pretreated with spironolactone (50µM), or vehicle control and extracellular ATP levels were measured after 15 minutes of stimulation with isoproterenol (ISO) (2 and 20µM). (N=4)

D) Yo-Pro-1 dye uptake by H9c2 cells treated with isoproterenol (20µM) after pretreatment with spironolactone, carbenoxolone (CBX), or probenecid at the listed concentrations. (N=4)

Data are represented as mean ± standard error of the mean (SEM). Data shown are representatives of 2 independent experiments. Significance determined using One-way ANOVA (A, B, C, D) with Sidak's multiple comparison test for post-hoc analysis for comparisons between individual groups. ns = not significant See also S1 in reference to figure 1.
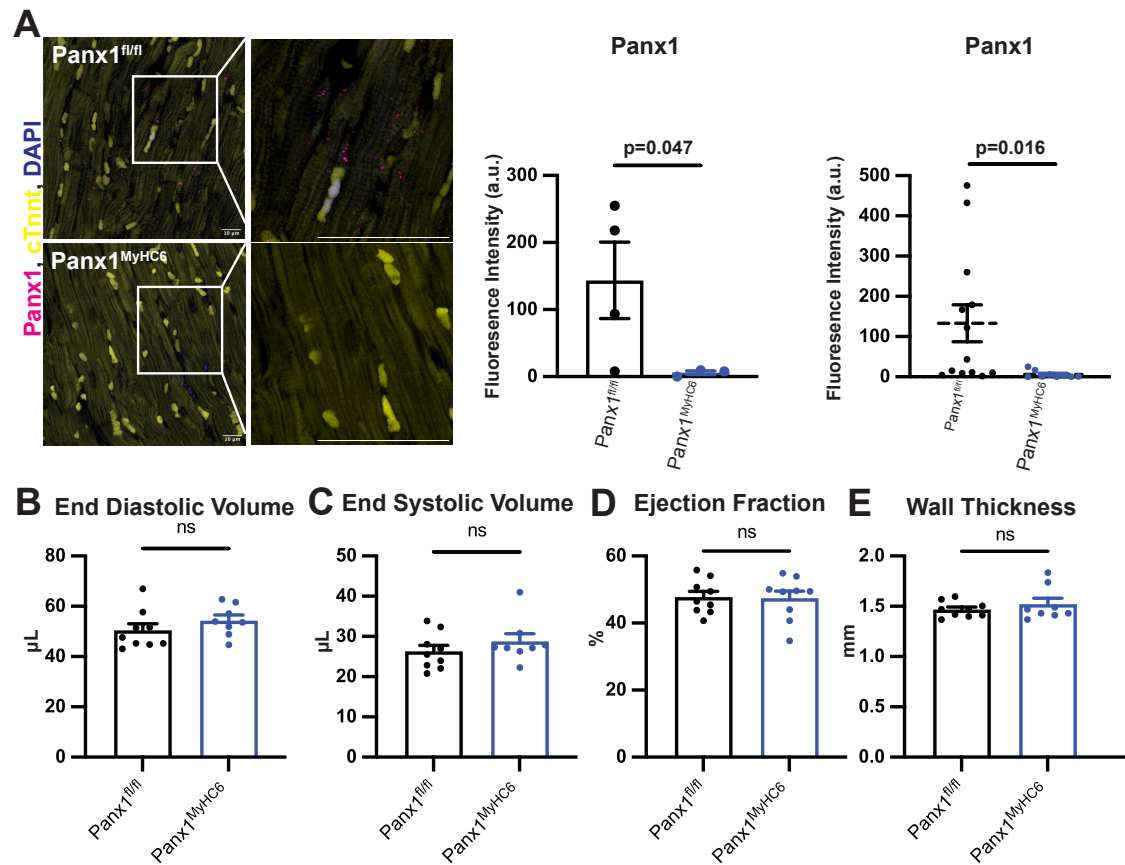
Figure 3.2: Generation and Characterization of a novel Pannexin 1 cardiomyocyte specific deletion mouse

A) Confocal micrographs of cardiomyocyte-rich whole heart sections from 12-week-old male Panx1$^{fl/fl}$ and Panx1^{MyHC6} mice. Knockout of PANX1 in cardiomyocytes was assessed using immunofluorescent staining. Cardiac troponin T (cTnnt) was used to stain cardiomyocytes; DAPI was used as a nuclear stain. Left, representative micrographs with insets showing PANX1 punctate; middle, average Panx1 fluorescence intensity for individual mice; right, fluorescence intensities for individual micrographs showing demonstrating of PANX1 signal. (Panx1$^{fl/fl}$ N=4 mice N=13 images, Panx1^{MyHC6} N=3 mice N=9 images, 3-5 images per mouse averaged).

B) End-diastolic volume C) End-systolic volume D) Ejection fraction and E) Wall thickness were measured in anesthetized 8- to 10-week-old male Panx1$^{fl/fl}$ and Panx1^{MyHC6} mice using *in vivo* 2D-echocardiography. (Panx1$^{fl/fl}$ N= 9 mice, Panx1^{MyHC6} N=8)

Data represented as mean $\pm$ SEM. Significance was determined by Welch's t-test (A-E).

ns = not significant. See also S2 in reference to figure 2.

A Uniquely Expressed Genes

B Cardiomyocyte at Baseline

C Glycolysis

D Glucose Uptake

E

F Basal ECAR

G Max ECAR

H Max OCR

I ATP Production
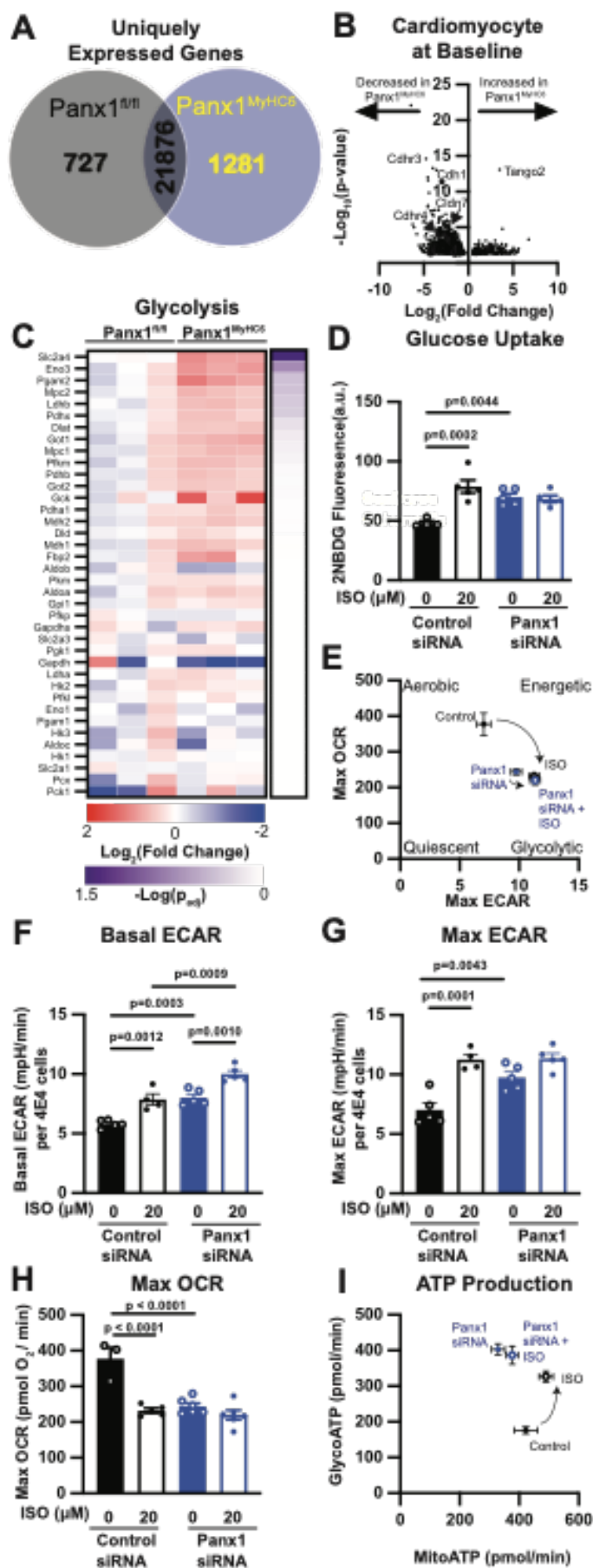
Figure 3.3: Figure 3: Pannexin 1 deletion shifts cardiomyocyte metabolism from oxidative phosphorylation to glycolysis both *in vivo* and *in vitro*

A) Quantification of uniquely expressed genes from bulk RNA-Sequencing of isolated cardiomyocytes from untreated 12-week-old male Panx1$^{fl/fl}$ and Panx1^{MyHC6} mice.

B) Volcano plot of differentially expressed genes with a cut off of $p < 0.05$. Individual genes are indicated with gene name and arrow.

C) Heatmap showing relative gene expression of glycolysis associated genes from isolated cardiomyocytes of untreated Panx1$^{fl/fl}$ and Panx1^{MyHC6} mice plotted as the Log$_2$ (fold change) from Panx1$^{fl/fl}$ mouse. Purple heatmap represents -log(p-value) of two-tailed t-tests comparing fold change of Panx1$^{fl/fl}$ and Panx1^{MyHC6}. (Panx1$^{fl/fl}$ N=3 mice, Panx1^{MyHC6} N=3 mice)

D) Glucose uptake as measured by 2NBD-glucose fluorescence intensity of control or Panx1-targeted siRNA treated after 1 hour ISO (20µM) stimulation. (N=4)

E) Phenogram of bioenergetic profile of control siRNA treated H9c2 cells reveals a shift to more glycolytic phenotype after ISO treatment. siRNA mediated PANX1 knock-down demonstrates a more glycolytic phenotype without ISO stimulation which is only minimally shifted after ISO treatment.

F) Quantification of Basal extracellular acidification rate (ECAR) and

G) Maximal ECAR of control of Panx1-targeted siRNA treated H9c2 cells after stimulation with either vehicle or ISO (20µM) for 1 hour. (N=5)

H) Maximal OCR of control of Panx1-targeted siRNA treated H9c2 cells after stimulation with either vehicle or ISO (20µM) for 1 hour. (N=5)

I) Phenogram of ATP production of control siRNA treated H9c2 cells reveals a shift to more glycolytic phenotype after ISO treatment. siRNA mediated PANX1 knock-down demonstrates a more glycolytic phenotype without ISO stimulation which is not shifted after ISO treatment.

Data represented as mean $\pm$ SEM. Significance determined using One-way ANOVA (D, F-H) with Sidak's multiple comparison test for post-hoc analysis for comparisons between individual groups.   ns = not significant. See also S3 in reference to figure 3.
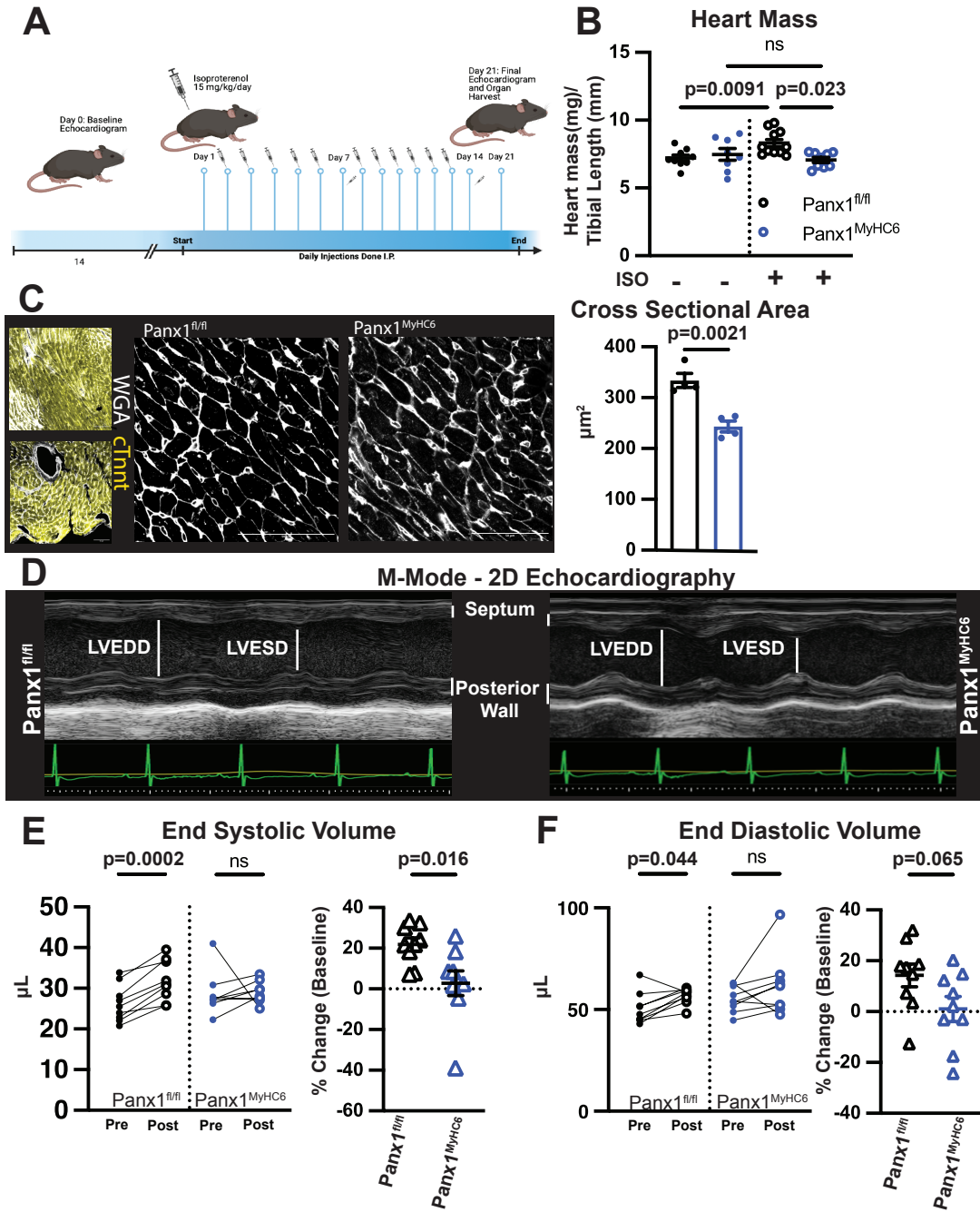
Figure 3.4: Isoproterenol induced cardiac hypertrophy and dysfunction is abrogated in Panx1^{MyHC6} mice

A) Schematic of experimental model of isoproterenol induced non-ischemic heart failure.

B) Normalized heart mass from 10–12-week-old Panx1$^{fl/fl}$ or Panx1^{MyHC6} mice treated for 14 days with isoproterenol (15 mg/kg/day), or saline control normalized to tibial length. (Saline: Panx1$^{fl/fl}$ N=9, Panx1^{MyHC6} N= 8; Isoproterenol Panx1$^{fl/fl}$ N=11, Panx1^{MyHC6} N= 9)

C) Representative confocal micrographs of wheat germ agglutinin (WGA) staining at 20X (Left) and 60X (Right) from Panx1$^{fl/fl}$ or Panx1^{MyHC6} mice treated with isoproterenol for 14 days. Cardiomyocyte cross sectional area was calculated from WGA. (Panx1$^{fl/fl}$ N=4 mice, Panx1^{MyHC6} N=4, data points represent average of 50 cells per mouse).

D) Representative M-mode images of Panx1$^{fl/fl}$ mice or Panx1^{MyHC6} after 14 days of isoproterenol treatment, visualized by 2D echocardiography.

E) Left, paired analysis of left ventricle end-systolic volume (μL) pre- and post-isoproterenol treatment; right, percent change from baseline after isoproterenol treatment. (Panx1$^{fl/fl}$ N=8, Panx1^{MyHC6} N=9)

F) Left, paired analysis of left ventricle end-diastolic volume (μL) pre- and post-isoproterenol treatment; right, percent change from baseline after isoproterenol treatment. (Panx1$^{fl/fl}$ N=8, Panx1^{MyHC6} N=9)

Data represented as mean $\pm$ SEM. Significance determined using One-way ANOVA (B with Sidak's multiple comparison test for post-hoc analysis for comparisons between individual groups; Student's t-test (C) and Welch's t-test

(E, F) was used for comparison between two groups. Significance of paired data

was determined using Mixed effects analysis (E, F) with Sidak's multiple

comparison test for post-hoc analysis for comparisons between timepoints.   ns =

not significant. See also S4, S5 in reference to figure 4.
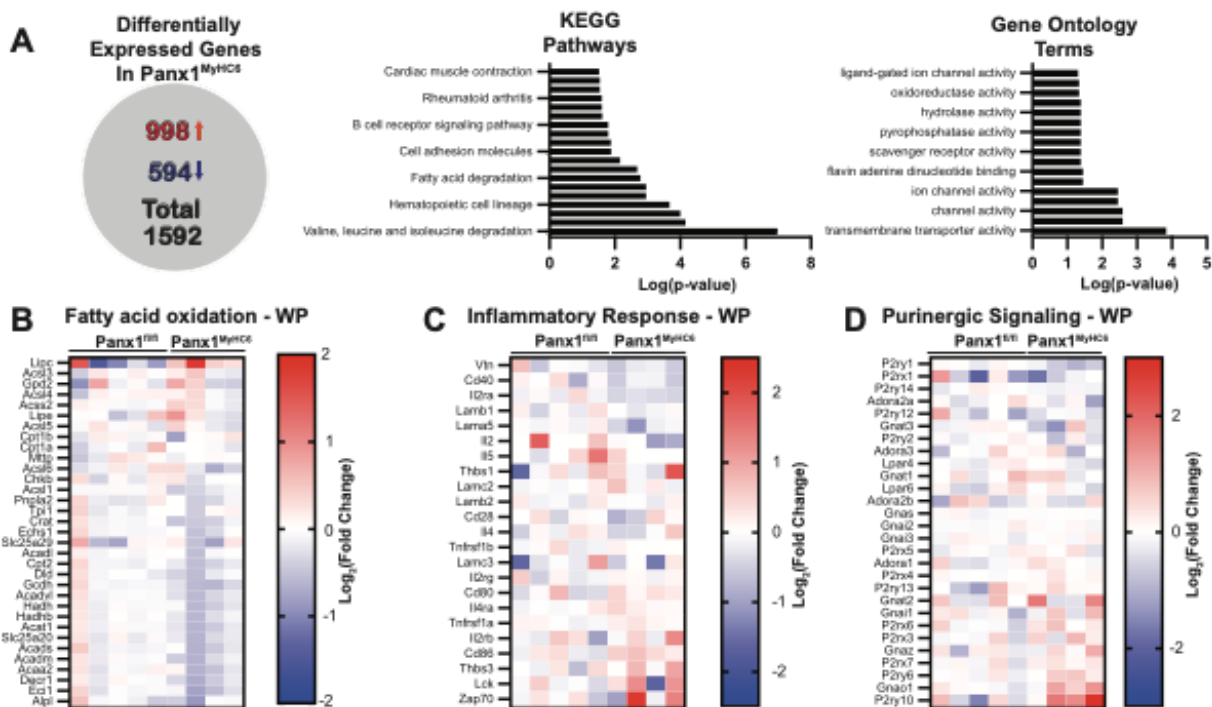
Figure 3.5: Cardiomyocyte PANX1 knockout leads to transcriptional downregulation of fatty acid metabolism and immune activation pathways during non-ischemic heart failure

A) Quantification of differentially expressed genes identified in bulk RNA-Sequencing between whole hearts of Panx1$^{fl/fl}$ and Panx1^{MyHC6} mice after 14 days of isoproterenol treatment. Differentially expressed gene determined by cut off of $p < 0.05$. Significantly changed, as determined by cut off of $p < 0.05$, KEGG Pathways and Gene Ontology (GO) Terms identified from differentially expressed genes plotted as ordered by -log(p-value).

B) Heatmap demonstrating genes identified in WikiPathways "Inflammatory response".

C) Heatmap demonstrating genes identified in WikiPathways "Fatty acid oxidation and Fatty acid beta-oxidation".

D) Heatmap demonstrating genes identified in WikiPathways "Purinergic signaling". Gradient plotted as Log$_2$(Fold Change) of Panx1^{MyHC6} compared to Panx1$^{fl/fl}$. (Panx1$^{fl/fl}$ N=5, Panx1^{MyHC6} N=4)
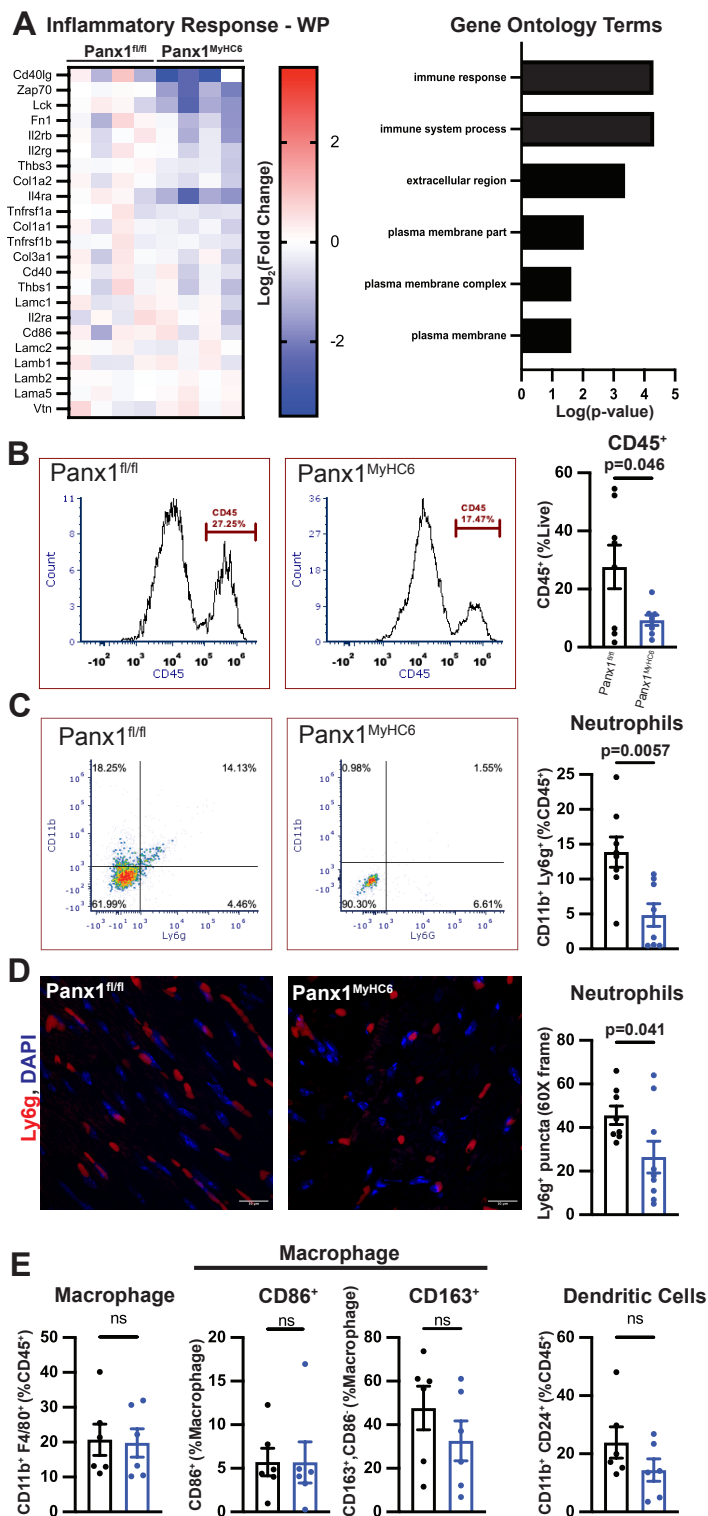
Figure 3.6: Neutrophil infiltration is significantly blunted in Panx1^MyHC6 mice during

heart failure induced by isoproterenol

A) Heatmap demonstrating genes identified in WikiPathway "Inflammatory response". Gradient plotted as Log_2(Fold Change) of Panx1^{MyHC6} isolated cardiomyocytes after 14-days of isoproterenol treatment compared to Panx1$^{fl/fl}$. Significantly decreased, as determined by cut off of $p < 0.05$, GO terms in Panx1^{MyHC6} cardiomyocytes compared with Panx1$^{fl/fl}$ cardiomyocytes. (Panx1$^{fl/fl}$ N=4, Panx1^{MyHC6} N=4 mice).

B) Flow cytometric analysis of CD45$^+$ cells as a percentage of total live cells isolated from Panx1$^{fl/fl}$ and Panx1^{MyHC6} hearts after 14-days of isoproterenol treatment as identified. Representative histograms of the CD45 populations from live parent gate. (Panx1$^{fl/fl}$ N=8, Panx1^{MyHC6} N=8 mice)

C) Flow cytometric analysis of neutrophils (CD11b$^+$, Ly6g$^+$) as a percentage of the CD45$^+$ cells in Panx1$^{fl/fl}$ and Panx1^{MyHC6} hearts after 14-days of isoproterenol treatment. Representative plots of the identified neutrophils from Panx1$^{fl/fl}$ and Panx1^{MyHC6} mice hearts. (Panx1$^{fl/fl}$ N=8, Panx1^{MyHC6} N=8 mice)

D) Representative confocal micrographs of Ly6g staining at 60X from Panx1$^{fl/fl}$ and Panx1^{MyHC6} mice treated with isoproterenol for 14 days. Ly6g was used to stain neutrophils; DAPI was used as a nuclear stain. Quantification of number of neutrophils, Ly6g$^+$ puncta, per 60X field in whole heart tissue from Panx1$^{fl/fl}$ and Panx1^{MyHC6} mice after 14-days of isoproterenol treatment. (Panx1$^{fl/fl}$ N=8, Panx1^{MyHC6} N=9 mice, 3-5 images per mouse averaged)

E) Flow cytometric analysis of macrophages (CD11b$^+$, F4/80$^+$) as a percentage of CD45$^+$ cells from Panx1$^{fl/fl}$ and Panx1^{MyHC6} hearts after 14-days of isoproterenol

treatment. Macrophages expressing the co-stimulatory activation marker

(CD86$^+$) and macrophages expressing the anti-inflammatory marker (CD163$^+$,

CD86$^-$) as a percentage of the macrophages (CD11b$^+$, F4/80$^+$). Flow cytometric

analysis of dendritic cells (DC) (CD11b$^+$, CD24$^+$) as a percentage of CD45$^+$ cells

from Panx1$^{fl/fl}$ and Panx1^{MyHC6} hearts after 14-days of isoproterenol treatment.

(Panx1$^{fl/fl}$ N=6, Panx1^{MyHC6} N=6 mice)

Data represented as mean $\pm$ SEM. Significance determined using Welch's t-test

(B, C, D, E) was used for comparison between two groups. ns = not significant.

See also S6 in reference to figure 6.

A   Panx1 Protein

B   Panx1 mRNA

C   Cell Death

Gating Scheme

Singlets	Live	Annexin V Negative	Yo-Pro-1 Postive

D
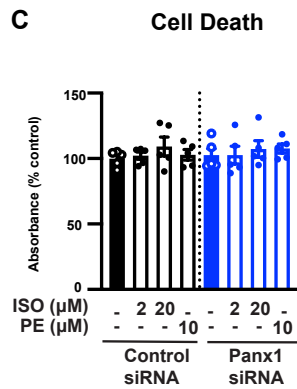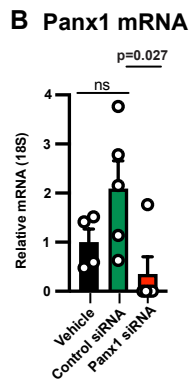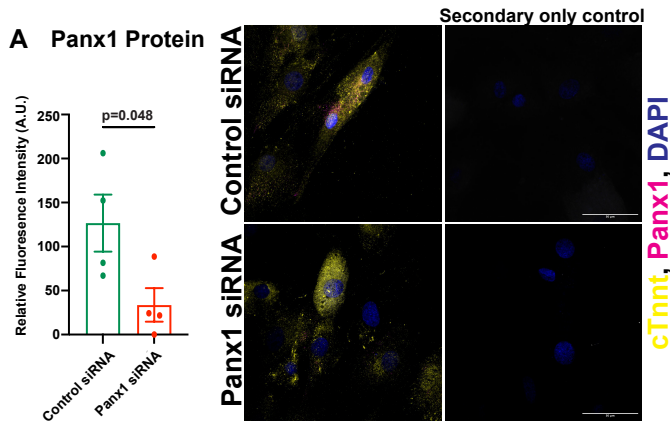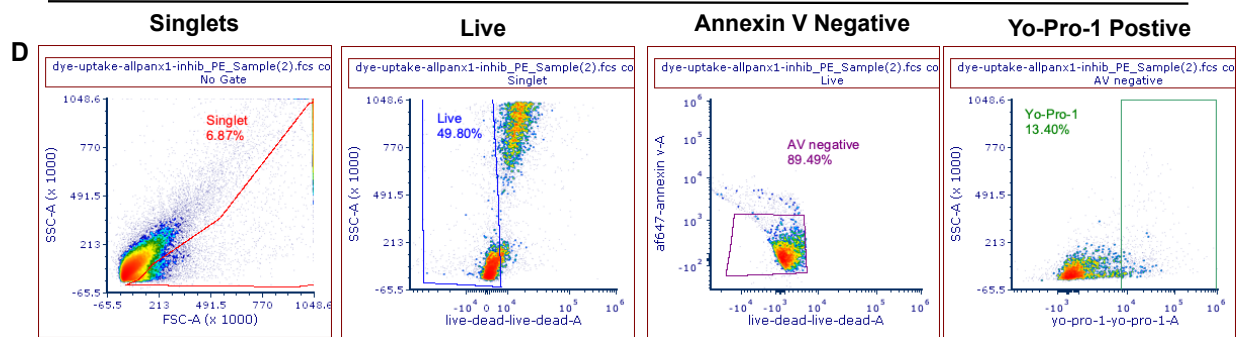
Figure 3.7:

A) Left, quantification from confocal micrographs of Panx1 in control siRNA and

    Panx1-targeted siRNA in H9c2 cells after 72 hours of treatment for mean

    fluorescence intensity. Cardiac troponin T (cTnnt) was used to stain

    cardiomyocytes; DAPI was used as a nuclear stain. Right, secondary only controls

    included for cTnnt and Panx1 staining. (N=4)

B) Relative mRNA expression of *Panx1* (18S) in vehicle, control siRNA, and Panx1-

    targeted siRNA treated H9c2 cells after 48 hours of treatment (Vehicle N=4,

    Control siRNA N=5, Panx1 siRNA N=5).

C) H9c2 rat myoblasts were transfected with control or Panx1-targeted siRNA for 72

    hours. LDH was measured after stimulation with ISO (2 or 20 µM), phenylephrine

    (10 µM), or vehicle control as a proxy for cell death. All data was normalized to

    the absorbance of the vehicle control. (N=5)

D) Gating scheme for the identification of Yo-Pro-1 positive H9c2 rat myoblasts.

    Data represented as mean $\pm$ SEM. Significance determined using Student's t-test

    (A) or One-way ANOVA (B) with Sidak's multiple comparison test for post-hoc

    analysis for comparisons between individual groups. * $p < 0.05$, ns = not

    significant
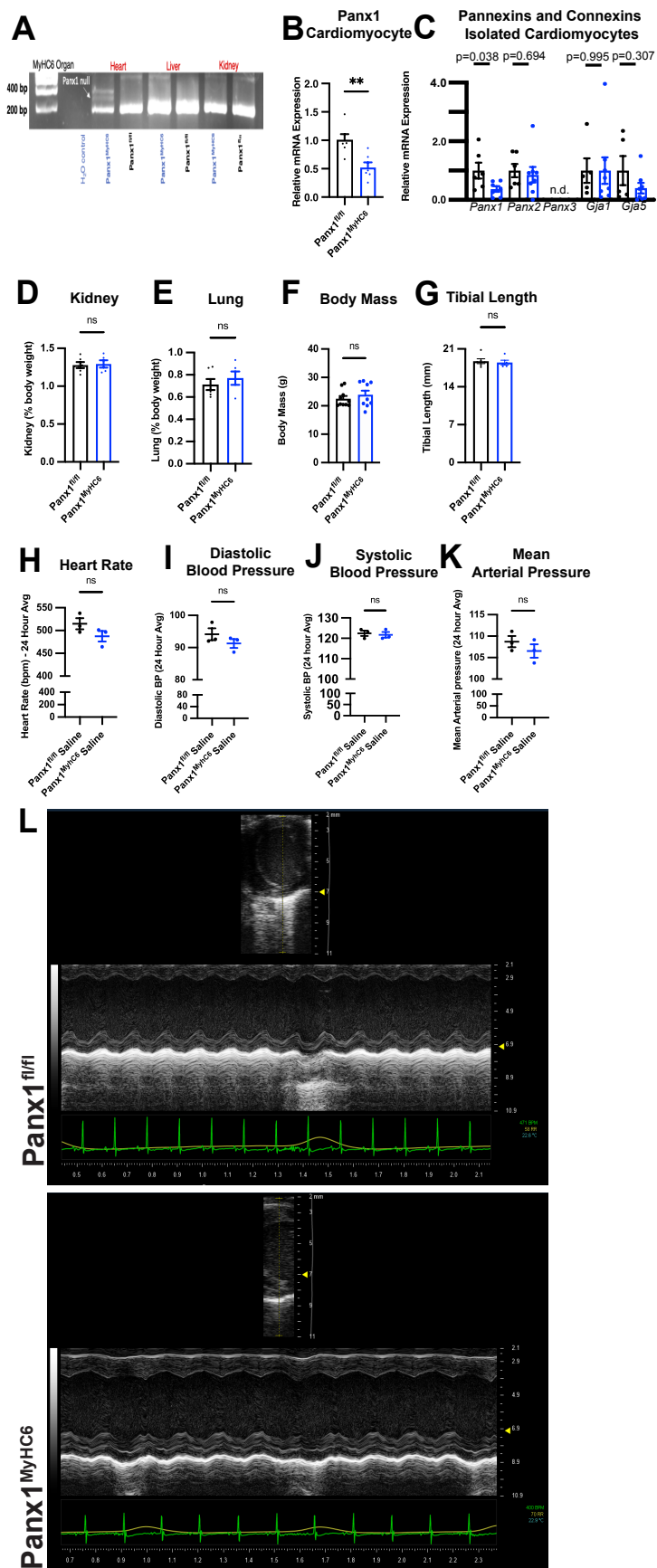
Figure 3.8:

A) Genomic DNA from PCR for Panx1 in heart of Panx1$^{fl/fl}$ and Panx1^{MyHC6} mouse with null band present in Panx1^{MyHC6} heart. Panx1 null band absent from genomic DNA from PCR for Panx1 in heart of Panx1$^{fl/fl}$ and from liver or kidney of Panx1$^{fl/fl}$ and Panx1^{MyHC6} mice.

B) Relative mRNA expression of *Panx1* (Hprt) in isolated cardiomyocytes from untreated Panx1$^{fl/fl}$ and Panx1^{MyHC6} mice. (Panx1$^{fl/fl}$ N=6, Panx1^{MyHC6} N=6)

C) Relative mRNA expression of *Panx1, Panx2, Panx3, Gja1* (Cx43)*, Gja5* (Cx40) in isolated cardiomyocytes from untreated Panx1$^{fl/fl}$ and Panx1^{MyHC6} mice. (Panx1, Panx2: Panx1$^{fl/fl}$ N=6, Panx1^{MyHC6} N=8; Gja1, Gja5: Panx1$^{fl/fl}$ N=5, Panx1^{MyHC6} N=8)

D) Kidney weight as a percentage of body weight of 12-week-old male untreated Panx1$^{fl/fl}$ and Panx1^{MyHC6} mice. (Panx1$^{fl/fl}$ N=6, Panx1^{MyHC6} N=5)

E) Lung weight as a percentage of body weight of 12-week-old male untreated Panx1$^{fl/fl}$ and Panx1^{MyHC6} mice. (Panx1$^{fl/fl}$ N=6, Panx1^{MyHC6} N=5)

F) Body mass of 12-week-old male untreated Panx1$^{fl/fl}$ and Panx1^{MyHC6} mice. (Panx1$^{fl/fl}$ N=10, Panx1^{MyHC6} N=9)

G) Tibial length of 12-week-old male untreated Panx1$^{fl/fl}$ and Panx1^{MyHC6} mice measured with manual calipers. (Panx1$^{fl/fl}$ N=6, Panx1^{MyHC6} N=5)

H) 24-hour average heart rate measured by radio telemetry for 5 days averaged in 12-week-old male saline treated (14 days i.p.) Panx1$^{fl/fl}$ and Panx1^{MyHC6} mice. (Panx1$^{fl/fl}$ N=3, Panx1^{MyHC6} N=3)

I) 24-hour average diastolic blood pressure measured by radio telemetry for 5 days averaged in 12-week-old male saline treated (14 days i.p.) Panx1$^{fl/fl}$ and Panx1^{MyHC6} mice. (Panx1$^{fl/fl}$ N=3, Panx1^{MyHC6} N=3)

J) 24-hour average systolic blood pressure measured by radio telemetry for 5 days averaged in 12-week-old male saline treated (14 days i.p.) Panx1$^{fl/fl}$ and Panx1^{MyHC6} mice. (Panx1$^{fl/fl}$ N=3, Panx1^{MyHC6} N=3)

K) 24-hour average mean arterial pressure measured by radio telemetry for 5 days averaged in 12-week-old male saline treated (14 days i.p.) Panx1$^{fl/fl}$ and Panx1^{MyHC6} mice. (Panx1$^{fl/fl}$ N=3, Panx1^{MyHC6} N=3)

L) Representative images of short-axis B-mode and M-mode 2D echocardiography of Panx1$^{fl/fl}$ and Panx1^{MyHC6} mice prior to the beginning of isoproterenol injections. Data represented as mean $\pm$ SEM. Significance determined using Student's t-test (B-J).

ns = not significant

A Gene Ontology Terms

B KEGG Pathways

C Glycolytic Stress Test

D Mitochondrial Stress Test

E Intracellular ATP

F Total ATP

G Mitochondrial ATP

H Glycolytic ATP

I GLUT Isoforms
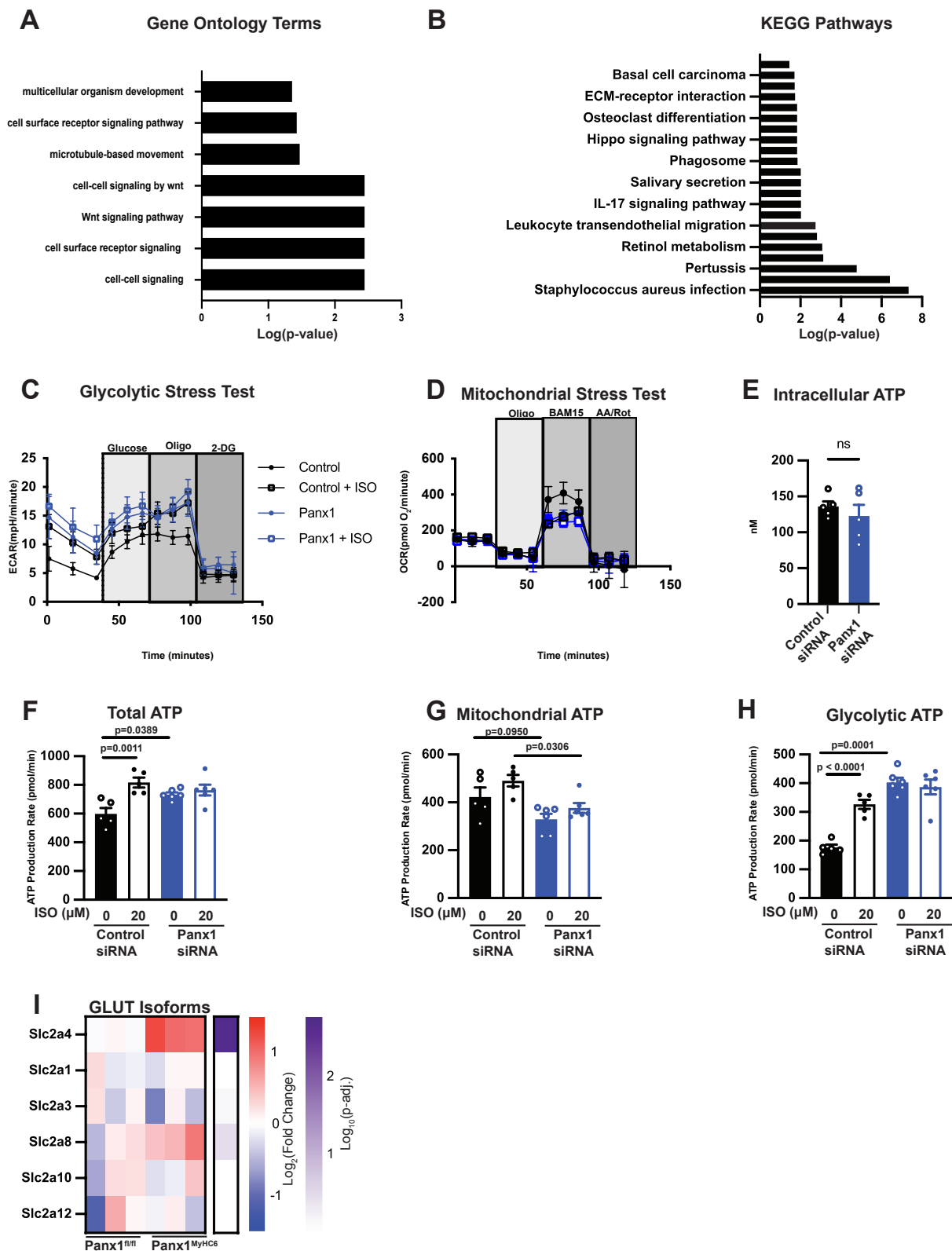
Figure 3.9:

A) Significant, as determined by a cutoff of p < 0.05, GO Terms identified from the differential gene expression in isolated cardiomyocytes of untreated Panx1$^{fl/fl}$ and Panx1^{MyHC6} mice. (Panx1$^{fl/fl}$ N=3, Panx1^{MyHC6} N=3)

B) Significant, as determined by a cut off of p < 0.05, KEGG pathways identified from the differential gene expression in isolated cardiomyocytes of untreated Panx1$^{fl/fl}$ and Panx1^{MyHC6} mice. (Panx1$^{fl/fl}$ N=3, Panx1^{MyHC6} N=3)

C) H9c2 cells were transfected with either control or Panx1-targeting siRNA and treated with either vehicle or ISO (20µM) for 1 hour. Extracellular acidification was measured after the addition of glucose, oligomycin (oligo), and 2-deoxyglucose (2-DG). (N=5)

D) H9c2 cells were transfected with either control or Panx1-targeting siRNA and treated with either vehicle or ISO (20µM) for 1 hour. Oxygen consumption rate was measured after the addition of oligomycin (oligo), BAM15, and antimycin A and rotenone. (N=3-6)

E) H9c2 cells were transfected with either control or Panx1-targeting siRNA for 72 hours and intracellular concentration of ATP was measured. (N=5)

H9c2 cells were transfected with either control or Panx1-targeting siRNA and treated with either vehicle or ISO (20µM) for 1 hour. F) Total ATP, G) Mitochondrial ATP, H) Glycolytic ATP production was measured by proton extrusion rate after the addition of oligomycin (oligo), and antimycin A and rotenone. (N=5-6)

I) Heatmap showing relative gene expression of predominate GLUT isoforms in isolated cardiomyocytes of untreated Panx1$^{fl/fl}$ and Panx1^{MyHC6} mice plotted as the Log$_2$ (fold change) from Panx1$^{fl/fl}$ mouse. Purple heatmap represents -log(p-value) of two-tailed t-tests comparing fold change of Panx1$^{fl/fl}$ and Panx1^{MyHC6}. (Panx1$^{fl/fl}$ N=3 mice, Panx1^{MyHC6} N=3 mice)

Data represented as mean $\pm$ SEM. Significance determined using Student's t-test (E). One-way ANOVA (F-H) with Sidak's multiple comparison test for post-hoc analysis for comparisons between individual groups. ns = not significant
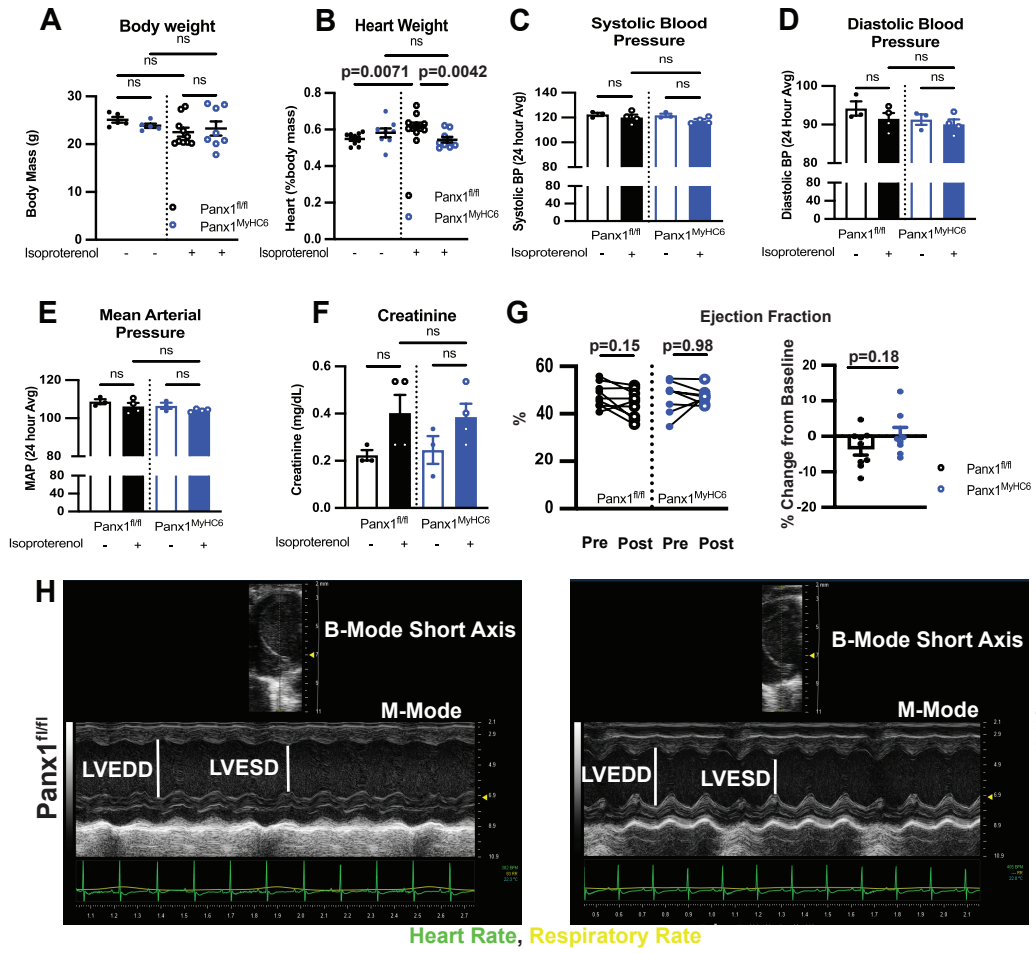
Figure 3.10:

A) Body weight of Panx1$^{fl/fl}$ and Panx1^{MyHC6} mice treated with isoproterenol (15

mg/kg/day) or saline control for 14 days. (Saline: Panx1$^{fl/fl}$ N=9, Panx1^{MyHC6} N= 8;

Isoproterenol Panx1$^{fl/fl}$ N=11, Panx1^{MyHC6} N= 9)

B) Normalized heart weight as a percentage of body weight of Panx1$^{fl/fl}$ and

Panx1^{MyHC6} mice treated with isoproterenol (15 mg/kg/day) or saline control for

14 days. (Saline: Panx1$^{fl/fl}$ N=9, Panx1^{MyHC6} N= 8; Isoproterenol Panx1$^{fl/fl}$ N=11,

Panx1^{MyHC6} N= 9).

C) 24-hour average systolic blood pressure measured by radio telemetry for 5 days

averaged in Panx1$^{fl/fl}$ and Panx1^{MyHC6} mice treated with isoproterenol (15

mg/kg/day) or saline control for 14 days. (Saline: Panx1$^{fl/fl}$ N=3, Panx1^{MyHC6} N= 3;

Isoproterenol Panx1$^{fl/fl}$ N=4, Panx1^{MyHC6} N= 4)

D) 24-hour average diastolic blood pressure measured by radio telemetry for 5 days

averaged in Panx1$^{fl/fl}$ and Panx1^{MyHC6} mice treated with isoproterenol (15

mg/kg/day) or saline control for 14 days. (Saline: Panx1$^{fl/fl}$ N=3, Panx1^{MyHC6} N= 3;

Isoproterenol Panx1$^{fl/fl}$ N=4, Panx1^{MyHC6} N= 4)

E) 24-hour average mean arterial pressure measured by radio telemetry for 5 days

averaged in Panx1$^{fl/fl}$ and Panx1^{MyHC6} mice treated with isoproterenol (15

mg/kg/day) or saline control for 14 days. (Saline: Panx1$^{fl/fl}$ N=3, Panx1^{MyHC6} N= 3;

Isoproterenol Panx1$^{fl/fl}$ N=4, Panx1^{MyHC6} N= 4)

F) Serum creatinine in Panx1$^{fl/fl}$ and Panx1^{MyHC6} mice treated with isoproterenol (15 mg/kg/day) or saline control for 14 days. (Saline: Panx1$^{fl/fl}$ N=3, Panx1^{MyHC6} N= 3; Isoproterenol Panx1$^{fl/fl}$ N=4, Panx1^{MyHC6} N= 4)

G) Left, paired analysis of left ventricle ejection fraction (%) pre- and post-isoproterenol treatment; right, percent change from baseline after isoproterenol treatment. (Panx1$^{fl/fl}$ N=9, Panx1^{MyHC6} N=8)

H) Representative images of short-axis B-mode and M-mode 2D echocardiography of Panx1$^{fl/fl}$ and Panx1^{MyHC6} mice treated with isoproterenol (15 mg/kg/day) for 14 days.

Data represented as mean $\pm$ SEM. Significance determined using One-way ANOVA (A-F) with Sidak's multiple comparison test for post-hoc analysis for comparisons between individual groups. Significance of paired data was determined using Mixed effects analysis (G) with Sidak's multiple comparison test for post-hoc analysis for comparisons between timepoints. ns = not significant

A Baseline Echo · Panx1^{MyHC6} · Pump Implantation · Day 14 Echo · Day 28 Echo · Sacrifice and Harvest Organs

Isoproterenol · Pump Implantation · Pump Ends · End

B Col1a1 — MFI (A.U.) — p=0.023 — Panx1$^{fl/fl}$, Panx1^{MyHC6}

Col1a1 — % Area / 20X Field — p=0.038 — Panx1$^{fl/fl}$, Panx1^{MyHC6}

C Fractional Shortening — % — p=0.24 — Panx1$^{fl/fl}$, Panx1^{MyHC6}

D Wall Thickness — mm — p=0.019 — Panx1$^{fl/fl}$, Panx1^{MyHC6}
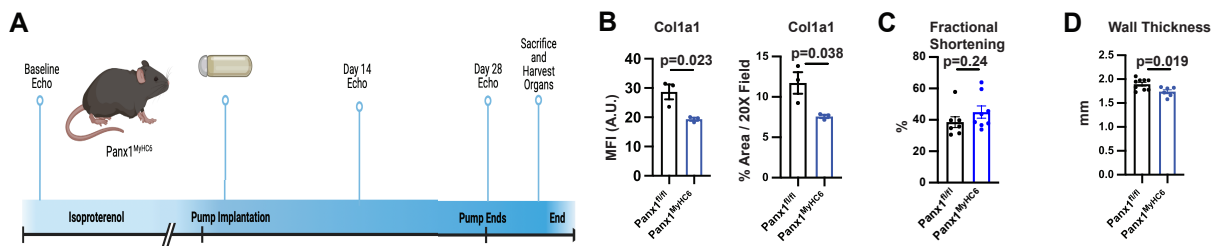
Figure 3.11:

A) Schematic of experimental design for osmotic pump implantation for isoproterenol treatment for 28 days continuous administration (15 mg/kg/day) in Panx1$^{fl/fl}$ and Panx1^{MyHC6} mice.

B) Quantification of confocal micrographs of Collagen 1a1 for intensity (mean fluorescence intensity) and percent area (20X field) after 28 days of isoproterenol administration in 8–10-week-old male Panx1$^{fl/fl}$ and Panx1^{MyHC6} mice. (Panx1$^{fl/fl}$ N=3, Panx1^{MyHC6} N=3)

C) Fractional shortening as measured by echocardiography after 28 days of isoproterenol administration in 8–10-week-old male Panx1$^{fl/fl}$ and Panx1^{MyHC6} mice. (Panx1$^{fl/fl}$ N=7, Panx1^{MyHC6} N=8)

D) Wall thickness of combined anterior and posterior wall of the left ventricle (mm) after 28 days of isoproterenol administration in 8–10-week-old male Panx1$^{fl/fl}$ and Panx1^{MyHC6} mice. (Panx1$^{fl/fl}$ N=7, Panx1^{MyHC6} N=8)

Data represented as mean $\pm$ SEM. Significance determined using Student's t-test (B-D).

A Differentially Expressed Genes

Increase 402 — Total 1439 — Decrease 1037

B

C Secondary only control

Panx1^fl/fl — Panx1^MyHC6

DAPI, Ly6g

D

Macrophage — CD86⁺ — CD163⁺

Macrophage

DC

E

Cd86 — p = 0.1879

Il1b — p = 0.0335

Cxcl2 — p = 0.0200

Chil3

Relative mRNA (Hprt)

Panx1^fl/fl Panx1^MyHC6
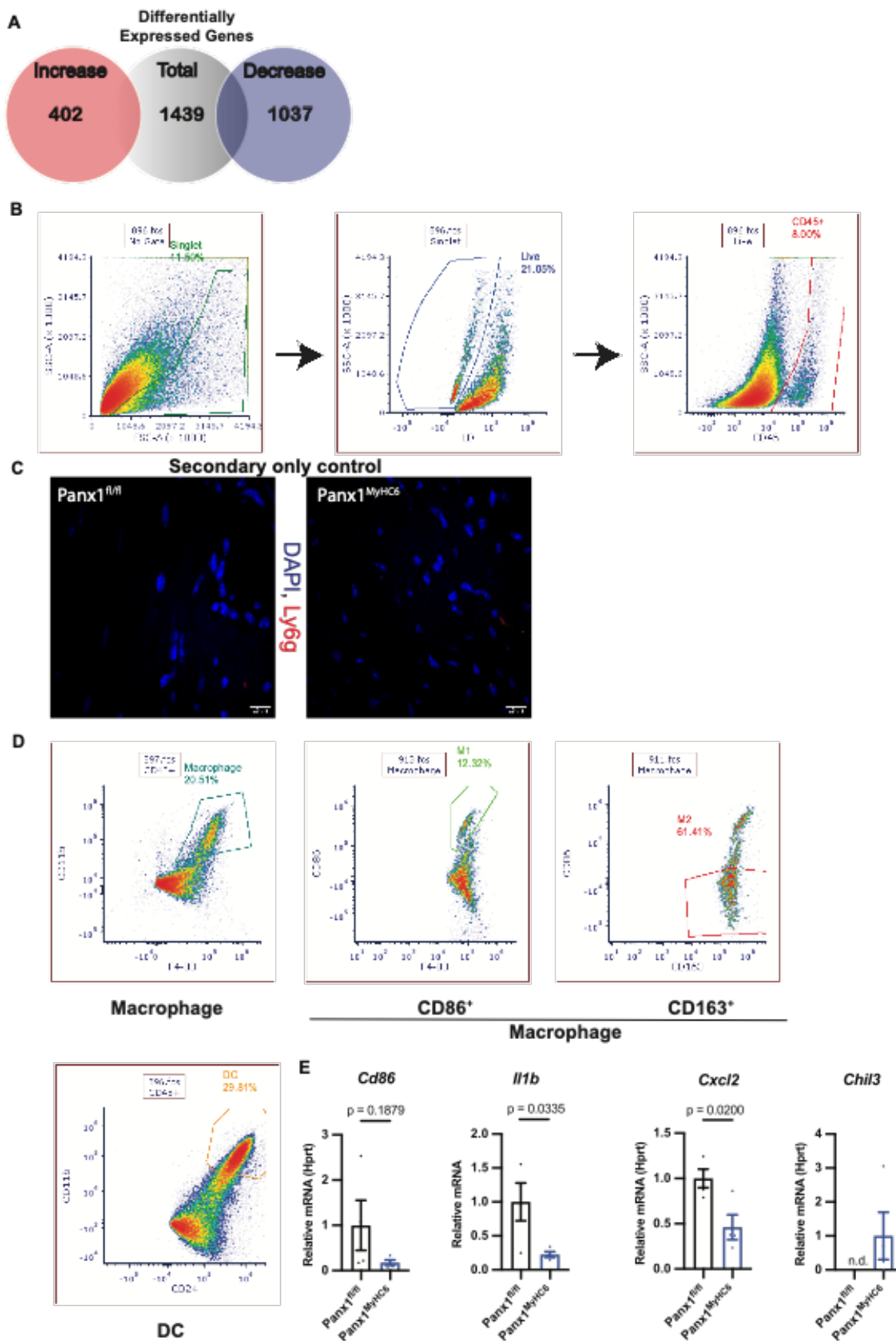
Figure 3.12:

A) Venn Diagram of the quantification of significantly increased (left, red), total (middle), and decreased (right, blue) differentially expressed genes, as determined by a cut off of $p < 0.05$, in isolated cardiomyocytes from Panx1$^{fl/fl}$ and Panx1^{MyHC6} mice treated with isoproterenol for 14 days (15 mg/kg/day).

B) Gating scheme and representative gates for the identification of CD45$^+$ cells from the non-myocyte fraction of mouse myocardial tissue.

C) Confocal micrographs of secondary only controls from cardiac sections from Panx1$^{fl/fl}$ and Panx1^{MyHC6} mice treated with isoproterenol (15mg/kg/day) for 14 days. Sections were stained with secondary antibody Goat anti-donkey Alexa Fluor 647; DAPI was used as a nuclear stain.

D) Flow cytometric analysis with representative gates for the identification of macrophages (CD11b$^+$, F4/80$^+$), macrophages expressing the co-stimulatory activation marker CD86 (CD86$^+$), macrophages expressing the anti-inflammatory M2 marker (CD163$^+$). Flow cytometric analysis with representative gates for the identification of dendritic cells (CD11b$^+$, CD24$^+$) from the CD45$^+$ cells of the non-myocyte fraction of the myocardium of Panx1$^{fl/fl}$ and Panx1^{MyHC6} mice treated with isoproterenol for 14 days (15 mg/kg/day).

E) Relative mRNA expression (Hprt) of *Cd86, Il1b, Cxcl2, and Chil3* in isolated immune cells from the myocardium of Panx1$^{fl/fl}$ and Panx1^{MyHC6} mice treated with isoproterenol for 14 days (15 mg/kg/day). (N=4)

Data represented as mean $\pm$ SEM. Significance determined using Student's t-test

(E).

Chapter 4: ***Oxidized Lipids and Sex-dependent differences in a murine model of heart failure with preserved ejection fraction***

Abstract: Heart failure with preserved ejection fraction (HFpEF) is the predominant form of heart failure, yet its treatment is largely limited due to the lack of therapeutics and multifactorial nature of the disease. We sought to explore the role of oxidized phospholipids (oxPLs) in HFpEF induced by high fat high sucrose (HFHS) feeding as model of cardiometabolic HFpEF. OxPLs have been shown to play key roles cardiovascular disease including atherosclerosis and non-alcoholic fatty liver disease, and lowering oxPLs using over expression of scFv-E06, a naturally occurring IgM which decreases plasma oxPL levels, was protective against disease onset and progression. We induced cardiometabolic HFpEF in male mice with 16 weeks of HFHS feeding and find increases in end-diastolic volume as well as development of insulin resistance. We then sought to reduce plasma oxPLs using a previously established AAV8-scFv-E06 system, which protected mice against increased end-diastolic volume and significantly reduced heart size. We demonstrate that systemic expression of scFv-E06 has differing roles in heart and kidney damage incurred during cardiometabolic HFpEF using bulk RNA-sequencing. Finally, we determine that these transcriptomic changes are sex-dependent in our model especially as it pertains to oxidative phosphorylation and inflammation in multiple organ systems. All together our data elucidates another layer to the complexity of cardiometabolic HFpEF by not only implicating an important role for oxPLs in disease onset, but further by demonstrating that at the transcriptional level there are disparate effects of scFv-E06 on the disease mechanism on the basis of biological sex.

Introduction

4.1 Oxidized Lipids in Cardiovascular Disease*: Lipids are central mediators of cellular health; in their many formats they serve as both a fuel source as well as integral membrane components. Phospholipids are a specialized lipid which is composed of a phosphate attached to a glycerol making the head group which then has two hydrophobic fatty-acyl tails. The two tails can contain a variety of carbon-chain lengths and functional groups, which can make these chains saturated or unsaturated. Unsaturated tails are susceptible to oxidation, either from enzymatic processes or free radicals generated as part of reactive oxygen species created during oxidative stress[119]. Phosphocholine containing species create the greatest proportion of phospholipids in the serum, with many oxidized phospholipids species which can be made from this parent molecule (oxPCs)[120].

There is evidence from several studies in mice that decreasing plasma oxPLs is protective against cardiometabolic diseasing including atherosclerosis, non-alcoholic fatty liver disease, and ischemia reperfusion injury in the heart[121–123]. Decreasing plasma oxPLs in mice has previously been mediated by overexpression of a naturally occurring mouse IgM – E06 using a genetic or viral vector model[122,124]. E06 has been described to bind to the PC head group of oxPLs only once oxidized and to be specific to the PC head group and not other common species such as phosphorylserine. The specificity of the peptide has been described both *in vitro* and *in vivo* by validating that non-oxidized PC species are not decreased in mice with E06 over expression[124–126]. Overexpression of E06 has

previously been done using either a mouse with constitutive overexpression of the peptide or through delivery of an AAV which has a Cre-dependent expression system developed by **Upchurch et al**[124,122]. Furthermore, AAV mediated delivery of E06 was shown to be protective against both the onset and the progression of NAFLD, making it a useful tool to understand the impact of oxPLs in disease onset but also from a therapeutic avenue[122].

Previous work has demonstrated that oxPLs play many important roles in cardiovascular disease including in endothelial cells as mediators of cell death and angiogenesis, in macrophages as differentiation factors driving metabolism, in smooth muscle cells driving phenotypic switching, and in cardiomyocytes during ischemia reperfusion injury[123,127–130]. Treatment of endothelial cells *in vitro* with oxPAPC, a mixture of oxPLs made from oxidation of 1-palmitoyl-2-arachidonoyl-snphosphatidylcholine, in concert with TNFα mitigates expression of VCAM and ICAM, markers of endothelial cell activation[127]. Moreover, co-treatment of mice with oxPAPC *in vivo* at the time of LPS induced lung injury reduced vascular leak and improved metrics of endothelial barrier function[130]. Conversely, in smooth muscles cells in culture treatment with oxPAPC lead to dedifferentiation with decreased expression of alpha-smooth muscle actin and mouse models of atherosclerosis with overexpression of scFv-E06 demonstrate the beneficial effect of decreasing oxidized phospholipid levels[121,124,128]. In macrophages, treatment with oxPAPC results in the induction of a unique macrophage class, Mox, which is less metabolically active and primed for antioxidant capacity[129,131]. This can be driven to a more M1 inflammatory phenotype with treatment of truncated oxidized lipid species such

as those which are more abundant in obese adipose tissue[129]. Finally, in cardiomyocytes overexpression of scFv-E06 using a transgene on an *Ldlr*^{-/-} background reduced infarct size and cardiomyocyte death induced by multiple classes of oxPLs[123].

In total, these studies demonstrate the wide and complex functions of oxidized phospholipids both *in vivo* and *in vitro*. Further, this body of literature dissects that the impacts of oxPLs is cell type specific and can yield both pro- and anti-inflammatory effects which are both system and disease dependent. This leaves many open questions about the role for oxPLs in chronic and multi-organ disease which may have both diverging impacts at the cellular level as well as shifting ranges of individual lipid species.

4.2 Heart Failure with Preserved Ejection Fraction and Cardiometabolic Syndrome:

As previously discussed, heart failure can be divided in to two sub-classes: heart failure with preserved ejection fraction (HFpEF) and heart failure with reduced ejection fraction (HFrEF). HFpEF can be even further sub-divided in three phenotypes: cardiometabolic, renal, and age-induced, as demonstrated both at the patient and the sequencing level and these all demand type specific therapies at least to some degree[132–134]. While these three sub-groups have some degree of overlap, cardiometabolic HFpEF which is HFpEF that is initiated and propagated by cardiometabolic co-morbidities such as type-two diabetes, hypertension, and obesity is the most predominate[28,132].

Cardiometabolic HFpEF is a complex multi-organ disease dominated by diastolic dysfunction and hypertrophy of the heart, glucose intolerance and insulin resistance, and chronic inflammation[135]. Over time these systemic stressors cause a shift in

cardiomyocyte metabolism which results in an ATP deficit similar to that which is observed in HFrEF[135]. This energy insufficient results in fuel source switching and when left unchecked results in cardiomyocyte death, which in turn causes interstitial fibrosis and myocardial stiffening. Previous work in a "3-hit" model to recapitulate the multifaceted HFpEF phenotype in humans demonstrated that ketone supplementation in mice was able to reduce functional metrics of HFpEF including improving running endurance as well as reducing interstitial fibrosis[136]. In addition, the only proven therapy for HFpEF patients is SGLT2 inhibitors which reduces risk of hospitalization independent of diabetes status[29].

In addition to the strong indicator for dysregulation in cardiac metabolism, inflammation is known to play a major role in HFpEF. In patients with HFpEF, circulating levels of c-reactive protein, IL-1, and TNFα are increased[137,138] and differentially regulated compared with HFrEF patients. Furthermore, in human biopsies from HFpEF patients an inflammatory cell type which produces TGFβ has been well described[139]. In the two hit "LNAME + high fat diet" mouse model of HFpEF, the unfolded protein response and ER-damage/ stress has been implicated by multiple groups, which is also known to play a major role in inducing the sterile inflammatory response[140].

These findings demonstrate that cardiometabolic HFpEF is a multifactorial disease which is driven not only at the level of the heart, but also has a strong systemic component. This opens the doors for a systemic therapy which impacts not only the myocardium but also improves metabolic syndrome co-morbidities and reduces inflammation in order to mitigate disease burden.

4.3 Brief Summary of Chapter: Here we demonstrate that 16 weeks of HFHS feeding in male albumin-cre mice is able to induce a cardiometabolic HFpEF phenotype. We express scFv-E06 in these mice using a previously established AAV8-DIO-E06 construct and find that scFv-E06 is protective against cardiac and metabolic dysfunction. Mice expressing scFv-E06 have no significant change in end-diastolic volume compared to chow controls, as well as smaller hearts. Furthermore, RNA-sequencing in the hearts and kidneys of a mixed sex-cohort demonstrates that scFv-E06 expression has systemic effects on the transcriptomes of these organs including changes in fibrosis and inflammation. Additionally, these studies revealed that scFv-E06 expression has sex-dependent effects on these organs. All together, these studies indicate an important role for oxidized phospholipids in the initiation of cardiometabolic HFpEF.

Results:

4.4 High fat high sucrose (HFHS) feeding as a model of Heart Failure with Preserved Ejection Fraction (HFpEF): HFpEF has been historically challenging to model in a murine system as the disease is complex with several parameters being self-reported in the human condition. Murine models need to encompass not only the cardiac function, but also represent the multi-organ damage which is a classic hallmark of the cardiometabolic HFpEF phenotype. Furthermore, HFpEF is being further characterized as the different disease-causing mechanisms are being more thoroughly investigated in human patient populations. In order to understand the ability of HFHS feeding to mimic the human condition, we characterized the effect of HFHS in male Albumin-cre mice injected with AAV8-CMV-GFP and fed chow or HFHS for 16 weeks. Male mice were subject to serial echocardiography starting prior to the induction of feeding and then every two weeks following for the duration of the diet. At the conclusion of the study, cardiac MRI was performed to assess more detailed diastolic function which is not able to be determined via 2D imaging methods. Cardiac MRI analysis of ejection fraction revealed that mice fed HFHS diet for 16 weeks had no significant changes compared with age-matched virus-matched control mice **(Figure 4.1A)**. While ejection fraction was not significantly changed, end-diastolic volume (EDV) of the left ventricle (LV) was significantly increased by HFHS feeding **(Figure 4.1B)**. Finally, we find that while total heart mass normalized to tibial length is not significantly changed, there is a trending though not statistically significant increase with HFHS in LV mass as measured by cardiac MRI after HFHS feeding **(Figure 4.1C, D)**.

Additionally, we find that HFHS feeding induces a significant increase in fat mass compared with chow control fed mice, which is concurrent with a significant increase in gWAT mass (normalized to total body weight) after HFHS feeding **(Figure 4.1E, F)**. Other organ weights including liver, kidney, and spleen were not significantly changed by HFHS feeding **(data not shown)**. Furthermore, we measured metabolic parameters expected to be impacted by HFHS feeding. While GTT area under the curve (AUC) measurements in male GFP-expressing mice were not significant changed, ITT AUC was significantly reduced by HFHS feeding **(Figure 4.1 G)**. Fasting blood glucose was not significantly changed by HFHS feeding **(data not shown)**.

Taken together this data indicates that HFHS feeding is sufficient to induce an insulin resistant phenotype. Furthermore, our data demonstrates that HFHS feeding induces increases in heart mass and LV-volume which are concurrent with hypertrophy. Finally, we observe that HFHS feeding significantly increases fat mass at both the whole body and gonad specific depot levels.

4.5 Systemic svFv-E06 expression drives protective effects in the heart, liver, and kidneys of mice feed an HFHS diet:

In order to understand the role for oxPLs in HFpEF we used an AAV8-DIO-E06 virus which had been previously established in the lab to express scFv-E06 systemically in mice in an inducible manner. Previous work has demonstrated that administration of AAV8-DIO-E06 driven by albumin Cre expression is sufficient to induce E06 expression in the liver after 2 weeks post injection[122]. The expression of scFv-E06 is then found in the liver and plasma of mice up to 14 weeks post-injection, with plasma levels reaching an average of

40 µg/mL at 14 weeks after injection. We confirmed the expression by mRNA in the liver of mice fed HFHS diet for 16 weeks and find that E06 transcripts are significantly increased after HFHS feeding similar to previously described.

We characterized the cardiac function of male mice expressing scFv-E06 compared with GFP controls all fed HFHS using cardiac MRI. scFv-E06 did not significantly change ejection fraction compared with GFP or with mice expressing scFv-E06 fed a chow diet **(Figure 4.2A)**. While HFHS feeding in mice expressing GFP resulted in significantly increased LV EDV compared with chow fed controls, scFv-E06 expression was sufficient to protect against this increase. Furthermore, mice expressing scFv-E06 had a trending decrease (p=0.1) compared with GFP controls both fed a HFHS diet **(Figure 4.2B)**. We compared the heart mass normalized to tibial length and find that after HFHS scFv-E06 expression protects mice with a significantly smaller total heart mass **(Figure 4.2C)**. Finally, we compared the LV mass as calculated from cardiac MRI and find that compared with GFP controls, scFv-E06 drives a significant decrease in LV mass which is concurrent with the decrease in total heart mass **(Figure 4.2C)**.

While we find that scFv-E06 protects mice from changes in heart mass and LV dysfunction induced by HFHS feeding, body mass and total weight gain were not significantly different compared with GFP controls **(Figure 4.2E)**. Additionally, we find that scFv-E06 expression does not change fat mass compared with GFP expressing mice and that HFHS diet still induces a significant increase in fat mass and fat pad mass compared with scFv-E06 chow fed control mice **(Figure 4.2D)**. Furthermore, we find no differences

in organ mass including kidney, liver, or spleen compared with GFP expressing mice fed HFHS diet or scFv-E06 chow fed control mice **(Figure 4.2I)**.

We tested the effect of scFv-E06 expression in HFHS feeding on metabolic changes induced with cardiometabolic HFpEF. We find that scFv-E06 expression does not induce a significant change in 16-hour fasting glucose compared with GFP controls after HFHS feeding, though we find that scFv-E06 expression induces a trending though not significant improvement in glucose tolerance as measured by glucose tolerance test area under the curve **(Figure 4.2 G)**. We tested insulin tolerance via an insulin tolerance test (ITT) after 16 weeks of HFHS feeding and determined GFP expressing mice fed an HFHS diet after 16 weeks had a significant decrease in the AUC determined by an ITT, scFv-E06 expressing mice fed an HFHS diet had no significant difference compared with their respective chow controls **(Figure 4.1G, Figure 4.2H)**. Furthermore, when comparing only HFHS fed mice scFv-E06 expression induced a significant increase in insulin sensitivity as measured by an increased insulin tolerance test area under the curve compared with compared with GFP controls **(Figure 4.2H)**. We tested plasma AST to determine whether scFV-E06 expression protected against liver injury induced by HFHS feeding. scFv-E06 expressing mice had significantly lower plasma AST compared with GFP expressing mice also fed HFHS diet **(Figure 4.2F)**.

Finally, we performed untargeted oxylipidomics to examine the role for scFv-E06 in removing oxPLs during HFHS feeding. We found that expression of scFv-E06 was sufficient to significant decrease the plasma concentration of many oxPL species, mostly those in the truncated fraction but also a small number of full-length species **(Figure 4.2I)**.

We find no significant difference in non-oxidized parent species which indicates the specificity of E06 for oxidized phospholipids. When we compare mice expressing scFv-E06 fed HFHS diet for 14 weeks we find they have significantly lower levels of oxidized lipids when comparing both truncated and full-length fractions over GFP control mice.

In order to better understand the protective mechanisms of scFv-E06 expression during cardiometabolic HFpEF we performed RNA-sequencing on the heart and kidneys of mice fed HFHS diet for 14 weeks. When we examine the effects of scFv-E06 expression on the transcriptome of the heart we find that in a mixed sex cohort there are 364 significantly differentially expressed genes, 167 upregulated and 197 down regulated **(Figure 4.3A)**. Gene Ontology pathway analysis of these genes revealed significant changes in molecular function pathways of manganese, calcium, and potassium channel activity, as well as NFκB- binding **(Figure 4.3B)**. KEGG pathway analysis revealed significant changes in glyoxylate and pyrimidine metabolism. Further analysis of the NFκB- binding pathway demonstrated that there was a decrease in genes such as *Anxa4* and *Npm1* **(Figure 4.3C)**. Previous work has demonstrated that *Anxa4* is increased in the failing human heart and in a *Anxa4* null mouse cardiomyocyte contractional force was increased after stimulation with isoproterenol[141]. Conversely there was an increase in *Hdac1*, which has been previously shown to play an important role in promoting expression of anti-hypertrophic genes such as *Klf4* and *Inpp5f* [142]. This transcriptomic data taken with the functional metrics indicates that decreasing plasma oxPLs via expression of scFv-E06 during the progression of cardiometabolic HFpEF serves as a cardioprotective mechanism. scFv-E06 expression systemically is sufficient to decrease cardiac size and protect against

cardiac dysfunction, while also preventing transcriptional changes which are associated with cardiac hypertrophy and promoting gene expression associated with improved cardiomyocyte contractile function.

We also performed bulk RNA-sequencing on the kidneys of mice from this same cohort in order to examine the role of systemic scFv-E06 expression on the renal-axis which is commonly implicated in HFpEF[44,133]. We found that in the kidney of a mix-sex cohort fed HFHS diet for 14 weeks there were 467 significantly differentially expressed genes **(Figure 4.4A)**. There were 369 upregulated genes, 98 downregulated genes when comparing scFv-E06 expressing mice to GFP controls. Reactome pathway analysis revealed that there were significant changes in pathways associated with extracellular matrix assembly and degradation, including "assembly of collagen fibrils", "collagen formation", "collagen chain trimerization", "degradation of the extracellular matrix", and "collagen degradation" **(Figure 4.4B)**. Further analysis of the genes associated with the "collagen formation" pathway revealed that while several collagen isoforms in the kidney are upregulated by scFv-E06 expression including multiple subunits of *Col4*, that *Col1* expression is downregulated **(Figure 4.4C)**. Previous work has demonstrated deficiency of *Col4* expression causes Alport's syndrome which results in kidney failure due to loss of basement membrane integrity in the glomeruli, while increased expression of *Col1* is generally associated with increased in fibrotic content and decreased glomerular function[143,144]. Taken together this data indicated that scFv-E06 expression driven by the liver is sufficient to decrease fibrotic gene expression in the kidney during cardiometabolic HFpEF.

4.6 Sex differences in mice fed a HFHS diet during HFpEF

Since we performed RNA-sequencing on mixed sex cohorts and found differences at multiple organs which were driven by systemic scFv-E06 expression, we next examined whether scFv-E06 expression could be affecting different pathways in male and female mice fed an HFHS diet. Gross analysis of the heart revealed that while inflammatory response genes did not appear changed by scFv-E06 expression in a mixed sex cohort, by splitting the sexes inflammatory response genes are changed in opposite directions in males and females **(Figure 4.5)**. In male mice expressing scFv-E06, inflammatory response genes are upregulated during HFHS feeding. While in female mice, we find that scFv-E06 expression drives a significant decrease in genes associated with inflammatory response.

We further investigated these sex dependent effects in the kidneys of mice fed HFHS diet after administration of scFv-E06 or GFP as a control. Deeper analysis of the bulk RNA-sequencing in the kidneys revealed that in male mice there are 195 significantly differentially expressed genes, while in females there are 1809 **(Figure 4.6A)**. This stark difference demonstrates that understanding sex dependent effects in our model system is key to drawing conclusions about disease mechanisms and systemic impacts.

We further performed KEGG pathway analysis on each sex from the kidneys in order to understand the broader picture of these transcriptional differences. We find that the most changed pathways in male mice are "protein export", "complement and coagulation cascade", and "PPAR signaling mechanisms" **(Figure 4.6B)**. These pathways together indicate that the differentially expressed genes in the kidneys of male mice

regulated by scFv-E06 expression point towards inflammatory response signaling. Meanwhile, in kidneys of female mice we observed that the most significantly changed pathways were "reactive oxygen species" and "oxidative phosphorylation" **(Figure 4.6B)**. These pathways demonstrate the role for systemic scFv-E06 in female mice in altering gene transcription involved in metabolic stress response most significantly.

We then further assessed the "oxidative stress response" pathway in the male and female kidneys. This pathway was of specific interest as it has been previously demonstrated that oxPLs drive increased oxidative stress and it would be hypothesized that sequestering these with E06 expression would decrease gene expression in this pathway. Interestingly we find that when we perform a mixed sex analysis there is a clear pattern by biological sex **(Figure 4.6C)**. We then performed sex-independent analysis and find that while in the kidneys of males scFv-E06 expression does not drive obvious changes, in female mice scFv-E06 expression drives an obvious decrease in genes involved in the oxidative stress response **(Figure 4.6C)**.

In summary, we find that scFv-E06 expression driven from the liver has systemic effects on the transcriptome of multiple organs in a murine model of cardiometabolic HFpEF. In a mixed sex cohort, this reveals changes which are drive improved organ function including reduced inflammatory and fibrotic genes. Deeper analysis on the basis of biological sex demonstrates that the effects of scFv-E06 expression are largely sex dependent as it comes to inflammatory response in the heart and oxidative stress in the kidney. This work demonstrates the importance of examining effects in both mixed sex and single biological sex cohorts to understand the impact of systemic oxPLs in

cardiometabolic HFpEF, especially considering the disparate number of HFpEF diagnoses

in female human patients.

Discussion

Previous work has elegantly demonstrated that scFv-E06 expression in mouse models of other cardiometabolic syndromes can be protective in both onset and progression of disease. Here we demonstrate that scFv-E06 expression is protective against the onset of cardiometabolic HFpEF using a murine model of inducible scFv-E06 systemic expression and high fat high sucrose (HFHS) feeding.

We first demonstrate that HFHS feeding for 16 weeks in male mice is sufficient to induce significant increases in left ventricular end-diastolic volume, while maintaining ejection fraction compared with chow controls **(Figure 4.1A, B)**. Furthermore, we show that mice significantly increase their fat mass on after HFHS feeding and develop insulin resistance as determined an insulin tolerance test **(Figure 4.1 E, F,G)**. This fat mass is both at the whole-body level, as well as specifically shown in the visceral adipose depot of the gonadal white adipose tissue. As HFpEF has been difficult to model in a murine system due to the complex nature of the disease, we sought to test whether our model mimicked both the cardiac and cardiometabolic syndrome components of the human condition. Other diet models have been used to similarly mimic the human condition, including the popular high fat diet plus L-NAME model (HFD + L-LNAME) "two-hit" model. HFD + L-NAME induced similar to HFHS feeding a significant induction diastolic dysfunction as well as an increase in body weight and decreased glucose sensitivity[140]. Furthermore, authors observed in the "two-hit" model reduced running distance and pulmonary edema assessed by wet/dry lung weight, as well as marked endothelial dysfunction evidenced by the increase in both diastolic and systolic blood pressure present after five-weeks of L-

NAME treatment alone or HFD+ L-NAME treatment[140]. While, we have not tested for endothelial dysfunction, our model is slower progressing, which does more closely resemble human cardiometabolic HFpEF compared with the HFD+L-NAME system and therefore we will test this in future work. In order to determine whether endothelial dysfunction is occurring in our model, analysis of the hypertensive status of these mice would be necessary. Furthermore, it would be worthwhile to look at markers of endothelial activation and blood flow either *ex vivo* or *in vivo* at the end of feeding. As other studies have demonstrated the delicate balanced role that oxPAPC can play in maintaining or causing vascular leakiness during acute sterile inflammation, understand the impact of scFv-E06 treatment in this balance during a chronic injury model would allow for novel insights for the role of oxPAPC on the endothelium during long-term injury[130].

We further demonstrated that liver-driven expression of scFv-E06 is protective against increases in end-diastolic volume and results in lower heart mass and LV mass over GFP mice also fed HFHS diet **(Figure 4.2B, C)**. These changes were observed without concurrent changes to fat mass or overall body weight **(Figure 4,2 D, E)**. The smaller heart mass is a likely indicator of less hypertrophy as a result of HFHS feeding, but this needs to be further investigated by measuring cardiomyocyte cross sectional area and cardiomyocyte number. Moreover, this needs to be evaluated in the context of female mice which are not included in the present study. Comparable studies have found that HFHS feeding in males for 16 weeks induces significant changes in cardiac function, whereas female mice did not develop significant changes in cardiac parameters after

feeding[145]. Though the diet used in this study does not exactly mimic ours, its similarities are striking and therefore we need to understand not only the impact of HFHS feeding in both male and female mice, but also whether scFv-E06 expression in female mice induces differences at both baseline and after feeding. We additionally demonstrated in male mice that markers of metabolic health we improved by scFv-E06 expression during feeding, including increased insulin tolerance test and glucose tolerance test area under the curve, as well as decreases in markers of liver damage with reduced plasma AST **(Figure 4.2 F-H)**.

We performed RNA-sequencing on mice expressing scFv-E06 compared to GFP controls which demonstrated changes in not only the hearts, but also kidneys, of a mixed sex cohort. In the heart we find that there were significant pathway level changes in channel activation including calcium and potassium channels as well as NFkB-binding **(Figure 4.3B)**. Deeper analysis of the genes in the NFkB-binding pathway revealed changes in genes including *Anxa4*, *Nmp1, and Hdac1* **(Figure 4.3C)**. While previous work indicated a clear protective effect from scFv-E06 in an ischemia reperfusion model, they were not able to clearly delineate the impacts of oxPLs in cardiomyocyte damage outside of causing mitochondrial dysfunction and cell death *in vitro*[123]. Together the shifts in these genes in addition to the pathway level changes in calcium and potassium channel activation point to an improvement in cardiac contractile force and function, which may be driven by changes in calcium handling[141,142,146,147]. This could link the previous finding as calcium overload directly impacts mitochondrial health and cardiomyocyte contraction.

RNA-sequencing in the kidneys of these mice demonstrated that scFv-E06 expression significantly alters collagen and extracellular matrix regulation **(Figure 4.4A, B)**.

We find that there is an upregulation of *Col4* subunits and a decrease in *Col1a1* **(Figure 4.4C)**. Upregulation of the *Col4* subunits would be indicative of improved basement membrane integrity which is associated with increased glomerular filtration rate and improved kidney function[143]. This would need further validation by electron microscopy assessment of the histology, as well as functional metrics of urine albumin and serum creatinine[148]. Though we do not demonstrate that renal function is changed, renal disease is a common comorbidity of HFpEF and our findings here would indicate that reducing oxPLs may support improved renal integrity in the context of cardiometabolic disease, just as increased oxPLs are associated with worsened diabetic kidney disease and reducing these improves kidney function[149].

Finally, we assessed whether the impact of scFv-E06 expression altered transcriptomic changes in a sex-dependent manner. We found that the inflammatory pathway in the heart was only significantly changed in female mice expressing scFv-E06 compared with their GFP counterparts. Additionally, we observe that when comparing male and female mice both expressing scFv-E06 using the same 10 genes in this pathway male mice respond in the opposite direction to female mice **(Figure 4.5)**. We performed this same analysis format in the kidney and demonstrate a similar finding regarding the oxidative stress response pathway **(Figure 4.6B, C)**. These findings highlight the hole in the field regarding sex as a biological variable in HFpEF. In the human condition, HFpEF is more common in women and being biologically female is associated with worse diastolic function and clinical outcomes[150]. Despite this, most studies in mice or in humans either only evaluate males or do lumped analysis without accounting for sex as a biological

variable, therefore our findings are particularly meaningful. We identify two pathways that may serve as therapeutic targets in females, but not males as administration of scFv-E06 causes pathway level decreases in genes only in female mice.

Limitations

Currently our study is limited by the small cohort size in the female group, as well as lack of chow control in this group. Those mice are in progress and will be considered in future analysis. In addition, we have not yet assessed metrics of microvascular dysfunction which is a key hallmark of HFpEF and would need to be determined in order to claim that HFHS feeding encompasses the full complexity of the human condition. Finally, we have identified multiple pathways which could be at play in the molecular mechanism of the role for oxPLs and in using the scFv-E06 model we do not target one specific lipid species; therefore, it is very likely our findings are due to the impact of the overall oxidized lipid profile and do not describe any singular pathway or receptor-ligand pair.
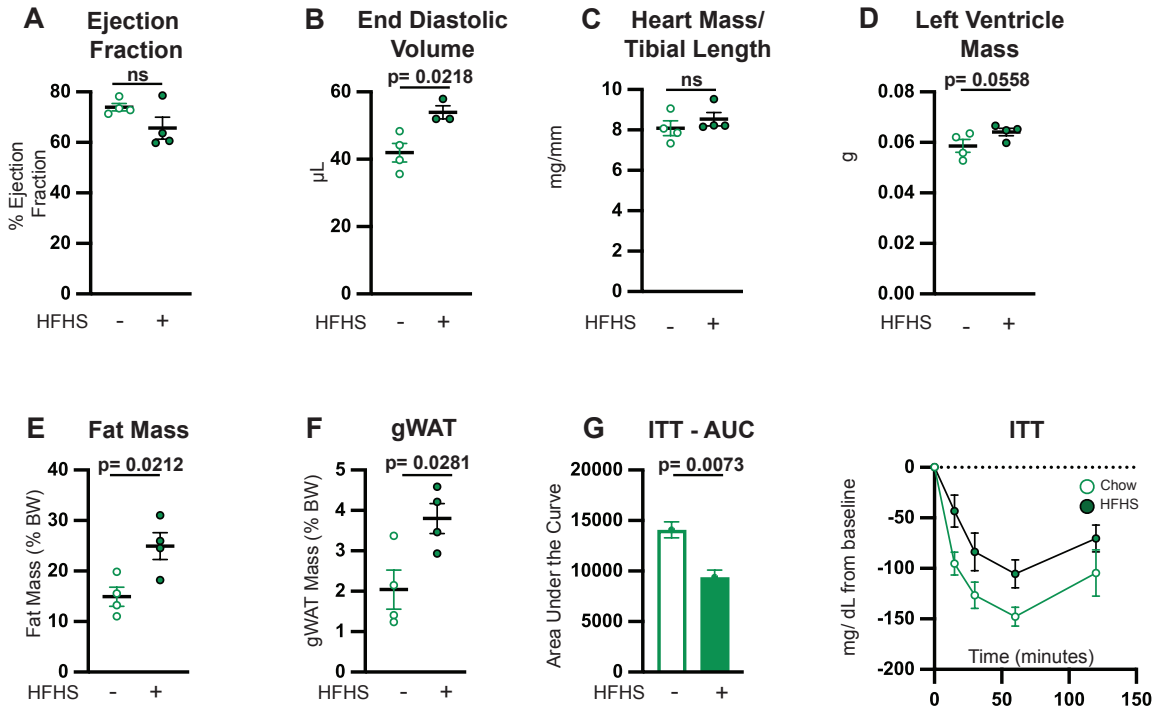
Figure 4.1: High Fat High Sucrose Feeding for 16 weeks is a murine model of Heart Failure with Preserved Ejection Fraction

Figure 4.1: High Fat High Sucrose Feeding for 16 weeks is a murine model of Heart Failure with Preserved Ejection Fraction

A) Left ventricle ejection fraction calculated from cardiac MRI in male mice fed chow (left) or HFHS diet (right) for 16 weeks after administration of AAV8-GFP.

B) Left ventricle end-diastolic volume measured from cardiac MRI in male mice fed chow or HFHS diet for 16 weeks after AAV8-GFP administration. (N=4 chow, N=4 HFHS feedings – one outlier determined by ROUT test)

C) Heart mass normalized to tibial length in male mice fed chow or HFHS diet for 16 weeks after administration of AAV8-GFP.

D) Left ventricle mass calculated from cardiac MRI in male mice fed chow or HFHS diet for 16 weeks after AAV8-GFP administration.

E) Fat mass as a percent of body weight in male mice fed chow of HFHS diet for 16 weeks after administration of AAV8-GFP.

F) Gonadal white adipose tissue (gWAT) fat pad mass normalized to total body weight in male mice fed chow or HFHS diet for 16 weeks after administration of AAV8-GFP.

G) Insulin tolerance test after 16 weeks of chow or HFHS feeding in male GFP expressing mice area under the curve (left) and representative curves (right).

Statistics: Data represented as mean $\pm$ SEM. Student's t-test; N=4 chow, N=4 HFHS
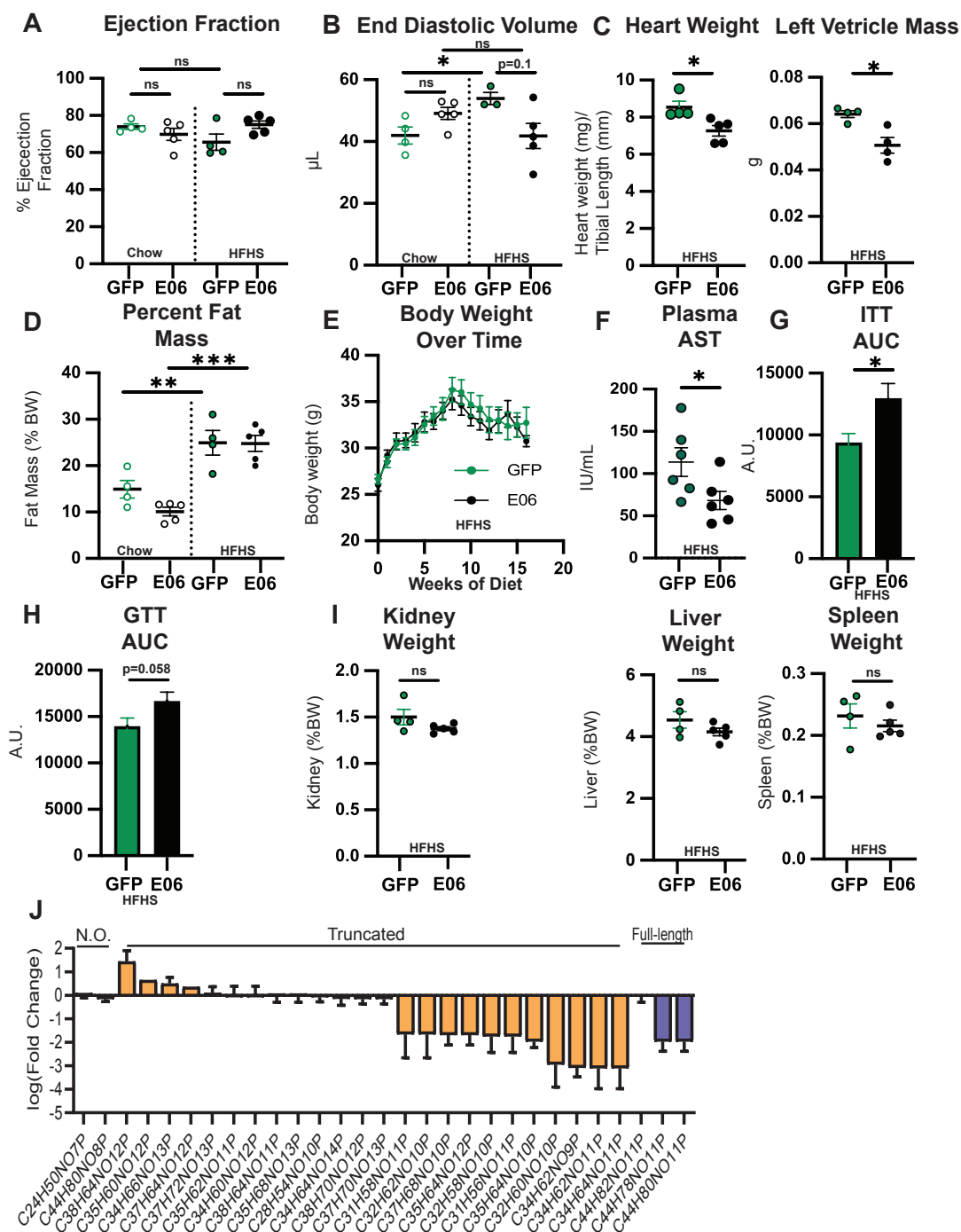
Figure 4.2: Liver driven expression of scFv-E06 protects mice against cardiometabolic HFpEF and significantly reduces plasma oxidized lipids

Figure 4.2: Liver driven expression of scFv-E06 protects mice against cardiometabolic HFpEF and significantly reduces plasma oxidized lipids

A) Left ventricle ejection fraction calculated from cardiac MRI in male mice fed chow (left) or HFHS diet (right) for 16 weeks after administration of AAV8-GFP or AAV8-scFv-E06. (N=4 GFP chow, N=4 GFP HFHS, N=5 scFv-E06 chow, N=5 scFv-E06 HFHS)

B) Left ventricle end-diastolic volume measured from cardiac MRI in male mice fed chow or HFHS diet for 16 weeks after AAV8-GFP or AAV8-scFv-E06 administration. (N=4 GFP chow, N=3 GFP HFHS, N=5 scFv-E06 chow, N=4 scFv-E06 HFHS, outlier determined by ROUT test)

C) Heart mass normalized to tibial length (left) and left ventricle mass calculated by cardiac MRI (right) in male mice fed HFHS diet for 16 weeks after administration of AAV8-GFP or AAV8-scFv-E06 administration. (N=4 GFP, N=5 scFv-E06 – left, (N=4 GFP, N=4 scFv-E06 – right, outlier determined by ROUT test)

D) Fat mass as a percent of body weight in male mice fed chow of HFHS diet for 16 weeks after administration of AAV8-GFP or AAV8-scFv-E06. (N=4 GFP chow, N=4 GFP HFHS, N=5 scFv-E06 chow, N=5 scFv-E06 HFHS)

E) Total body weight over 16 weeks HFHS feeding in male mice administered AAV8-GFP or AAV8-scFv-E06. (N=4 GFP, N=5 scFv-E06)

F) Plasma AST in mice fed HFHS diet after administration of AAV8-GFP or AAV8-scFv-E06. (N=6 in each group, 3M, 3F)

G) Area under the curve from insulin tolerance test performed after 16 weeks of HFHS feeding in male mice expressing GFP or scFv-E06. (N=4 GFP, N=5 scFv-E06)

H) Area under the curve from glucose tolerance test performed after 14 weeks of HFHS feeding in male mice expressing GFP or scFv-E06. (N=7 GFP, N=8 scFv-E06)

I) Kidney (left), liver (middle), and spleen (right) weight normalized to body weight in male mice fed HFHS diet for 16 weeks expressing either GFP or scFv-E06. (N=4 GFP, N=5 scFv-E06)

J) Log (fold change) of Plasma non-oxidized (N.O.) or truncated or full-length oxidized phospholipids detected by LC-MS/MS in mice fed HFHS diet comparing mice expressing scFv-E06 with GFP control mice. (N=6 in each group, 3M, 3F)

Statistics: Student's t-test (C, F-I), One-Way ANOVA with Sidak's multiple comparison test (A, B, D)
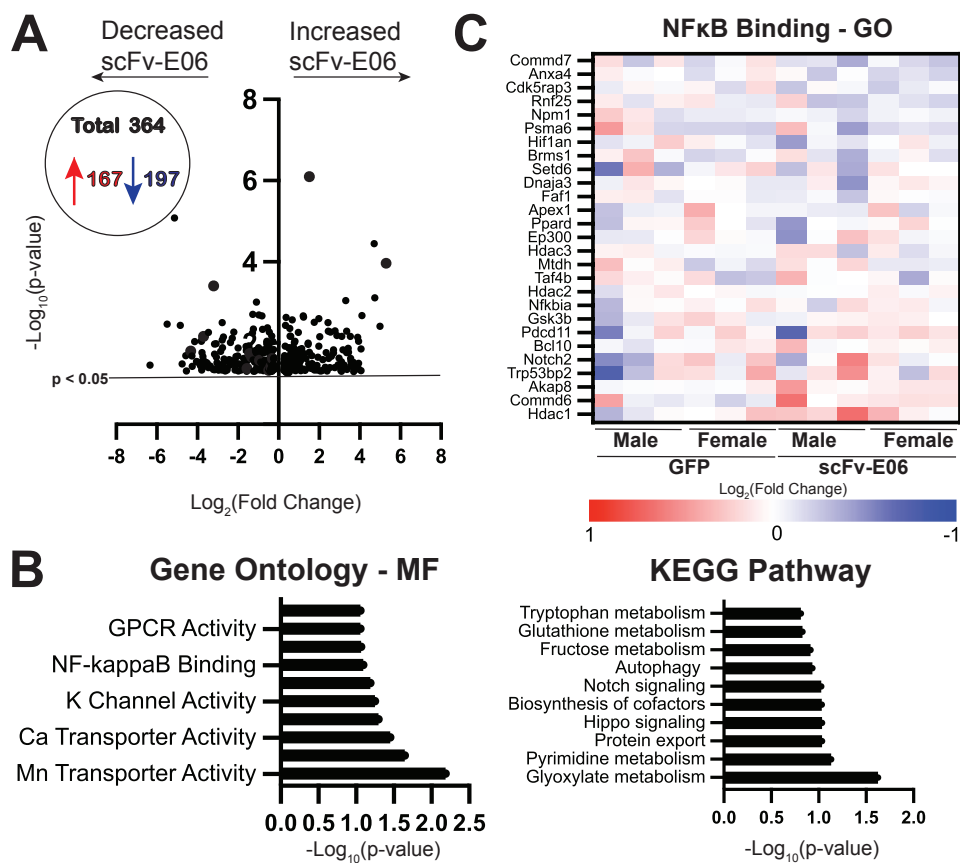
Figure 4.3: **Bulk RNA-Sequencing of hearts from mice fed high fat high sucrose diet reveals liver-driven scFv-E06 expression drives decreased in inflammation and plasma membrane transporter activity**

Figure 4.3: **Bulk RNA-Sequencing of hearts from mice fed high fat high sucrose diet reveals liver-driven scFv-E06 expression drives decreased in inflammation and plasma membrane transporter activity**

A) Volcano plot of differentially expressed genes in hearts of mice expressing E06 versus mice expressing GFP control after 12 weeks of high fat high sucrose (HFHS) feeding demonstrates 364 significantly differentially expressed genes. 167 genes are upregulated, and 197 genes are downregulated of the 364 changed.

B) Enriched Gene Ontology- molecular function and KEGG pathway analysis in hearts of mice expressing E06 versus GFP controls after 12 weeks of high fat high sucrose (HFHS) feeding revealed pathways of membrane channel transporter activity, NFκB binding, protein export, and biosynthesis of co-factors as being regulated by systemic expression of scFv-E06.

C) Heatmap showing relative gene expression of NFκB binding genes from hearts of mice expressing E06 versus mice expressing GFP control plotted as $\log_2$ (Fold Change) from kidneys of GFP expressing mice.

Statistics: Differentially expressed genes have -log(p-value) > 1.3 analyzed by DESeq2, Pathway Analysis performed by clusterProfiler, N=6 (3M,3F)
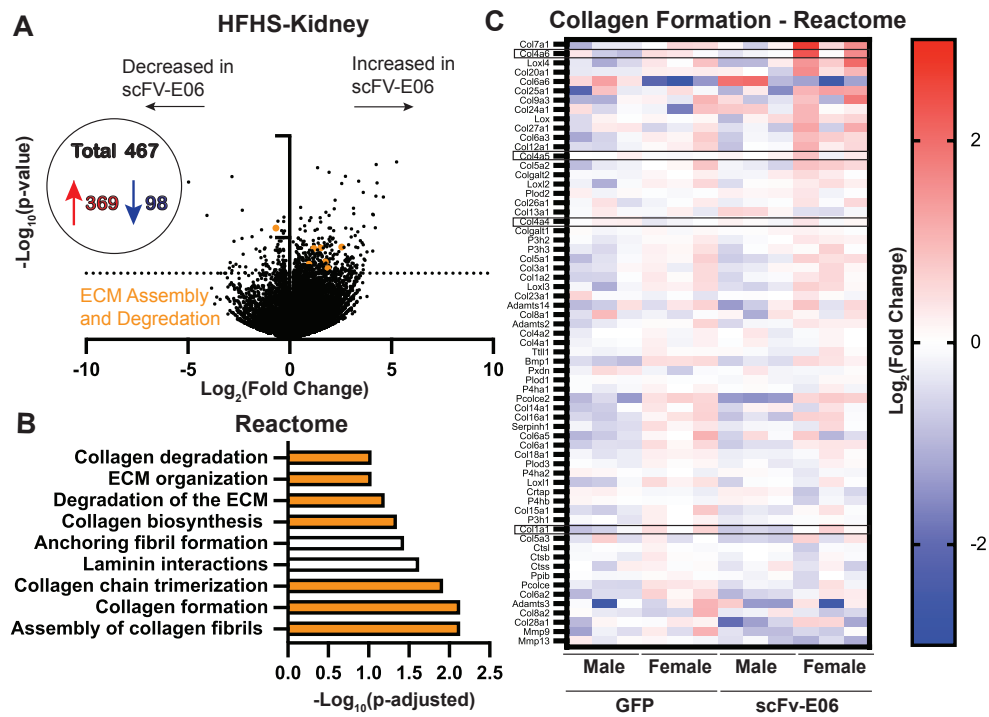
Figure 4.4: **Bulk RNA-Sequencing of kidneys from mice fed high fat high sucrose diet reveals differential gene expression associated with extracellular matrix maintenance**

Figure 4.4: **Bulk RNA-Sequencing of kidneys from mice fed high fat high sucrose diet reveals differential gene expression associated with extracellular matrix maintenance**

A) Volcano plot of differentially expressed genes in kidney of mice expressing E06 versus mice expressing GFP control after 12 weeks of high fat high sucrose (HFHS) feeding demonstrates 467 significantly differentially expressed genes. 369 genes are upregulated, and 98 genes are downregulated of the 467 changed. Orange dots corresponds to genes included in pathways of extracellular matrix assembly and degradation.

B) Enriched reactome pathway analysis in kidneys of mice expressing E06 versus GFP controls after 12 weeks of high fat high sucrose (HFHS) feeding revealed pathways of ECM assembly and degradation as significantly regulated by liver driven scFv-E06 expression.

C) Heatmap showing relative gene expression of collagen formation associated genes from kidney of mice expressing E06 versus mice expressing GFP control plotted as $\log_2$ (Fold Change) from kidneys of GFP expressing mice.

Statistics: Differentially expressed genes have -log(p-value) > 1.3 analyzed by DESeq2, Pathway Analysis performed by clusterProfiler, N=6 (3M,3F)
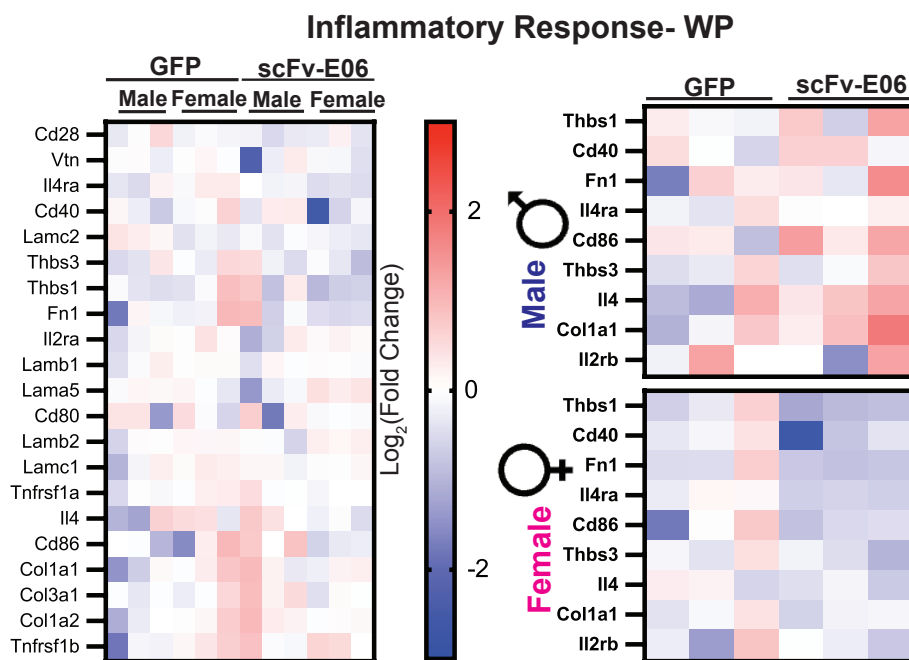
Figure 4.5: Bulk RNA-Sequencing of hearts from mice fed HFHS diet reveals liver-driven scFv-E06 expression drives sex-dependent changes in inflammatory response

Figure 4.5: Bulk RNA-Sequencing of hearts from mice fed HFHS diet reveals liver-driven scFv-E06 expression drives sex-dependent changes in inflammatory response

Heatmap showing relative gene expression of "inflammatory response" genes (WikiPathways) from hearts of mice expressing E06 versus mice expressing GFP control plotted as $\log_2$ (Fold Change) from hearts of GFP expressing mice. Further analysis of males only or females only reveals divergent expression of genes when biological sex is considered. Male mice expressing scFv-E06 demonstrate increased expression, while females demonstrate decreased expression relative to GFP controls.

Statistics: Differentially expressed genes have -log(p-value) > 1.3 analyzed by DESeq2, Pathway Analysis performed by clusterProfiler, N=6 (3M,3F)
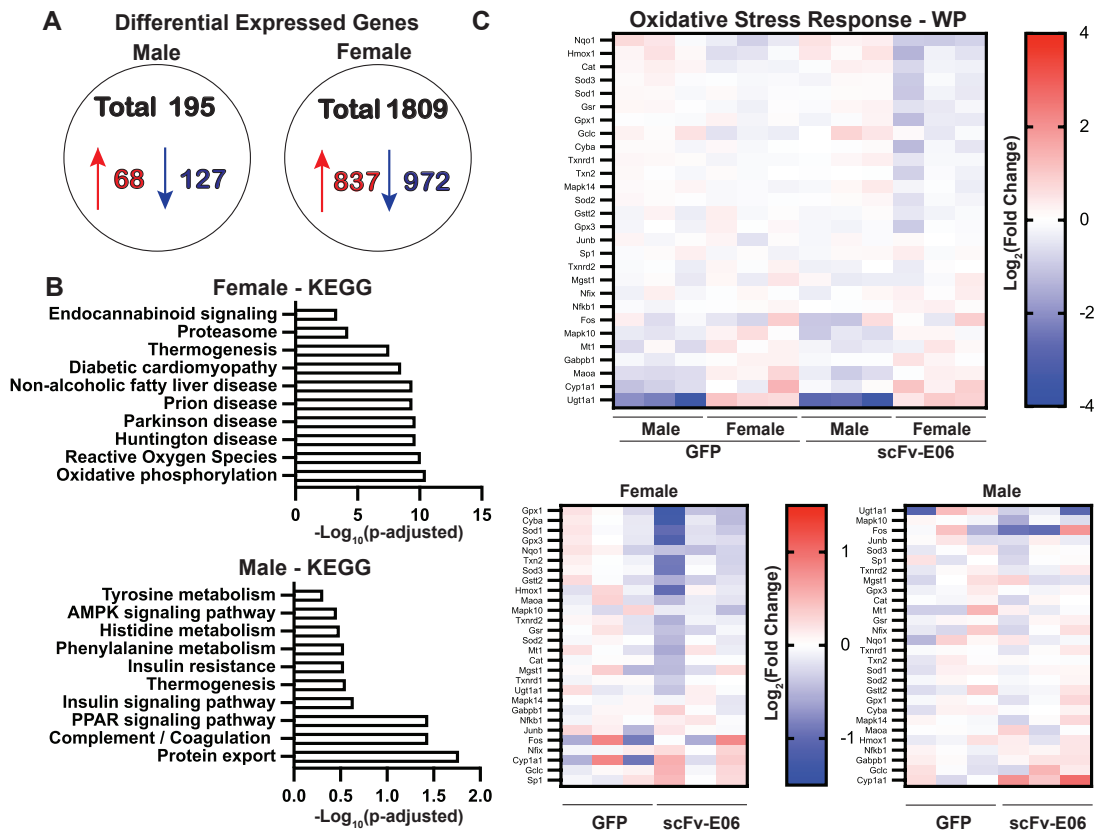
Figure 4.6: Bulk RNA-Sequencing analysis of kidneys from male and female mice fed high fat high sucrose diet demonstrate unique pathway regulation after scFv-E06 on the basis of biological sex

Figure 4.6: **Bulk RNA-Sequencing analysis of kidneys from male and female mice fed high fat high sucrose diet demonstrate unique pathway regulation after scFv-E06 on the basis of biological sex**

A) Differentially expressed genes from male mice expressing E06 versus mice expressing GFP control after 12 weeks of high fat high sucrose (HFHS) feeding have 195 significantly changed genes, 68 upregulated and 127 down regulated. Differentially expressed genes from female mice expressing E06 versus mice expressing GFP control after 12 weeks of high fat high sucrose (HFHS) feeding have 1809 significantly changed genes, 837 upregulated and 972 down regulated.

B) KEGG pathway analysis from the kidneys of female mice expressing E06 compared with GFP controls after 12 weeks of HFHS feeding have significant changes in pathways associated with oxidative phosphorylation, reactive oxygen species, and diseases including diabetic cardiomyopathy, revealing transcriptional changes associated with oxidative stress. KEGG pathway analysis from the kidneys of male mice have significant changes in pathways of protein export, complement and coagulation cascade, and PPAR signaling, demonstrating changes in inflammatory signaling.

C) Heatmap showing relative gene expression of collagen formation associated genes from kidney of mice expressing E06 versus mice expressing GFP control plotted as $\log_2$ (Fold Change) from kidneys of GFP expressing mice. Further heatmaps showing the breakout of changes in female or male mice exclusively

revealing the significant downregulation of oxidative stress associated genes in

female but not male.

Statistics: Differentially expressed genes have -log(p-value) > 1.3 analyzed by

DESeq2, Pathway Analysis performed by clusterProfiler, N=6 (3M,3F)

**Acknowledgments**

Chapter 5: Discussion and Future Directions

In this work we discover novel regulators of the metabolic and inflammatory

pathways in heart failure, which can be regulated by both systemic manipulation of

oxidized phospholipids and cardiomyocyte specific deletion of PANX1.

In order to understand how PANX1 in cardiomyocytes plays a role in both

inflammation and metabolism during heart failure, we developed a novel mouse with

cardiomyocyte specific deletion of PANX1 under the control of the alpha-myosin heavy

chain driven Cre. We determined that while these mice had no developmental or cardiac

function deficits in the unstressed state, the cardiomyocyte metabolism was shifted to a

hyper glycolytic state. Using bulk RNA-sequencing we uncovered a significant

upregulation in the transcription of *Scl2a4* which encodes the GLUT4, one of the

predominate glucose transporters in cardiomyocytes[151]. We then validated these

findings *in vitro* using H9c2 rat myoblasts and demonstrated that siRNA-mediated knock-

down of PANX1 resulted in a significant increase in maximal ECAR and total as well as

glycolysis associated ATP production. We further demonstrated, as had been previously

described, that isoproterenol stimulation results in increased maximal ECAR and

glycolytic ATP production. We then described for the first time that in PANX1 knock-

down cells isoproterenol stimulation does not further increase glycolytic bioenergetics

or total ATP production. This data suggests that in cardiomyocytes PANX1 serves to

regulate glycolytic metabolism even in the unstimulated and unstressed states.

Furthermore, it demonstrates that PANX1 deletion in cardiomyocyte serves to push cells

to a glycolytic ceiling from which they cannot further increase glycolytic metabolism or

total ATP production according to our *in vitro* data.

These findings not only provided new insights into the role of PANX1 in metabolism, but also yield additional questions in the context of cardiomyocytes. In order to better probe the fate of the increased glucose, it would be worthwhile to perform further tracing experiments to determine the downstream metabolites made from carbon labelled glucose. It would be hypothesized that this is simply made into ATP through glycolysis based on our data, but further confirmation of this is warranted. Additionally, PANX1's role in metabolism is not unique to cardiomyocytes and therefore it would be interesting to determine whether this metabolic shift is present in other predominate cells of the heart including endothelial cells and fibroblasts. Finally, our study is limited as we determine mechanistically how this shift is protective in the context of non-ischemic heart failure. The current paradigm in the field is that the shift to glycolytic metabolism in cardiomyocytes is detrimental to cardiomyocyte survival under stress, but our data demonstrates that this may not be the case. More work needs to be done to understand why the metabolic switch to increasing glucose utilization is detrimental and whether in our system other fuel sources such as fatty acids and ketones are used equally to control cardiomyocytes.

As we describe, the PANX1 deletion in cardiomyocyte is concurrent with an increase in GLUT4 expression and increased ATP production through upregulation of the glycolytic rate. In this work we do not describe the mechanism by which this metabolic shift occurs, but we hypothesize that the activation of PANX1 as an ATP leak in cardiomyocytes may play a role in this process. Leak of ATP through PANX1 may serve to regulate the ATP to ADP ratio within the cell controlling metabolic processes and when

this ratio is shifted the increased presence of ATP in the cell may be used to upregulate ATP dependent process which can then use ATP as either an allosteric regulator or use ATP hydrolysis to fuel biochemical reactions. PANX1 can be activated by mechanical stretch of cells potentially mediated by PIEZO channels, namely in cardiomyocytes PIEZO1 is the predominate isoform[62,152]. This mechanical activation as a result of PIEZO1 and cardiomyocyte contraction may allow for the constant leak of ATP at low levels to regulate the intracellular ATP content. Even without this leak, which has not been demonstrated by us or others and is simply conjecture, the absence of PANX1 increases total ATP production and this excess ATP maybe stored and this is why we observed no difference in intracellular ATP concentration. If this storage of ATP is increased and mitochondrial oxidative phosphorylation dependent ATP production is decreased this could also act as the feed-forward mechanism by which increased glycolysis is maintained in our PANX1 deficient cardiomyocytes. This could be tested in our system by measuring phosphocreatine which is used as a storage mechanism for ATP to be mobilized to the sarcoplasmic reticulum and measuring creatine kinase activity in the cardiomyocytes of Panx1$^{fl/fl}$ mice relative to Panx1^{MyHC6} mice[153]. Taken together our data as well as further work would hope to demonstrate how PANX1 presence in the cardiomyocyte drives oxidative phosphorylation and why its deletion results in alter glycolytic metabolism. Furthermore, understanding this mechanism may allow us to understand whether this increase in glycolytic is causal to the protection against hypertrophy and neutrophil recruitment or whether these are two separate mechanisms which are not linked.

In additional to our finding regarding the novel metabolic role for PANX1 in cardiomyocytes, we determined that during isoproterenol induced non-ischemic heart failure PANX1 deletion in cardiomyocyte significantly reduces neutrophil recruitment to the myocardium. We determined that this recruitment was specific to neutrophils and not macrophages by both flow cytometry and confocal microscopy. This finding fills a hole in the field which had previously demonstrated that PANX1 deletion in the myocardium significantly reduces immune cell recruitment in both myocardial infarction and ischemia reperfusion injury[55,68] but did not identify a specific cell type. However, our study did not evaluate whether this phenotype persists into the longer term model which would be worthwhile to understand in considering PANX1 as a therapeutic target. Additionally, future work should evaluate whether there are any changes to adaptive immune cell populations such as B and T cells as well as natural killer cells considering the significant decrease in total immune cells, CD45^{+}, we observe in Panx1[MyHC6] hearts at the early disease timepoint.

In our work identifying the role for PANX1 in neutrophil recruitment, we did not explore the ligand receptor pair which results in this recruitment nor whether this is driven through an endothelial dependent or resident immune cell dependent process. Based on RNA-Seq analysis of whole heart tissue in which we identify three key purinergic receptors which we attribute to neutrophils, we postulate that neutrophils could be called by ATP, ADP, or UDP-glucose released through PANX1 during isoproterenol-induced cardiac hypertrophy. While we did not do so for this study, it would be worthwhile to attempt to measure whether it is any of these metabolites

individually or in combination which is being released through PANX1 and is changed in the effulent of Panx1$^{fl/fl}$ hearts versus Panx1^{MyHC6} hearts which have been hung and stimulated ex-vivo utilizing a Langendorff apparatus. As UDP-glucose is the longest-lived of these three metabolites, from previous cell culture studies directly comparing ATP and UDP-glucose, it is the most likely to result in prolonged neutrophil recruitment, but this could be determined using both the effluence measurements and an *in vitro* migration assay[154]. Further work could then study *in vitro* migration in the presence of one or multiple metabolites identified from the effluence of the hearts as a way to narrow down the results of cardiomyocyte damage result and neutrophil migration. Furthermore, it would be worthwhile to perform in-vivo imaging of labelled neutrophils through the process of isoproterenol induced injury in the presence or absence of resident leukocytes which could be depleted in adulthood using a diptheria toxin driven promoter to demonstrate how these cells are called to the myocardium. One may presume that this is done in an endothelial dependent manner through activation of endothelial cells in the vascular and endocardial surface, but elegant design of a construct which results in the death of resident immune cells upon activation and re-entry into the cell cycle could determine whether signaling from resident leukocytes is required or if cardiomyocyte release of damage signals is sufficient to drive recruitment.

Finally, we evaluated whether systemic manipulation of oxidized phospholipids impacts cardiometabolic HFpEF. We used a previously validated AAV8-DIO-scFv-E06 expression vector which is driven in a liver-specific manner, but results in plasma expression of scFv-E06[122]. We demonstrated that HFHS feeding in male mice results in

no change in ejection fraction but significantly increases left-ventricle end-diastolic volume. Furthermore, HFHS feeding induces significant decreases in insulin tolerance test area under the curve indicating insulin resistance. We find through RNA-sequencing on hearts of these mice that scFv-E06 expression results in changes in NFkB-binding, potentially promoting the expression of anti-hypertrophic genes. Additionally, we determined that the effects of scFv-E06 expression are sex-dependent as they result in transcriptome level changes which are significantly different between male and female mice in both the heart and the kidney. Together these findings promote the question of how oxidized lipids are interacting with cardiomyocytes to change NFkB-binding. Identifying a potential membrane receptor or secondary messenger within cardiomyocytes would elucidate how oxidized lipids impact cardiomyocyte physiology. Moreover, understanding whether this mechanism is sex dependent would provide opportunity for novel therapeutic strategies within HFpEF. Further work will characterize the response of female mice to HFHS feeding and determine whether scFv-E06 expression affects the *in vivo* cardiac and metabolic dysfunction observed in male mice after HFHS feeding.

Studies on female mice are currently ongoing and recently published work has begun to explore these sex-dependent difference[145]. The recently published work elucidates that HFHS feeding results in sex-dependent changes in cardiac function where males have significant changes in diastolic dysfunction which is not present in female mice. Furthermore, this study demonstrates that the metabolic dysfunction induced by HFHS feeding is ubiquitous if not more prevalent in female mice. In our work we expect

that we will observe similar *in vivo* physiology due to HFHS feeding, and we with the preliminary cohort of mice which expressed GFP or scFv-E06 all fed HFHS diet observed that the effect of scFv-E06 expression in increasing glucose tolerance by decreasing area under the curve compared with GFP controls was more pronounced in female mice over males. We would hypothesize that this data will be reinforced with the addition of more mice to the cohort and chow controls for understanding the role of HFHS feeding in inducing insulin resistance in this model. Moreover, we identified one pathway which in which the impact of scFv-E06 expression is sex-dependent in the hearts of inflammation which could be further explored in the ongoing cohort. This would be of particular interest because it is well recognized that inflammation has a strong sex dependent component and that HFpEF differentially affects females over males making the potential for targeting oxidized lipids in females as a therapeutic strategy particularly appealing. Furthermore, the data from the sex-dependent affects in the kidney would allow for speculation that scFv-E06 expression may also affect cellular metabolism and reactive oxygen species generation in a sex dependent manner, particularly oxidative phosphorylation. It would be of interest to understand whether this is a multi-organ affect which can be generalized due to the known role of metabolism shifting in the heart failure. This may reveal whether anti-oxidant therapy or removal of oxidized lipid species from the plasma is protective against cardiac dysfunction due to protection of cardiomyocyte metabolism or another process all together.

Taken together the data in this dissertation demonstrates novel roles for oxidized phospholipids and PANX1 in cardiomyocyte metabolism and inflammation. We evaluated

multiple murine models of non-ischemic heart failure using both isoproterenol and high fat high sucrose feeding. We identified that PANX1 deletion shifts cardiomyocyte metabolism in an unstressed state and protects against isoproterenol induced hypertrophy by decreasing immune cell recruitment to the myocardium. Finally, we evaluated the impact of scFv-e06 expression in HFpEF in both male and female mice. We determined that in male mice scFv-E06 expression protects mice against HFHS induced cardiac and metabolic dysfunction. We also determined that the cellular mechanism by which this may be occurring is potentially sex-dependent based on RNA-sequencing.

References:

1. Später, D., Hansson, E. M., Zangi, L. & Chien, K. R. How to make a cardiomyocyte. *Development* **141**, 4418–4431 (2014).

2. Walker, C. A. & Spinale, F. G. The structure and function of the cardiac myocyte: A review of fundamental concepts. *J. Thorac. Cardiovasc. Surg.* **118**, 375–382 (1999).

3. Weinhaus, A. J. & Roberts, K. P. Anatomy of the Human Heart. in *Handbook of Cardiac Anatomy, Physiology, and Devices* (ed. Iaizzo, P. A.) 51–79 (Humana Press, Totowa, NJ, 2005). doi:10.1007/978-1-59259-835-9_4.

4. Doevendans, P. A. F. M. Cardiac specific gene expression of the regulatory myosin light chains. (maastricht university, 1997). doi:10.26481/dis.19971212pd.

5. Fearnley, C. J., Roderick, H. L. & Bootman, M. D. Calcium Signaling in Cardiac Myocytes. *Cold Spring Harb. Perspect. Biol.* **3**, (2011).

6. Lopaschuk, G. D. & Jaswal, J. S. Energy Metabolic Phenotype of the Cardiomyocyte During Development, Differentiation, and Postnatal Maturation. *J. Cardiovasc. Pharmacol.* **56**, 130–140 (2010).

7. Gupta, M. P. Factors controlling cardiac myosin-isoform shift during hypertrophy and heart failure. *J. Mol. Cell. Cardiol.* **43**, 388–403 (2007).

8. Litviňuková, M. *et al.* Cells of the adult human heart. *Nature* 1–10 (2020) doi:10.1038/s41586-020-2797-4.

9. Frieler, R. A. & Mortensen, R. M. Immune Cell and Other Non-Cardiomyocyte Regulation of Cardiac Hypertrophy and Remodeling. *Circulation* **131**, 1019–1030 (2015).

10. Brutsaert, D. L. Cardiac Endothelial-Myocardial Signaling: Its Role in Cardiac Growth, Contractile Performance, and Rhythmicity. *Physiol. Rev.* **83**, 59–115 (2003).

11. Zhang, H., Lui, K. O. & Zhou, B. Endocardial Cell Plasticity in Cardiac Development, Diseases and Regeneration. *Circ. Res.* **122**, 774–789 (2018).

12. Fang, M., Xiang, F.-L., Braitsch, C. M. & Yutzey, K. E. Epicardium-derived fibroblasts in heart development and disease. *J. Mol. Cell. Cardiol.* **91**, 23–27 (2016).

13. Frangogiannis, N. G. Cardiac fibrosis: Cell biological mechanisms, molecular pathways and therapeutic opportunities. *Mol. Aspects Med.* **65**, 70–99 (2019).

14. Hinderer, S. & Schenke-Layland, K. Cardiac fibrosis – A short review of causes and therapeutic strategies. *Adv. Drug Deliv. Rev.* **146**, 77–82 (2019).

15. Ivey, M. J. & Tallquist, M. D. Defining the Cardiac Fibroblast. *Circ. J. Off. J. Jpn. Circ. Soc.* **80**, 2269–2276 (2016).

16. Lewis, G. A. *et al.* Pirfenidone in heart failure with preserved ejection fraction: a randomized phase 2 trial. *Nat. Med.* **27**, 1477–1482 (2021).

17. Revelo, X. *et al.* Cardiac Resident Macrophages Prevent Fibrosis and Stimulate Angiogenesis. *Circ. Res.* CIRCRESAHA.121.319737 (2021) doi:10.1161/CIRCRESAHA.121.319737.

18. Hu, S. *et al.* Different Roles of Resident and Non-resident Macrophages in Cardiac Fibrosis. *Front. Cardiovasc. Med.* **9**, 818188 (2022).

19. Liao, X. *et al.* Distinct roles of resident and nonresident macrophages in nonischemic cardiomyopathy. *Proc. Natl. Acad. Sci.* **115**, (2018).

20. Neubauer, S. The Failing Heart — An Engine Out of Fuel. *N. Engl. J. Med.* **356**, 1140–1151 (2007).

21. Fragasso, G. Deranged Cardiac Metabolism and the Pathogenesis of Heart Failure. *Card. Fail. Rev.* **2**, 8–13 (2016).

22. Razeghi, P. *et al.* Metabolic Gene Expression in Fetal and Failing Human Heart. *Circulation* **104**, 2923–2931 (2001).

23. Li, X. *et al.* Inhibition of fatty acid oxidation enables heart regeneration in adult mice. *Nature* **622**, 619–626 (2023).

24. Tsao, C. W. *et al.* Heart Disease and Stroke Statistics—2023 Update: A Report From the American Heart Association. *Circulation* CIR.0000000000001123 (2023) doi:10.1161/CIR.0000000000001123.

25. Berthiaume, J. M. *et al.* Chapter 8 - Pathophysiology of Heart Failure and an Overview of Therapies. in *Cardiovascular Pathology (Fourth Edition)* (eds. Buja, L. M. & Butany, J.) 271–339 (Academic Press, San Diego, 2016). doi:10.1016/B978-0-12-420219-1.00008-2.

26. Oka, T., Akazawa, H., Naito, A. T. & Komuro, I. Angiogenesis and Cardiac Hypertrophy: Maintenance of Cardiac Function and Causative Roles in Heart Failure. *Circ. Res.* **114**, 565–571 (2014).

27. Simmonds, S. J., Cuijpers, I., Heymans, S. & Jones, E. A. V. Cellular and Molecular Differences between HFpEF and HFrEF: A Step Ahead in an Improved Pathological Understanding. *Cells* **9**, (2020).

28. Schiattarella, G. G. & Hill, J. A. Cardiometabolic HFpEF: Mechanisms and Therapies. *CardioMetabolic Syndr. J.* **1**, 117 (2021).

29. Anker, S. D. *et al.* Empagliflozin in Heart Failure with a Preserved Ejection Fraction. *N. Engl. J. Med.* **385**, 1451–1461 (2021).

30. Ranek, M. J. *et al.* Pathophysiology of heart failure and an overview of therapies. *Cardiovasc. Pathol.* 149–221 (2022) doi:10.1016/B978-0-12-822224-9.00025-6.

31. Resident cardiac macrophages mediate adaptive myocardial remodeling: Immunity. https://www.cell.com/immunity/fulltext/S1074-7613(21)00289-2.

32. Kumar, S. & Dikshit, M. Metabolic Insight of Neutrophils in Health and Disease. *Front. Immunol.* **10**, 2099 (2019).

33. Silvestre-Roig, C., Fridlender, Z. G., Glogauer, M. & Scapini, P. Neutrophil Diversity in Health and Disease. *Trends Immunol.* **40**, 565–583 (2019).

34. Chaar, D. *et al.* Neutrophils pro-inflammatory and anti-inflammatory cytokine release in patients with heart failure and reduced ejection fraction. *ESC Heart Fail.* **8**, 3855–3864 (2021).

35. Scapini, P. *et al.* Neutrophil-derived chemokines. *Immunol. Rev.* **177**, 195–203.

36. Ma, Y. *et al.* Temporal neutrophil polarization following myocardial infarction. *Cardiovasc. Res.* **110**, 51–61 (2016).

37. Coffelt, S. B., Wellenstein, M. D. & De Visser, K. E. Neutrophils in cancer: neutral no more. *Nat. Rev. Cancer* **16**, 431–446 (2016).

38. Fridlender, Z. G. *et al.* Polarization of Tumor-Associated Neutrophil Phenotype by TGF-β: "N1" versus "N2" TAN. *Cancer Cell* **16**, 183–194 (2009).

39. Sager, H. B. *et al.* Proliferation and Recruitment Contribute to Myocardial Macrophage Expansion in Chronic Heart Failure. *Circ. Res.* **119**, 853–864 (2016).

40. Lavine, K. J. *et al.* The Macrophage in Cardiac Homeostasis and Disease. *J. Am. Coll. Cardiol.* **72**, 2213–2230 (2018).

41. Garrido, C. *et al.* Mechanisms of cytochrome c release from mitochondria. *Cell Death Differ.* **13**, 1423–1433 (2006).

42. Frangogiannis, N. G. & Entman, M. L. Chemokines in Myocardial Ischemia. *Trends Cardiovasc. Med.* **15**, 163–169 (2005).

43. Mouton, A. J. *et al.* Mapping macrophage polarization over the myocardial infarction time continuum. *Basic Res. Cardiol.* **113**, 26 (2018).

44. Ter Maaten, J. M. *et al.* Connecting heart failure with preserved ejection fraction and renal dysfunction: the role of endothelial dysfunction and inflammation. *Eur. J. Heart Fail.* **18**, 588–598 (2016).

45. Dusi, V., Ghidoni, A., Ravera, A., De Ferrari, G. M. & Calvillo, L. Chemokines and Heart Disease: A Network Connecting Cardiovascular Biology to Immune and Autonomic Nervous Systems. *Mediators Inflamm.* **2016**, (2016).

46. Russo, S., Kwiatkowski, M., Govorukhina, N., Bischoff, R. & Melgert, B. N. Meta-Inflammation and Metabolic Reprogramming of Macrophages in Diabetes and Obesity: The Importance of Metabolites. *Front. Immunol.* **12**, 746151 (2021).

47. Poon, I. K. H. *et al.* Unexpected link between an antibiotic, pannexin channels and apoptosis. *Nature* **507**, 329–334 (2014).

48. Agah, R. *et al.* Gene recombination in postmitotic cells. Targeted expression of Cre recombinase provokes cardiac-restricted, site-specific rearrangement in adult ventricular muscle in vivo. https://www.jci.org/articles/view/119509/pdf (1997) doi:10.1172/JCI119509.

49. Poon, I. K. H. *et al.* Unexpected link between an antibiotic, pannexin channels and apoptosis. *Nature* **507**, 329–334 (2014).

50. Ackers-Johnson Matthew *et al.* A Simplified, Langendorff-Free Method for Concomitant Isolation of Viable Cardiac Myocytes and Nonmyocytes From the Adult Mouse Heart. *Circ. Res.* **119**, 909–920 (2016).

51. Billaud, M. *et al.* A molecular signature in the pannexin1 intracellular loop confers channel activation by the α1 adrenoreceptor in smooth muscle cells. *Sci. Signal.* **8**, ra17–ra17 (2015).

52. Heiberg, E. *et al.* Design and validation of Segment - freely available software for cardiovascular image analysis. *BMC Med. Imaging* **10**, 1 (2010).

53. Senthivinayagam, S. *et al.* Adaptive thermogenesis in brown adipose tissue involves activation of pannexin-1 channels. *Mol. Metab.* **44**, 101130 (2021).

54. Zhang, Y. *et al.* Role of cAMP in Cardiomyocyte Viability: Beneficial or Detrimental? *Circ. Res.* **133**, 902–923 (2023).

55. Rusiecka, O. M. *et al.* Mitochondrial pannexin1 controls cardiac sensitivity to ischaemia/reperfusion injury. *Cardiovasc. Res.* **119**, 2342–2354 (2023).

56. Le Vasseur, M., Lelowski, J., Bechberger, J. F., Sin, W.-C. & Naus, C. C. Pannexin 2 protein expression is not restricted to the CNS. *Front. Cell. Neurosci.* **8**, (2014).

57. Zhang, H. *et al.* Cryo-EM structure of human heptameric pannexin 2 channel. *Nat. Commun.* **14**, 1118 (2023).

58. Wolpe, A. G. *et al.* Pannexin-3 stabilizes the transcription factor Bcl6 in a channel-independent manner to protect against vascular oxidative stress. *Sci. Signal.* **17**, eadg2622 (2024).

59. Narahari, A. K. *et al.* ATP and large signaling metabolites flux through caspase-activated Pannexin 1 channels. *eLife* **10**, e64787 (2021).

60. O'Donnell, B. L. & Penuela, S. Pannexin 3 channels in health and disease. *Purinergic Signal.* **17**, 577–589 (2021).

61. Sandilos, J. K. *et al.* Pannexin 1, an ATP Release Channel, Is Activated by Caspase Cleavage of Its Pore-associated C-terminal Autoinhibitory Region ♦. *J. Biol. Chem.* **287**, 11303–11311 (2012).

62. Chiu, Y.-H., Schappe, M. S., Desai, B. N. & Bayliss, D. A. Revisiting multimodal activation and channel properties of Pannexin 1. *J. Gen. Physiol.* **150**, 19–39 (2018).

63. Medina, C. B. *et al.* Metabolites released from apoptotic cells act as tissue messengers. *Nature* **580**, 130–135 (2020).

64. Good, M. E. *et al.* Pannexin 1 Channels as an Unexpected New Target of the Anti-Hypertensive Drug Spironolactone. *Circ. Res.* **122**, 606–615 (2018).

65. Lohman, A. W. *et al.* Pannexin 1 channels regulate leukocyte emigration through the venous endothelium during acute inflammation. *Nat. Commun.* **6**, 7965 (2015).

66. Filiberto, A. C. *et al.* Endothelial pannexin-1 channels modulate macrophage and smooth muscle cell activation in abdominal aortic aneurysm formation. *Nat. Commun.* **13**, 1521 (2022).

67. Metz, L. M. *et al.* Platelet pannexin-1 channels modulate neutrophil activation and migration but not the progression of abdominal aortic aneurysm. *Front. Mol. Biosci.* **10**, 1111108 (2023).

68. Good, M. E. *et al.* Endothelial Pannexin 1 Regulates Cardiac Response to Myocardial Infarction. *Circ. Res.* **128**, 1211–1213 (2021).

69. Michalski, K. & Kawate, T. Carbenoxolone inhibits Pannexin1 channels through interactions in the first extracellular loop. *J. Gen. Physiol.* **147**, 165–174 (2016).

70. Silverman, W., Locovei, S. & Dahl, G. Probenecid, a gout remedy, inhibits pannexin 1 channels. *Am. J. Physiol. Cell Physiol.* **295**, C761-767 (2008).

71. Pitt, B. *et al.* The Effect of Spironolactone on Morbidity and Mortality in Patients with Severe Heart Failure. *N. Engl. J. Med.* **341**, 709–717 (1999).

72. Anand, I. S. *et al.* Interaction Between Spironolactone and Natriuretic Peptides in Patients With Heart Failure and Preserved Ejection Fraction. *JACC Heart Fail.* **5**, 241–252 (2017).

73. Ferreira, J. P. *et al.* Proteomic and Mechanistic Analysis of Spironolactone in Patients at Risk for HF. *JACC Heart Fail.* (2021) doi:10.1016/j.jchf.2020.11.010.

74. Dolmatova, E. *et al.* Cardiomyocyte ATP release through pannexin 1 aids in early fibroblast activation. *Am. J. Physiol. - Heart Circ. Physiol.* **303**, H1208–H1218 (2012).

75. Li, L., He, L., Wu, D., Chen, L. & Jiang, Z. Pannexin-1 channels and their emerging functions in cardiovascular diseases. *Acta Biochim. Biophys. Sin.* **47**, 391–396 (2015).

76. Chavey, W. E., Hogikyan, R. V., Harrison, R. V. & Nicklas, J. M. Heart Failure Due to Reduced Ejection Fraction: Medical Management. *Am. Fam. Physician* **95**, 13–20 (2017).

77. McMurray, J. J. V. & Packer, M. How Should We Sequence the Treatments for Heart Failure and a Reduced Ejection Fraction? A Redefinition of Evidence-Based Medicine. *Circulation* CIRCULATIONAHA.120.052926 (2020) doi:10.1161/CIRCULATIONAHA.120.052926.

78. Zhang, Y., Bauersachs, J. & Langer, H. F. Immune mechanisms in heart failure. *Eur. J. Heart Fail.* **19**, 1379–1389 (2017).

79. Travers, J. G., Tharp, C. A., Rubino, M. & McKinsey, T. A. Therapeutic targets for cardiac fibrosis: from old school to next-gen. *J. Clin. Invest.* **132**, e148554 (2022).

80. Benjamin, I. J. *et al.* Isoproterenol-induced myocardial fibrosis in relation to myocyte necrosis. *Circ. Res.* **65**, 657–670 (1989).

81. Blanton, R. M., Carrillo-Salinas, F. J. & Alcaide, P. T-cell recruitment to the heart: friendly guests or unwelcome visitors? *Am. J. Physiol.-Heart Circ. Physiol.* **317**, H124–H140 (2019).

82. Hartman, M. H. T., Groot, H. E., Leach, I. M., Karper, J. C. & van der Harst, P. Translational overview of cytokine inhibition in acute myocardial infarction and chronic heart failure. *Trends Cardiovasc. Med.* **28**, 369–379 (2018).

83. Sesma, J. I. *et al.* The UDP-sugar-sensing P2Y $_{14}$ receptor promotes Rho-mediated signaling and chemotaxis in human neutrophils. *Am. J. Physiol.-Cell Physiol.* **303**, C490–C498 (2012).

84. Whitehead, G. S. *et al.* Effects of Purinergic Receptor Deletion or Pharmacologic Modulation on Pulmonary Inflammation in Mice. *ACS Pharmacol. Transl. Sci.* **5**, 973–984 (2022).

85. Wang, X. *et al.* P2RX1-Involved Glycolytic Metabolism Supports Neutrophil Activation in Acute Pancreatitis. *Front. Immunol.* **11**, 549179 (2021).

86. Wang, X. & Chen, D. Purinergic Regulation of Neutrophil Function. *Front. Immunol.* **9**, 399 (2018).

87. Barrett, M. O. *et al.* A selective high-affinity antagonist of the P2Y14 receptor inhibits UDP-glucose-stimulated chemotaxis of human neutrophils. *Mol. Pharmacol.* **84**, 41–49 (2013).

88. Battistone, M. A. *et al.* Proinflammatory P2Y14 receptor inhibition protects against ischemic acute kidney injury in mice. *J. Clin. Invest.* **130**, 3734–3749 (2020).

89. Chen, Y. *et al.* ATP Release Guides Neutrophil Chemotaxis via P2Y2 and A3 Receptors. *Science* **314**, 1792–1795 (2006).

90. Burnstock, G. & Boeynaems, J.-M. Purinergic signalling and immune cells. *Purinergic Signal.* **10**, 529–564 (2014).

91. Burnstock, G. Purinergic Signaling in the Cardiovascular System. *Circ. Res.* **120**, 207–228 (2017).

92. Karmakar, M., Katsnelson, M. A., Dubyak, G. R. & Pearlman, E. Neutrophil P2X7 receptors mediate NLRP3 inflammasome-dependent IL-1β secretion in response to ATP. *Nat. Commun.* **7**, 10555 (2016).

93. McDonald, B. *et al.* Intravascular Danger Signals Guide Neutrophils to Sites of Sterile Inflammation. *Science* **330**, 362–366 (2010).

94. Oudit, G. Y. *et al.* Phosphoinositide 3-Kinase γ–Deficient Mice Are Protected From Isoproterenol-Induced Heart Failure. *Circulation* **108**, 2147–2152 (2003).

95. Balakumar, P., Singh, A. P. & Singh, M. Rodent models of heart failure. *J. Pharmacol. Toxicol. Methods* **56**, 1–10 (2007).

96. Yang, Y. *et al.* Apelin-13/APJ induces cardiomyocyte hypertrophy by activating the Pannexin-1/P2X7 axis and FAM134B-dependent reticulophagy. *J. Cell. Physiol.* **237**, 2230–2248 (2022).

97. Valentine, C. D. & Haggie, P. M. Confinement of β $_1$ - and β $_2$ -adrenergic receptors in the plasma membrane of cardiomyocyte-like H9c2 cells is mediated by selective interactions with PDZ domain and A-kinase anchoring proteins but not caveolae. *Mol. Biol. Cell* **22**, 2970–2982 (2011).

98. Branco, A. F. *et al.* Isoproterenol Cytotoxicity is Dependent on the Differentiation State of the Cardiomyoblast H9c2 Cell Line. *Cardiovasc. Toxicol.* **11**, 191–203 (2011).

99. Heiman, P. *et al.* Mitochondrial dysfunction associated with TANGO2 deficiency. *Sci. Rep.* **12**, 3045 (2022).

100. Lujan, A. L. *et al.* Defects in lipid homeostasis reflect the function of TANGO2 in phospholipid and neutral lipid metabolism. *eLife* **12**, e85345 (2023).

101.   Lee, V. R. *et al.* Pannexin 1 regulates adipose stromal cell differentiation and fat

accumulation. *Sci. Rep.* **8**, 16166 (2018).

102.   Sayedyahossein, S. *et al.* Pannexin 1 binds β-catenin to modulate melanoma cell

growth and metabolism. *J. Biol. Chem.* **296**, 100478 (2021).

103.   Jorquera, G. *et al.* High extracellular ATP levels released through pannexin-1

channels mediate inflammation and insulin resistance in skeletal muscle fibres of

diet-induced obese mice. *Diabetologia* **64**, 1389–1401 (2021).

104.   Banuelos, A. *et al.* Pannexin-1 channels promotes CD8+ T cell effector and

memory responses through distinct metabolic pathways. *J. Immunol.* **210**, 226.15-

226.15 (2023).

105.   Adamson, S. E. *et al.* Pannexin 1 is required for full activation of insulin-

stimulated glucose uptake in adipocytes. *Mol. Metab.* **4**, 610–618 (2015).

106.   Sun, J. *et al.* Human Relaxin-2 Fusion Protein Treatment Prevents and Reverses

Isoproterenol-Induced Hypertrophy and Fibrosis in Mouse Heart. *J. Am. Heart Assoc.*

8, e013465 (2019).

107.   Von Hundelshausen, P. & Weber, C. Platelets as Immune Cells: Bridging

Inflammation and Cardiovascular Disease. *Circ. Res.* **100**, 27–40 (2007).

108.   Bisht, K. *et al.* Capillary-associated microglia regulate vascular structure and

function through PANX1-P2RY12 coupling in mice. *Nat. Commun.* **12**, 5289 (2021).

109.   Barletta, K. E., Ley, K. & Mehrad, B. Regulation of Neutrophil Function by

Adenosine. *Arterioscler. Thromb. Vasc. Biol.* **32**, 856–864 (2012).

110. Burnstock, G. Purinergic Signalling: Therapeutic Developments. *Front. Pharmacol.* **8**, 661 (2017).

111. Birkenfeld, A. L., Jordan, J., Dworak, M., Merkel, T. & Burnstock, G. Myocardial metabolism in heart failure: Purinergic signalling and other metabolic concepts. *Pharmacol. Ther.* **194**, 132–144 (2019).

112. Burnstock, G. & Pelleg, A. Cardiac purinergic signalling in health and disease. *Purinergic Signal.* **11**, 1–46 (2015).

113. Tran Diem H. & Wang Zhao V. Glucose Metabolism in Cardiac Hypertrophy and Heart Failure. *J. Am. Heart Assoc.* **8**, e012673 (2019).

114. Martini Elisa *et al.* Single-Cell Sequencing of Mouse Heart Immune Infiltrate in Pressure Overload–Driven Heart Failure Reveals Extent of Immune Activation. *Circulation* **140**, 2089–2107 (2019).

115. Li, X. *et al.* Systemic Adenosine Triphosphate Impairs Neutrophil Chemotaxis and Host Defense in Sepsis. *Crit. Care Med.* **45**, e97–e104 (2017).

116. Bao, Y., Chen, Y., Ledderose, C., Li, L. & Junger, W. G. Pannexin 1 Channels Link Chemoattractant Receptor Signaling to Local Excitation and Global Inhibition Responses at the Front and Back of Polarized Neutrophils. *J. Biol. Chem.* **288**, 22650–22657 (2013).

117. Chekeni, F. B. *et al.* Pannexin 1 channels mediate 'find-me' signal release and membrane permeability during apoptosis. *Nature* **467**, 863–867 (2010).

118. Good Miranda E *et al.* Endothelial Pannexin 1 Regulates Cardiac Response to Myocardial Infarction. *Circ. Res.* **0**,.

119. Bochkov, V. N. *et al.* Generation and Biological Activities of Oxidized Phospholipids. *Antioxid. Redox Signal.* **12**, 1009–1059 (2010).

120. Taleb, A., Witztum, J. L. & Tsimikas, S. Oxidized phospholipids on apoB-100-containing lipoproteins: a biomarker predicting cardiovascular disease and cardiovascular events. *Biomark. Med.* **5**, 673–694 (2011).

121. Berliner, J. A., Leitinger, N. & Tsimikas, S. The role of oxidized phospholipids in atherosclerosis. *J. Lipid Res.* **50**, S207–S212 (2009).

122. Upchurch, C. M. *et al.* Targeting oxidized phospholipids by AAV-based gene therapy in mice with established hepatic steatosis prevents progression to fibrosis. *Sci. Adv.* **8**, eabn0050 (2022).

123. Yeang, C. *et al.* Reduction of myocardial ischaemia–reperfusion injury by inactivating oxidized phospholipids. *Cardiovasc. Res.* **115**, 179–189 (2019).

124. Que, X. *et al.* Oxidized phospholipids are proinflammatory and proatherogenic in hypercholesterolaemic mice. *Nature* **558**, 301–306 (2018).

125. Hörkkö, S. *et al.* Monoclonal autoantibodies specific for oxidized phospholipids or oxidized phospholipid–protein adducts inhibit macrophage uptake of oxidized low-density lipoproteins. *J. Clin. Invest.* **103**, 117–128 (1999).

126. Sun, X. *et al.* Neutralization of Oxidized Phospholipids Ameliorates Non-alcoholic Steatohepatitis. *Cell Metab.* **31**, 189-206.e8 (2020).

127. Ke, Y. *et al.* Anti-Inflammatory Effects of OxPAPC Involve Endothelial Cell–Mediated Generation of LXA4. *Circ. Res.* **121**, 244–257 (2017).

128. Pidkovka, N. A. *et al.* Oxidized Phospholipids Induce Phenotypic Switching of Vascular Smooth Muscle Cells In Vivo and In Vitro. *Circ. Res.* **101**, 792–801 (2007).

129. Serbulea, V. *et al.* Macrophage phenotype and bioenergetics are controlled by oxidized phospholipids identified in lean and obese adipose tissue. *Proc. Natl. Acad. Sci.* **115**, (2018).

130. Nonas, S. *et al.* Oxidized Phospholipids Reduce Vascular Leak and Inflammation in Rat Model of Acute Lung Injury. *Am. J. Respir. Crit. Care Med.* **173**, 1130–1138 (2006).

131. Kadl, A. *et al.* Identification of a Novel Macrophage Phenotype That Develops in Response to Atherogenic Phospholipids via Nrf2. *Circ. Res.* **107**, 737–746 (2010).

132. Cohen, J. B. *et al.* Clinical Phenogroups in Heart Failure With Preserved Ejection Fraction. *JACC Heart Fail.* **8**, 172–184 (2020).

133. Shah, S. J. *et al.* Phenotype-Specific Treatment of Heart Failure With Preserved Ejection Fraction: A Multiorgan Roadmap. *Circulation* **134**, 73–90 (2016).

134. Hahn, V. S. *et al.* Myocardial Gene Expression Signatures in Human Heart Failure With Preserved Ejection Fraction. *Circulation* **143**, 120–134 (2021).

135. Capone, F. *et al.* Cardiac metabolism in HFpEF: from fuel to signalling. *Cardiovasc. Res.* **118**, 3556–3575 (2023).

136. Deng, Y. *et al.* Targeting Mitochondria-Inflammation Circuit by β-Hydroxybutyrate Mitigates HFpEF. *Circ. Res.* **128**, 232–245 (2021).

137.   Sanders-van Wijk, S. *et al.* Circulating biomarkers of distinct pathophysiological pathways in heart failure with preserved vs. reduced left ventricular ejection fraction. *Eur. J. Heart Fail.* **17**, 1006–1014 (2015).

138.   DuBrock, H. M., AbouEzzeddine, O. F. & Redfield, M. M. High-sensitivity C-reactive protein in heart failure with preserved ejection fraction. *PLOS ONE* **13**, e0201836 (2018).

139.   Westermann, D. *et al.* Cardiac Inflammation Contributes to Changes in the Extracellular Matrix in Patients With Heart Failure and Normal Ejection Fraction. *Circ. Heart Fail.* **4**, 44–52 (2011).

140.   Schiattarella, G. G. *et al.* Nitrosative stress drives heart failure with preserved ejection fraction. *Nature* **568**, 351–356 (2019).

141.   Heinick, A. *et al.* Annexin A4 is a novel direct regulator of adenylyl cyclase type 5. *FASEB J.* **29**, 3773–3787 (2015).

142.   Bush, E. W. & McKinsey, T. A. Protein Acetylation in the Cardiorenal Axis: The Promise of Histone Deacetylase Inhibitors. *Circ. Res.* **106**, 272–284 (2010).

143.   Cosgrove, D. & Liu, S. Collagen IV diseases: A focus on the glomerular basement membrane in Alport syndrome. *Matrix Biol.* **57–58**, 45–54 (2017).

144.   Baues, M. *et al.* A collagen-binding protein enables molecular imaging of kidney fibrosis in vivo. *Kidney Int.* **97**, 609–614 (2020).

145.   Croft, A. J. *et al.* Sex-based differences in short and longer-term diet-induced metabolic heart disease. *Am. J. Physiol.-Heart Circ. Physiol.* ajpheart.00467.2023 (2024) doi:10.1152/ajpheart.00467.2023.

146.   Camors, E., Monceau, V. & Charlemagne, D. Annexins and Ca2+ handling in the heart. *Cardiovasc. Res.* **65**, 793–802 (2005).

147.   Zhang, S., Zhang, Y., Duan, X., Wang, B. & Zhan, Z. Targeting NPM1 Epigenetically Promotes Postinfarction Cardiac Repair by Reprogramming Reparative Macrophage Metabolism. *Circulation* CIRCULATIONAHA.123.065506 (2024) doi:10.1161/CIRCULATIONAHA.123.065506.

148.   Stevens, M. & Oltean, S. Assessment of Kidney Function in Mouse Models of Glomerular Disease. *J. Vis. Exp.* 57764 (2018) doi:10.3791/57764.

149.   McCrimmon, A. *et al.* Redox phospholipidomics analysis reveals specific oxidized phospholipids and regions in the diabetic mouse kidney. *Redox Biol.* **58**, 102520 (2022).

150.   Sotomi, Y. *et al.* Sex Differences in Heart Failure With Preserved Ejection Fraction. *J. Am. Heart Assoc.* **10**, e018574 (2021).

151.   Shao, D. & Tian, R. Glucose Transporters in Cardiac Metabolism and Hypertrophy. in *Comprehensive Physiology* (ed. Prakash, Y. S.) 331–351 (Wiley, 2015). doi:10.1002/cphy.c150016.

152.   Yu, Z.-Y. *et al.* Piezo1 is the cardiac mechanosensor that initiates the cardiomyocyte hypertrophic response to pressure overload in adult mice. *Nat. Cardiovasc. Res.* **1**, 577–591 (2022).

153.   Bonora, M. *et al.* ATP synthesis and storage. *Purinergic Signal.* **8**, 343–357 (2012).

154.   Lazarowski, E. R., Shea, D. A., Boucher, R. C. & Harden, T. K. Release of Cellular

UDP-Glucose as a Potential Extracellular Signaling Molecule. *Mol. Pharmacol.* **63**,

1190–1197 (2003).